Dissertation
submitted to the
Combined Faculties for the Natural Sciences and for Mathematics
of the Ruperto-Carola University of Heidelberg, Germany
for the degree of
Doctor of Natural Sciences

presented by

Marco Raffaele Cosenza, Master of Science
born in Vico Equense, Italy

Oral examination:

Disruption of spindle pole symmetry by centriole overduplication induces chromosome instability in human malignancies

Referees: Prof. Dr Andreas Trumpp
Prof. Dr Alwin Krämer

TABLE OF CONTENTS

TABLE OF CONTENTS

SUMMARY

Disruption of spindle pole symmetry by centriole overduplication induces chromosome instability in human malignancies

Chromosomal instability (CIN) comprises an elevated rate of chromosome missegregation and correlates with the presence of extra centrosomes. Bipolar anaphases with clustered supernumerary centrosomes have been identified as a mechanism contributing to CIN via the formation of transient multipolar spindle intermediates, which promote merotelic kinetochore-microtubule attachment errors.

However, the contribution of this model and that of potential additional mechanisms in human malignancies has not been addressed.

Here we show that centriole rosettes, defined as multiple procentrioles engaged to a single parent, generate spindle asymmetry that favors kinetochore-microtubule attachment errors without centrosome clustering and ultimately results in CIN. Furthermore, we demonstrate that centriole rosettes, but not the progeny of clustered mitoses, are a common finding in primary human malignancies.

Centriole rosettes are capable of arranging bipolar mitotic spindles but cause an increased frequency of anaphase lagging chromosomes and chromosome missegregation. The CIN phenotype is aggravated when spindle pole have asymmetric centriole numbers and it is not rescued by enhancement of kinetochore-microtubule attachment correction.

Furthermore, by immunostaining for an array of centrosomal proteins, we find that, in primary human malignancies, centrosome amplification is characterized by supernumerary procentrioles forming rosettes around a single pair of parental centrioles, strongly arguing for a major contribution of this mechanism in the generation of CIN in vivo.

Our results indicate that asymmetric centriole rosettes produce unbalanced microtubule numbers on mitotic half-spindles, thereby skewing the chance of binding microtubules from the more prominent spindle pole, resulting in impaired correction of merotelic kinetochore attachments and subsequent chromosome missegregation. We propose that centriole numbers at spindle poles must be carefully controlled to ensure chromosome segregation fidelity and disruption of this mechanism is an important source of CIN in human cancer.

ZUSAMMENFASSUNG

Zentriolenrosetten induzieren chromosomale Instabilität durch Symmetrieverlust an Spindelpolen in humanen Tumorzellen

Chromosomale Instabilität (CIN) zeichnet sich durch erhöhte Raten fehlerhafter Chromosomenverteilung aus und korreliert mit der Präsenz überzähliger Zentrosomen. Als ein hierfür verantwortlicher Mechanismus wurden bipolare Anaphasen mit gebündelten, überzähligen Zentrosomen identifiziert, die, durch Bildung kurzlebiger, multipolarer Spindelintermediate, Fehler in den Kinetochor-Mikrotubulus-Verknüpfungen fördern.

Der Beitrag dieses sowie anderer potentiell beteiligter Mechasnismen zur Induktion chromosomaler Instabilität in primären Tumorzellen wurde bisher nicht untersucht.

In der vorliegenden Arbeit konnten wir zeigen, dass Zentriolenrosetten, definiert als mehrere ringförmig um eine Mutterzentriole angeordnete Prozentriolen, Spindelasymmetrien hervorrufen, welche Fehlverknüpfungen zwischen Kinetochoren und Mikrotubuli induzieren, und damit chromosomale Instabilität hervorrufen. Des Weiteren zeigen wir, dass Zentriolenrosetten, nicht jedoch die Nachkommen bipolarer Mitosen mit gebündelten Zentrosomen, häufig in primären humanen Neoplasien zu finden sind.

Bipolare mitotische Spindeln mit jeweils einer Zentriolenrosette pro Spindelpol sind mit einer erhöhten Frequenz an “anaphase lagging chromosomes” sowie einer daraus resultierenden mitotischen Fehlverteilung von Chromosomen vergesellschaftet. Dabei verstärkt eine ungleiche Zentriolenzahl an den beiden Spindelpolen das Ausmaß der mitotischen Chromosomenfehlverteilung. Darüber hinaus können die hierdurch hervorgerufenen fehlerhaften Kinetochor-Mikrotubulus-Verknüpfungen vom hierfür zuständigen Korrekturmechanismus nicht eliminiert werden.

Zusätzlich zeigen wir mithilfe von Immunfluoreszenzfärbungen, dass Zentriolenrosetten den prädominanten Zentrosomenamplifikationsphänotyp in allen von uns untersuchten primären humanen Neoplasien darstellen. Dies kann als starkes Argument für einen bedeutenden Beitrag dieses Mechanismus der Entstehung von CIN in vivo gewertet werden.

Diese Ergebnisse legen nahe, dass asymmetrische Zentriolenrosetten zur Nukleation unterschiedlicher Mengen an Mikrotubuli in den beiden Halbspindeln einer mitotischen Zelle führen, was wiederum beeinflusst die Wahrscheinlichkeit von Chromosomen, Mikrotubuli vom dominanten Spindelpol zu binden, erhöht und in einer Ungleichverteilung der Chromosomen resuliert.

Zusammenfassend kann geschlossen werden, dass die Zentriolenzahl pro Spindelpol sorgfältig kontrolliert sein muss, um eine korrekte Aufteilung der Chromosomen auf die Tochterzellen zu gewährleisten. Eine Beeinträchtigung dieses Mechanismus muss als Ursache chromosomaler Instabilität von Krebserkrankungen betrachtet werden.

ACKNOWLEDGEMENTS

The work here presented was conducted at the Clinical Cooperation Unit Molecular Hematology/Oncology of the German Cancer Research Center (DKFZ), under the supervision of Prof. Dr. Alwin Krämer.

First and foremost I want to thank my supervisor and referee Prof. Dr. Alwin Krämer, whose example and mentoring has greatly influenced my development as a scientist. I cannot express my gratitude for the time, ideas and funding Alwin put to promote my PhD. I am especially thankful for the intellectual freedom he granted me and that made my PhD successful. Contributing to the research on centrosomes and chromosome instability was my objective since I was a bachelor student. To Alwin, I owe a debt which I will never be able to repay.

I would like to acknowledge my thesis referee, Prof. Dr. Andreas Trumpp (DKFZ), who provided insightful discussions about the developing project during my thesis advisory meetings, and the other members, who kindly agreed to serve in my thesis defense committee, Prof. Dr. Elmar Schiebel and Prof. Dr. Karin Müller-Decker.

This work would have not been possible without the contribution of my students, Annik Roßberg and Anna Cazzola, which gave me a tremendous help in pushing this PhD to completion. I hope I returned to them as much as they gave me.

I would like to thank all the current and former lab members and especially Dr. Bettina Maier, Dr. Corinna Horrix and Dr. Gleb Konotop, whose experience helped me to solve the most difficult problems. I also have to thank Michael Kirsch for the priceless help he provided every day in keeping the lab running.

This work has microscopy at its core and wouldn't have been possible without the support of Dr. Damir Krunic from the DKFZ light microscopy facility. I want also to gratefully acknowledge Dr. Sven Poppelreuther from Carl Zeiss for giving me the opportunity to be among the first users of a new super-resolution technology and for inviting me as a speaker at the Mannheim's Planetarium.

Finally, I will be forever grateful to all the people that have been supporting me along these years: all the friends that shared this time with me in Heidelberg, all the friends that stayed despite the distance and my family that was always there for me whenever I needed it.

Last but not least I want to thank my fiancée, Aneczka, who has agreed to collaborate with me on the most difficult and important project of all: making a family.

CHAPTER 1

INTRODUCTION

1.1 CENTROSOME

1.1.1 CENTROSOME STRUCTURE

The centrosome is the primary microtubule-organizing center (MTOC) in metazoans. It is a cellular organelle of critical importance in many microtubule-dependent processes during both interphase and mitosis. In interphase, the centrosome organizes the microtubule cytoskeleton and is involved in the formation of the primary cilium; in mitosis the centrosome establishes microtubule arrays at the spindle poles[1].

In vertebrates, the centrosome is constituted by a pair of orthogonally oriented centrioles, which are embedded in a lattice of pericentriolar material (PCM). The two centrioles are not identical, as they are at different maturation stages. The fully mature one, defined mother, can be distinguished by the presence of two sets of protein appendages. The less mature daughter centriole, in contrast, is lacking these structures[2] (**Fig. 1**).

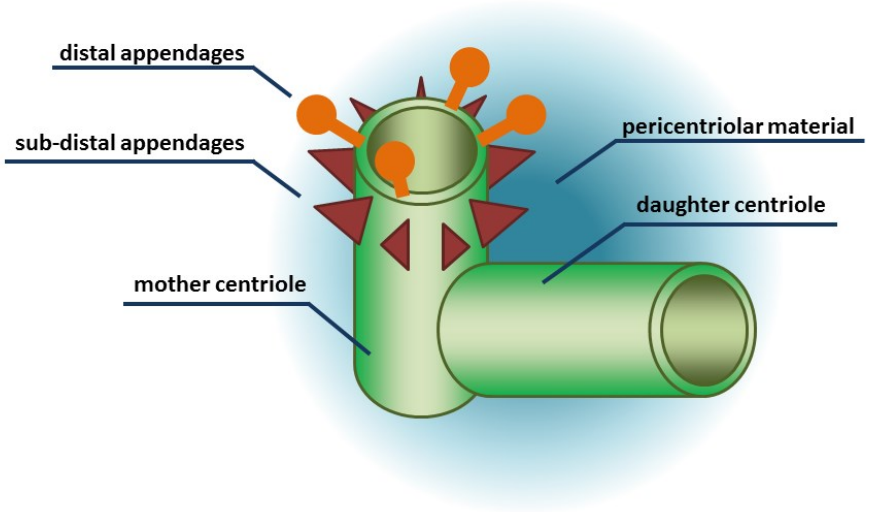

Figure 1 – Centrosome structure

The main centrosome components are depicted. The mother and daughter centrioles, oriented at 90° in respect to each other, are embedded in the pericentriolar material. The mother centriole is decorated by distal and sub-distal appendages. The daughter centriole is connected to the proximal end of the mother.

1.1.2 CENTRIOLE

A pair of centrioles is the core component of the centrosome[3]. Centrioles are small, barrel-shaped structures characterized by nine-fold symmetry. A centriole cross-section reveals the basic element of this structure: a repeated microtubule triplet, forming the wall of the cylinder (**Fig. 2**)[4].

The mother centriole comprises several highly specialized domains along its length. The distal end of the mother centriole is characterized by the presence of appendages that are necessary for accomplishing centrosome-related functions: subdistal appendages serve to anchor microtubules[5]; distal appendages are needed for anchoring the centriole to the plasma membrane during ciliogenesis[3].

The proximal end is responsible for recruiting pericentriolar material, needed for the microtubule nucleating ability of the centrosome (**Fig. 2**)[6]. Moreover, the proximal end is also the site of formation of the cartwheel, a structure needed for daughter centriole assembly[7].

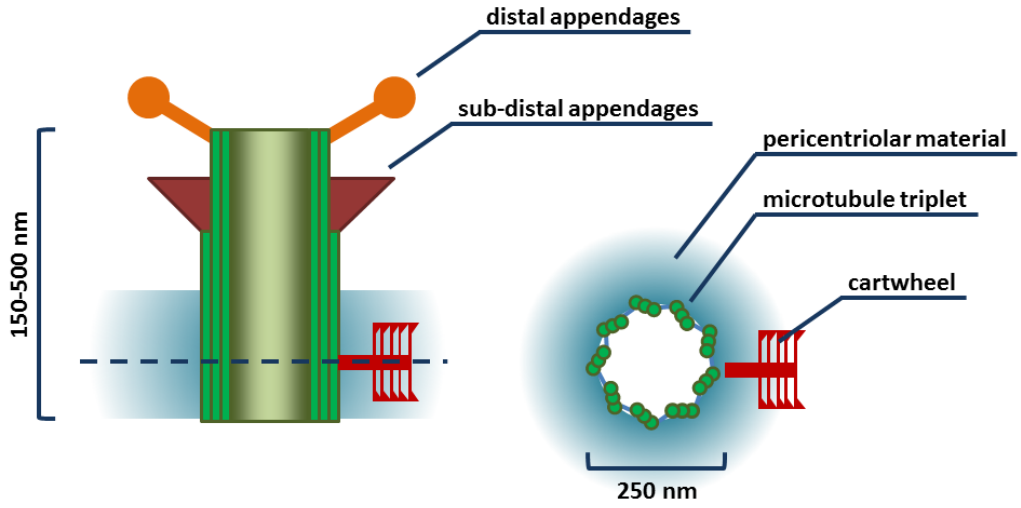

Figure 2 – Longitudinal and cross-section of a mother centriole

The fully mature mother centriole has a variable length of 150-500 nm and a diameter of 250 nm. The left side of the image represents a longitudinal section, the right side shows a cross-section corresponding to the dashed line within the longitudinal section. In the longitudinal section, the distal end is characterized by the presence of appendages. The pericentriolar material surrounds the proximal end. The cartwheel is also located at the proximal end, in orthogonal orientation. The daughter centriole is not depicted for clarity, but it is present and engaged to the cartwheel. In the cross-section, microtubule triplets can be observed arranged in typical nine-fold symmetry.

1.1.3 PERICENTRIOLAR MATERIAL

The pericentriolar material (PCM) is a matrix of proteins in which the centriole pair is embedded. It serves as a platform for regulation of biochemical pathways[8] including organelle trafficking[9], protein degradation[10] and most importantly spindle assembly[11].

The PCM forms a porous scaffold onto which γ-tubulin ring complexes (γ-TuRCs) are recruited for microtubule nucleation[12].

The main scaffolding proteins of the PCM there are: pericentrin (PCNT), CPAP, CEP192, CEP152 and CDK5RAP2. These proteins are characterized by the presence of coiled-coil domains, which regulate their mutual interaction and drive the formation of the PCM lattice (**Fig. 3**)[13].

During interphase, the scaffolding proteins arrange themselves as concentric toroids progressively extending from the centriole wall toward the cytoplasm[14]. Moreover, in *Drosophila*, a PCNT homologous protein is arranged in nine-fold symmetry, suggesting that it might be the mother centriole structure dictating the surrounding organization[15] (**Fig. 3**).

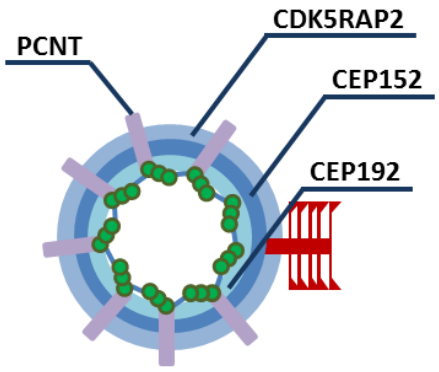

Figure 3 – Structural organization of the PCM

A ninefold radially symmetric centriole is depicted at the center. PCM proteins are arranged in concentric toroids around it. PCNT is depicted as a radial array, as described for PCNT–like protein in *Drosophila* by super-resolution microscopy. On the right side, the cartwheel is visible, where the daughter centriole is engaged, although not depicted.

1.2 THE CENTROSOME CYCLE

1.2.1 DEFINING THE PROCENTRIOLE DUPLICATION ORIGIN

Centrosome duplication is a tightly regulated process, synchronized with the cell cycle, as it is controlled by successive waves of cyclin-CDK complex activity[16]. Centriole duplication requires about one and a half cell cycles to be fully accomplished and is semi-conservative: each of the centrioles serves as seed for the formation of a new one[17]. An overview of the centrosome cycle in healthy cells is depicted in **Fig. 4**.

Every cell starts the cell cycle with a couple of centrioles, which in the previous cell cycle were a mother and a daughter. The two centrioles are disengaged, meaning that they do not have an orthogonal orientation. However, they are hold together by a protein linker structure (**Fig. 4**).

Centriole duplication starts at the G1/S boundary, when the new daughter centriole begins to nucleate from the mother. PLK4 protein is the kinase, which has been identified as the master regulator in this process[14,18].

In mammalian cells, two other proteins CEP152 and CEP192 recruit PLK4 to the centrosome[18]. For most of the cell cycle these proteins are evenly localized around the mother centriole, but, at the G1/S transition, this symmetry is broken via cooperative positive feedback interaction among the aforementioned proteins. As a result, PLK4 accumulates at the exact point where the procentriole will form, triggering cartwheel formation[18].

The cartwheel is characterized by nine-fold symmetry, thus being responsible for the peculiar centriole configuration[19]. Moreover, it is physically linked to the mother centriole through a structure called the stalk, giving its orthogonal orientation to the nascent centriole (**Fig. 5**)[20].

The cartwheel is named after its morphology, because at electron tomography it appears as a central hub from which nine filaments, or stokes, are protruding. Each stoke terminates with a pinhead, the structure to which the first microtubule of the triplet is connected (**Fig. 5**)[7].

The central hub and the proximal stoke structure are composed of nine SAS6 dimers, while the distal stoke and most of the pinhead consist of CEP135[7]. Two other proteins named STIL and CPAP have also been described to be involved in the formation of the cartwheel, but their exact localization and function in the assembly is still a matter of debate[7].

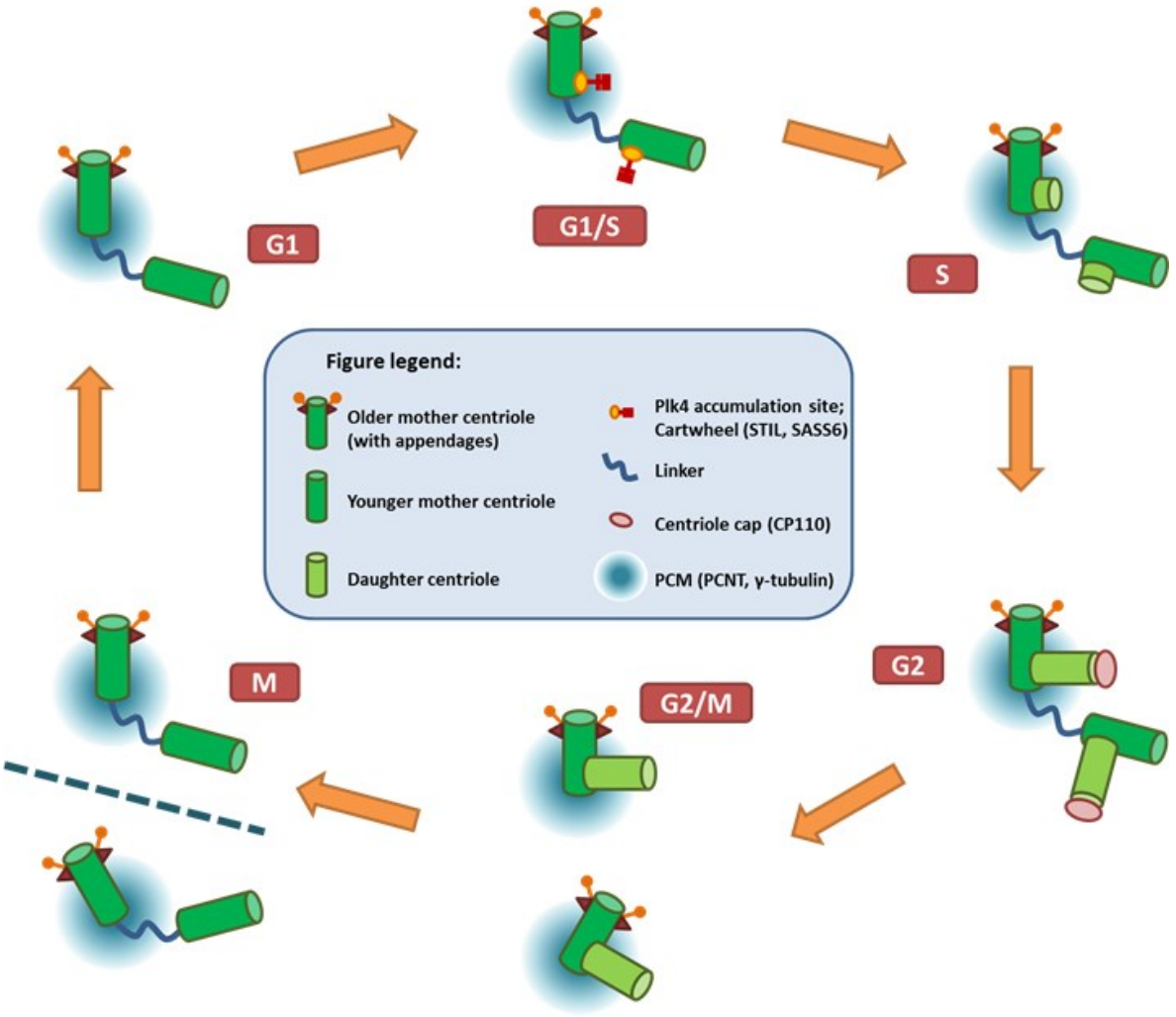

Figure 4 – A schematic overview of the centrosome cycle

The centrosome cycle is depicted in clockwise progression. It starts in G1 with two parental centrioles (*upper left*). Parents are disengaged, but stay connected by a linker. At the G1/S boundary, PLK4 (*yellow spot*) accumulates at the cartwheel origin site of both parents. This triggers SAS6 and STIL recruitment and formation of the cartwheel. During S phase the two nascent daughter centrioles elongate. At G2, the daughters reach full size and are capped by CP110. At this point the presence of three different generations of centrioles can be appreciated: an older mother, a younger mother and two daughter centrioles. At the G2/M boundary, the linker is dissolved; in addition, the younger mother acquires appendages and recruits PCM. During M phase, mother and daughter centriole pairs are disengaged. Each daughter cell will inherit a centrosome composed of two parent centrioles tethered by the linker. Notably, production of a fully developed centriole, decorated with appendages requires 1.5 cell cycles. During the first cell cycle a daughter centriole is produced and matures until becoming a new younger mother centriole. During the second cell cycle the younger mother continues its maturation until acquisition of appendages at the G2/M boundary.

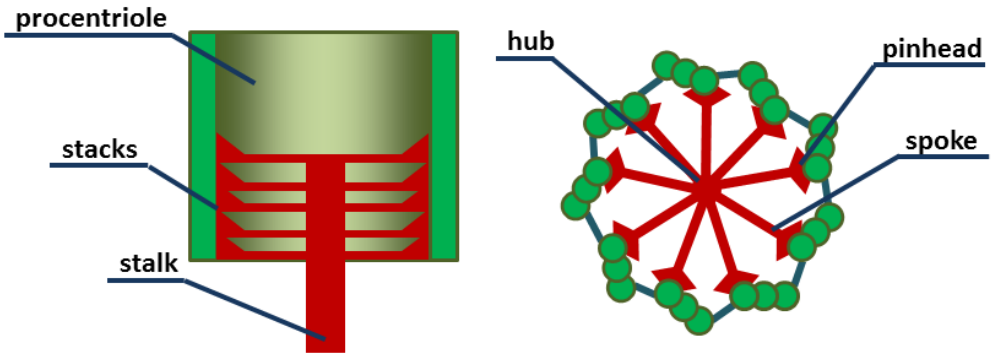

Figure 5 – Schematic representation of stalk and cartwheel structures

A longitudinal and cross-section of a stalk and cartwheel structure is depicted. In the longitudinal section (*left side*), the stalk is depicted; it connects the nascent procentriole to the parent centriole. Several cartwheel stacks are repeated in the distal lumen of the procentriole. At the cross-section (*right side*), the typical cartwheel morphology can be appreciated. A central hub is connected by nine radially symmetric spokes to the microtubule triplets. The pinhead is the part of the cartwheel structure that interacts with the first tubule of the triplet.

1.2.2 DAUGHTER CENTRIOLE ASSEMBLY

Following the formation of the cartwheel, the microtubule triplets are formed to compose the final structure of the daughter centriole.

The cartwheel stoke pinheads interact with γ-tubulin, which stabilizes the microtubule minus-ends, allowing nucleation and elongation of the A-tubule, the first microtubule belonging to the triplet of the centriole wall[20]. The following two microtubules designated as B- and C-tubules, are incomplete in the sense that they share part of their wall with the A- and B-tubule, respectively (**Fig. 5,6**)[17].

The triplet elongates during the whole S-phase, beyond the cartwheel length, with the A- and B- tubules being the longest and determining the different domains for appendages formation (**Fig. 6**)[3]. Centriole length is regulated in a process involving CPAP and capping of the plus-end by CP110[21].

At the end of the process a new daughter centriole is formed: it is composed by nine microtubule triplets, hold at the base by the cartwheel structure, which in turn is linked to the mother centriole through the stalk[20].

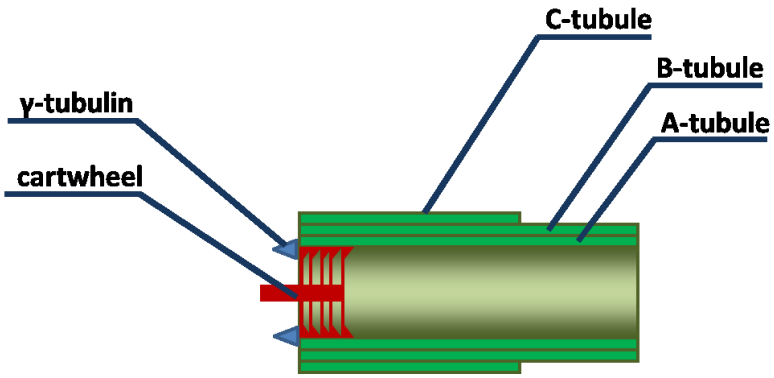

Figure 6 – Microtubule triplet longitudinal section

The cartwheel is connected to the mother centriole by the stalk. At the interface between the cartwheel and the A-tubule, γ-tubulin is recruited. The A-tubule is a complete microtubule. The B-tubule and C-tubule share part of their wall with the tubule they are in contact with. The C-tubule has a considerably shorter length as compared to A- and B-tubules. The distal end, left free by the C-tubule, will be the future site of appendages formation.

Notably, at this point of the cell cycle, there are three different generations of centrioles: the older mother centriole with appendages and the younger mother centriole without appendages, which are connected by the linker. In addition, there are the two newly formed daughters each one engaged to its parent in orthogonal position (**Fig. 4**).

1.2.3 MATURATION FROM DAUGHTER TO MOTHER CENTRIOLE

Once a daughter centriole is formed, two more steps are required for its complete maturation into a mother centriole with appendages. Both steps largely rely on PLK1 kinase activity[22].

Soon after the formation of the daughter centriole basal structure, the cell undergoes mitosis. During the metaphase/anaphase transition, the mother-daugher connection is lost through a process called disengagement. This requires PLK1 kinase activity and licenses the centriole couple for a new round of duplication[22,23].

Although the daughter centriole is now able to produce a new centriole, it is not fully mature, as it is still lacking its distal and subdistal appendages (**Fig. 4**). By the end of G2, PLK1 activity drives maturation of the younger mother centriole into a complete mother (**Fig. 4**)[22,24,25]. This way, a fully mature mother is formed, decorated with appendages and able to recruit PCM in mitosis[3].

1.2.4 CENTRIOLE NUMBER CONTROL

Centriole duplication is carefully regulated and synchronized with the cell cycle to ensure that each daughter cell will inherit a single pair of centrioles.

The main mechanism controlling that only one daughter per mother centriole is produced relies largely on protein abundance. In addition to this, there is evidence for a re-duplication block, which prevents the mother centriole to duplicate again, and for a licensing mechanism, which allows both the mother and daughter centriole to duplicate again only in the following cell cycle[17].

PLK4 has a central role in restricting the number of daughter centrioles to one. Indeed, PLK4 half-life is self-regulated by homodimerization and auto-phosphorylation, resulting in ubiquitin-dependent proteolysis by $SCF\beta^{TrCP}$ [26]. PLK4 overexpression leads to centriole overduplication[27], while its downregulation results in lack of centrioles[28].

The production of supernumerary centrioles occurs at parental centrioles, where, in case of PLK4 overexpression, the excess protein forms additional accumulation sites. This results in multiple procentrioles stemming from the same parent and forming a so called "centriole rosette" (**Fig. 7**)[27,29].

The cartwheel proteins SAS6 and STIL have also been described to induce centriole overduplication when overexpressed[30,31]. This mechanism is also dependent on ubiquitin dependent protein degradation: to ensure production of a single daughter centriole, SAS6 and STIL protein levels build up during G1 phase together with the formation of the cartwheel, but are fully degraded during anaphase as the cartwheel is destructed. When STIL or SAS6 mutants lacking the domain responsible for degradation are expressed, excess proteins are not fully degraded and their accumulation ultimately leads to centriole rosettes, similar to PLK4 overexpression[30,32,33].

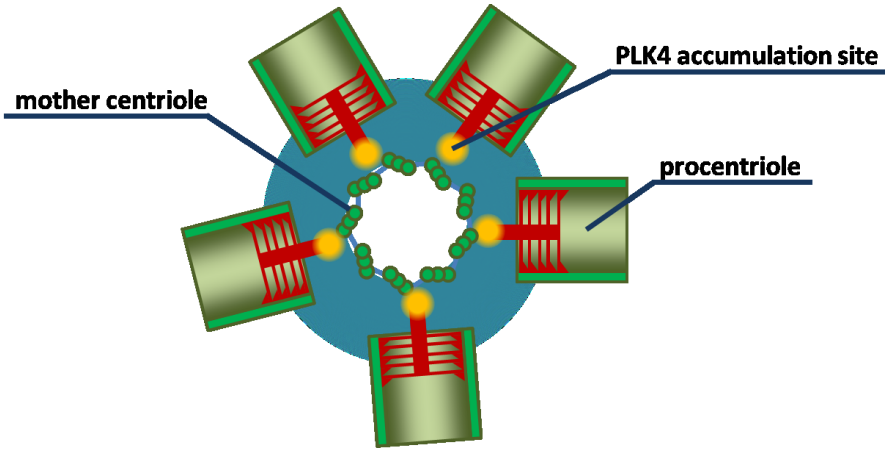

Figure 7 – Putative structure of a centriole rosette

A mother centriole surrounded by PCM is depicted at the center of the rosette. Multiple PLK4 accumulation sites are located radially around the PCM. Multiple procentrioles are formed, one for each PLK4 site.

PLK1-dependent modification of centrioles during late G2 and mitosis are also necessary to control centriole number. Early cell fusion experiment showed that previously duplicated centrioles cannot reduplicate when introduced in the cytoplasm of a cell whose centrioles are unduplicated[34]. The reduplication block is removed by centriole disengagement that is largely controlled by PLK1, as described above (see chapter 1.2.3)[23].

In addition to disengagement, PLK1 kinase activity is necessary to license the daughter centriole for the production of a new centriole in the following cell cycle. Therefore, this mechanism ensures that the daughter centriole does not produce another procentriole during a single cell cycle[25].

1.3 CENTROSOME AMPLIFICATION AND CHROMOSOME INSTABILITY IN CANCER

1.3.1 CHROMOSOME INSTABILITY

Chromosome segregation is orchestrated by the mitotic spindle. In vertebrates, centrosomes contribute to the formation and functioning of this complex apparatus by anchoring and nucleating microtubules and by establishing the spindle bipolar symmetry[35]. Other important players in this process are the kinetochores, big macromolecular complexes at chromosome centromeres, which regulate their attachment to microtubules[36].

Timely regulation of mitotic phases and accuracy of chromosome segregation are crucial in maintaining a normal, diploid chromosome content. A chromosome missegregation event produces aneuploidy, defined as a state of abnormal chromosome number. Instead, an elevated and persistent chromosome missegregation rate constitutes chromosome instability (CIN)[37].

Aneuploidy is a hallmark of cancer. More than 90% of solid tumors display an aneuploid karyotype and in many instances aneuploidy correlates with aggressiveness and tumor stage[35].

It is generally accepted that the advantage of a CIN phenotype is entailed in the development of intra-tumor heterogeneity. Genetic heterogeneity increases the chances of adaptation in a changing fitness landscape[38,39].

Indeed, experimental evidence in yeast shows that aneuploidy produces quantitative proteome changes that are related to gene copy numbers[40,41]. Aneuploid strains show slowed proliferation, however they have increased survival in stressful environments[42]. These studies suggest that modifying karyotypes affects cell fitness, and therefore CIN favors adaptation to changing environmental conditions.

In cancer, the relationship between CIN and poor prognosis probably is due to the fact that increased intra-tumor cell heterogeneity favors the emergence of drug-resistant clones[43]. Indeed, in evolutionary terms, chemotherapy is a selection agent and the emergence of a resistant clone the produced adaptation. In

support of this idea, some studies have shown an intrinsic multi-drug resistance phenotype in chromosomally unstable cells[44,45].

1.3.2 KINETOCHORE-MICROTUBULE ATTACHMENTS

CIN can be caused by various defects in mitotic spindle structure and regulation. All described CIN mechanisms ultimately lead to a decrease in chromosome segregation accuracy. In particular, CIN mechanisms deregulate the proper attachment of kinetochores to microtubules, which is controlled by the spindle assembly checkpoint (SAC)[36].

During mitosis progression, kinetochore-microtubule interactions are crucial to ensure correct chromosome bi-orientation between spindle poles. This occurs through several rounds of microtubule capture and release until sister kinetochores have connected to separate spindle poles, a configuration called amphitelic attachment (**Fig. 8A**). When all kinetochores are fully occupied by microtubules and have an amphitelic configuration, the cell enters anaphase. The SAC plays a fundamental role in this process, as it monitors microtubule attachment to kinetochores. This way, anaphase is triggered only when all kinetochores have correctly made contact with spindle microtubules[36,46,47].

However, erroneous attachments exist and commonly occur at early mitotic stages, but must be corrected, as only amphitelic attachments can ensure proper chromosome segregation[47].

Monotelic attachments occur when only one of the two kinetochores of a pair has captured microtubules (**Fig. 8B**). Since in this situation the free kinetochore is devoid of microtubule fibers, it produces a strong SAC signal, providing time for correction[36,48].

Syntelic attachments occur when both sister kinetochores are connected to the same spindle pole (**Fig. 8C**). Syntelically attached chromosomes lack tension across sister kinetochores. It is still controversial whether the SAC can sense this lack of tension; however, syntelic attachments are corrected before anaphase onset via Aurora B kinase activity[49,50].

Merotelic attachments occur when a single kinetochore is connected to microtubules coming from opposite spindle poles (**Fig. 8D**). In this case, sister kinetochores are fully occupied with microtubules, retain at least partial tension across themselves, and therefore do not provide a SAC signal[36,47]. Because of their ability to go undetected by the SAC, merotelic attachments have gained particular attention, as a plausible source of chromosome missegregation[48,51–53].

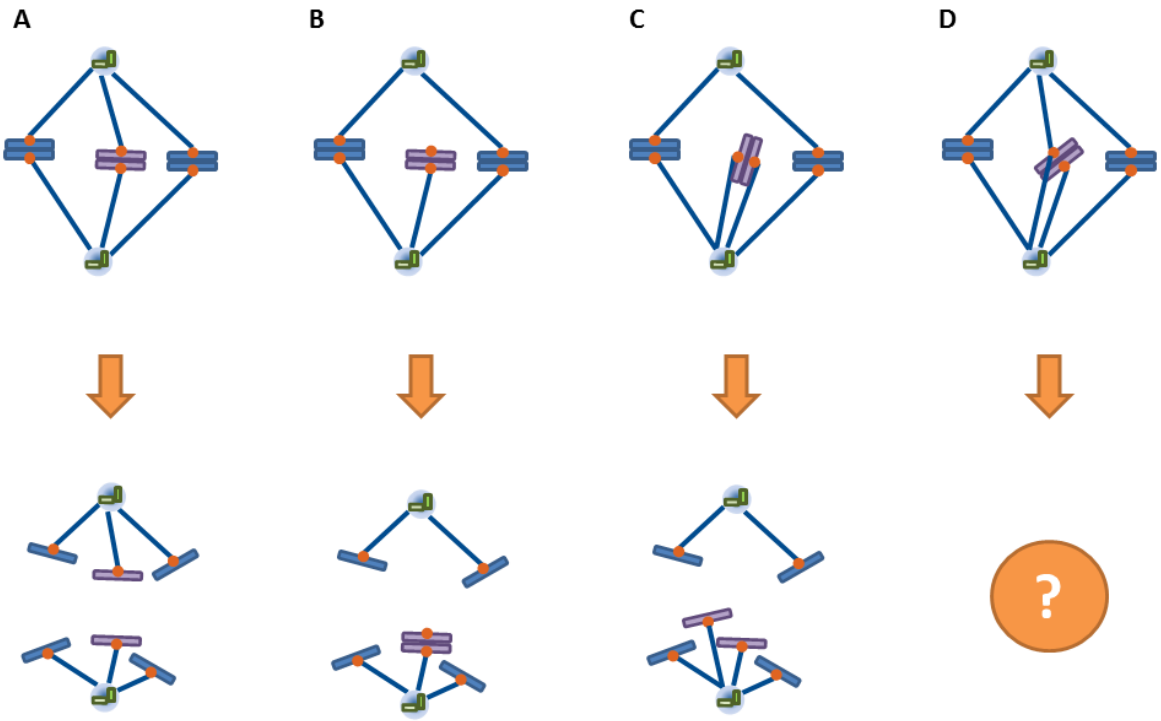

Figure 8 – Kinetochore-microtubule attachment types

Potential consequences of the different kinetochore-microtubule attachments depicted for the chromosome in purple color. With amphitelic attachment, each kinetochore is connected to the spindle pole it is facing. This results in proper chromatid segregation at anaphase (**A**). With monotelic attachment, only one kinetochore of a sister pair is connected to a spindle pole. If anaphase is triggered, it results in chromosome missegregation (**B**). With syntelic attachment, both sister kinetochores are connected to the same spindle pole. This attachment also results in chromosome missegregation (**C**). With merotelic attachment, one kinetochore in the pair is contacting simultaneously two opposite spindle poles. Its fate depends on the microtubule ratio between the numbers of microtubules in the two bundles (**D**).

When the kinetochore of a chromatid is merotelically attached, its fate at anaphase strictly depends on the microtubule ratio between the bundles to which it is connected. In a mero-amphitelic attached kinetochore, the bundle of microtubules connected to the spindle pole opposite to that of its sister is more prominent (**Fig. 9A**), while in a mero-syntelic attached kinetochore the opposite is true. Therefore, more fibers have to be exchanged in order to reach a proper amphitelic attachment starting from the mero-syntelic situation (**Fig. 9C**). There is also the possibility of a balanced merotelic attachment, where the bundles of microtubules coming from opposite poles are very similar. In this latter case, at anaphase the chromatid will be pulled in opposite directions with similar force, thus not moving in any particular direction. The chromatid will lag behind the two moving main chromosome masses, and can be detected as an “anaphase lagging chromosome” (**Fig. 9B**)[47,53–55].

Correction of erroneous attachments relies on the regulation of microtubule turnover at kinetochores, a process governed by Aurora B kinase[52]. Aurora B resides at the inner centromere. Therefore, it is spatially separated from kinetochores; however, in case of malattachments, kinetochores localize closer to Aurora B activity causing an increase in turnover through the microtubule depolymerases MCAK and KIF2B[56–58]. These two proteins stimulate microtubule catastrophe and thus detachment from kinetochores, which are

then free to capture other microtubules. When amphitelic attachment is attained, sister kinetochores are under tension and pulled well away from Aurora B leading to microtubule fiber stabilization[59].

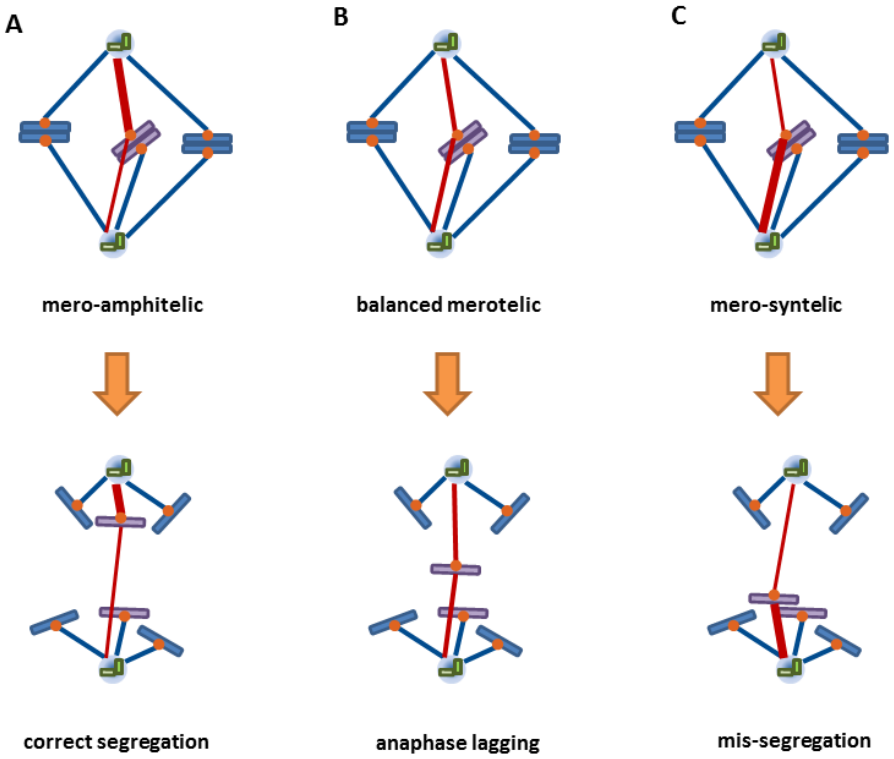

Figure 9 – Merotelic attachment resolution

The fate of a merotelically attached chromatid depends on the microtubule fiber ratio of the two bundles contacting it, here depicted in red. A kinetochore can connect to a definite amount of microtubules; therefore the opposing bundles compete for a limited number of binding sites. In mero-amphitelic attachment, the thicker fiber is connecting the kinetochore to the spindle pole opposite to its sister, which is the correct one. This attachment usually leads to correct segregation of the chromatid at anaphase (**A**). In balanced merotelic attachment, the ratio between the two fibers is close to one, resulting in the generation of an anaphase lagging chromosome (**B**). In mero-syntelic attachment, the thicker bundle is connected to the pole that the sister kinetochore is also facing. This attachment, if not resolved, results in chromosome mis-segregation (**C**).

1.3.3 CENTROSOME ABNORMALITIES IN CANCER

Theodor Boveri in his book "*Zur Frage der Entstehung Maligner Tumoren*" was the first to propose a connection between increased centrosome numbers, aneuploidy and tumorigenesis[60,61].

Centrosome aberrations are now recognized as a common feature of cancer cells, encompassing most kinds of solid and hematological tumors. Moreover, they are present in both early and late stages of tumor development and in most cases correlate with tumor grade. Importantly, in primary histology samples, centrosome aberrations are correlated with aneuploidy[1,61,62].

The landscape of centrosome aberrations in cancer is vast: both structural and numerical centrosome abnormalities have been reported. Common structural defects include changes in centrosome shape, size and protein composition, while, on the other hand, numerical abnormalities are defined by the presence of multiple centrosomes and are, by far, the most frequently reported and documented type[61,62].

However, due to the size of centrioles being very close to the microscope resolution limit, together with the fact that most often only one single PCM marker is used in studies for classification of abnormalities, structural and numerical aberrations can be confused and the actual frequency of these defects is difficult to assess [63,64].

1.3.4 ORIGIN OF SUPERNUMERARY CENTROSOMES IN CANCER

Mutations in several oncogenes and tumor suppressors have been connected to acquisition of supernumerary centrosomes; most often, this occurs indirectly by deregulation of the cell cycle to which centriole duplication is connected[65].

Three main routes for the origin of centrosome amplification in cancer cells have been described (**Fig. 10**). In principle supernumerary centrosome might arise through:

- centriole overduplication within a single cell cycle

- *de novo* centriole formation

- centrosome accumulation

Overduplication of multiple daughter centrioles within one cell cycle is probably the most common mechanism. In cancer cells, centrosome duplication cycle regulatory mechanisms, such as reduplication block and licensing, seem to be weakened, allowing for reduplication during prolonged cell cycle arrest[65,66]. Although it was formerly believed that centrosome amplification occurred through consecutive duplication rounds, recent *in vitro* data shows that overexpression of key players in centriole duplication can induce centriole amplification through the production of centriole rosettes in a single event (**Fig. 10A**)[27,30,31]. Higher levels of proteins involved in centriole duplication such as PLK4 and STIL, have been found in colorectal cancer and lung cancer, respectively[50,67,68]. However, it remains unclear, whether overexpression of these proteins is causally related to the presence of centrosome amplification.
Another studied route for centriole overduplication involves excessive production of centriolar satellites. It has been long known that cancer cells can accumulate multiple centrosomes in G2 phase following induction of DNA damage. In this study, it has been shown that the production of these supernumerary centrosomes requires dynein mediated transport of proteins and is preceded by the formation of centrin dots that are negative for canonical centriole components, but resemble centriole satellites at electron microscopy[1,66].

De novo centriole formation is defined as the production of supernumerary centrioles in cells devoid of centrosomes (**Fig. 10B**)[69]. In *Drosophila*, homologues of PLK4, SAS6 and STIL have been described as key regulators of this process[29,70]. In mammalian cells, it begins at the G1/S transition and is marked by the

appearance of faint centrin dots, which then become centrosomes before mitosis. As centrioles require more than one cell cycle to reach full maturation, these centrosomes are still unable to nucleate a full array of microtubules[71]. However, in normal settings, *de novo* formation is inhibited even by the presence of a single immature centriole. Moreover there seems to be a p38-p53-p21 checkpoint arresting cells with no centrosomes[72].

Centrosome accumulation is another route, where cancer cells, following cytokinesis abortion, cell fusion or mitotic slippage, acquire both supernumerary centrosomes and tetraploidy (**Fig. 10C**)[73,74]. However, although overexpression of some proteins like Aurora A have been described to induce cytokinesis failure and subsequent centrosome accumulation, it is important to notice that tetraploid cells spontaneously lose extra centrosomes in long term culture[74]. Neither transformed nor non-transformed cells accumulate extra centrosomes despite several rounds of cytokinesis failure[75].

Tetraploidy induction and subsequent centrosome accumulation therefore seems to only occur sporadically and at low frequencies. Indeed, even though up to 37% of all cancers undergo a genome doubling event in their clonal history, sustained cytokinesis failure would lead to the accumulation of highly polyploid genomes, which are only rarely observed in cancer[76,77].

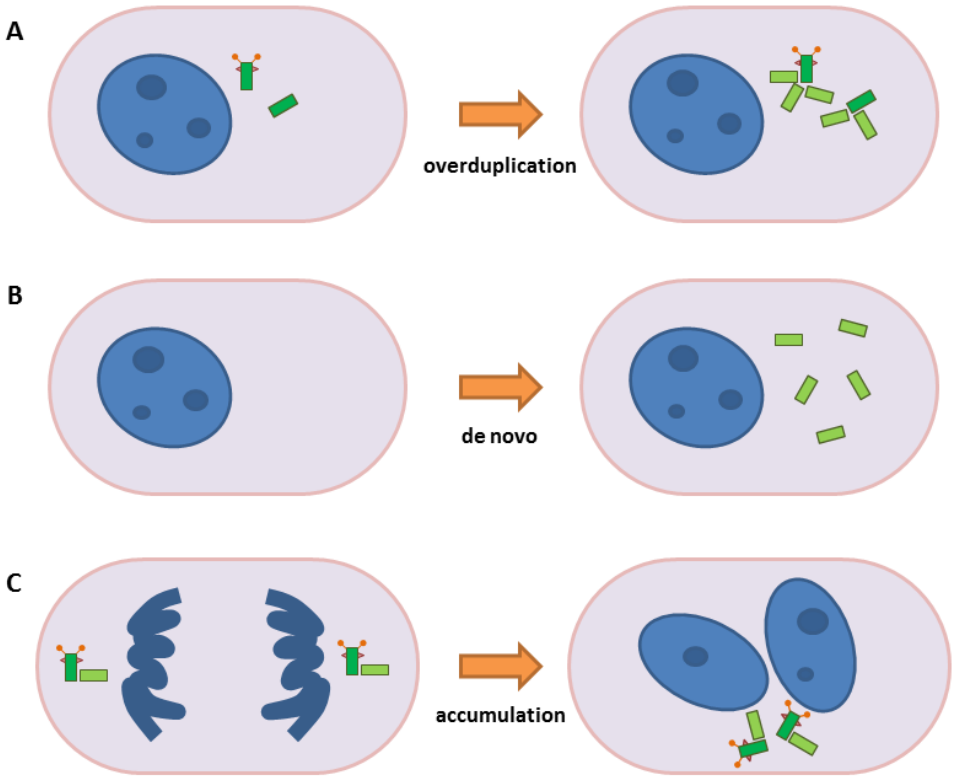

Figure 10 – Major routes to centrosome amplification

Centrosome amplification can be induced by three major routes. Overduplication consists in the generation of multiple daughter centrioles engaged to a pair of parental centrioles, thereby forming centriole rosettes (**A**). In cells devoid of centrosomes, *de novo* centriole formation can occur. In this case accumulation of centriolar proteins leads to the formation of multiple, supernumerary centrioles scattered within the cell cytoplasm **(B**). Centrosome accumulation can occur in case of cleavage failure. The cell fails to complete cytokinesis resulting in a binucleated cell with two mature centrosomes (**C**).

Most of the data regarding to these mechanisms has been collected in *in vitro* models. On the other hand, little is known about the exact mechanism by which centrosome amplification is generated *in vivo*. The major cause of this lies in the lack of accurate characterization of centrosome abnormalities in primary samples.

Therefore, investigating the characteristics of amplified centrosomes in primary tumor samples is critical for a better understanding of the factors that promote centrosome amplification in cancer and their relationship to tumor aggressiveness and aneuploidy.

1.3.5 SUPERNUMERARY CENTROSOMES AND CHROMOSOME INSTABILITY

One of the major sources of CIN in cancer is centrosome amplification, which is often observed in chromosomally unstable cell lines and in tumor types which show aneuploidy[62].

When multiple fully mature centrosomes reach mitosis, they can recruit PCM and establish supernumerary spindle poles, producing a multipolar mitosis (**Fig. 11A**)[78,79]. In this kind of mitosis a diploid genome is divided among multiple daughter cells. Very rarely multipolar mitoses produce viable cells as their progeny suffers severe aneuploidy (**Fig. 11B**)[79–81]. To limit the detrimental consequences of multipolar mitoses, cancer cells are described to group supernumerary centrosomes into two major spindle poles, a mechanism termed centrosome clustering (**Fig. 11C**)[78].

Centrosome clustering allows the formation of a pseudo-bipolar spindle even in the presence of multiple centrosomes, avoiding the dramatic effects of multipolarity. However, this kind of mitosis still bears an intrinsic risk of generating aneuploid progeny, albeit at a lower level: before collapsing in a clustered arrangement, supernumerary spindle poles form multipolar intermediates. During this process, kinetochores often attach to microtubules coming from different spindle poles, leading to the accumulation of merotelic attachments and subsequent generation of anaphase lagging chromosomes and aneuploidy (**Fig. 11D**)[79,80].

This model provides a mechanistic link between extra centrosomes and aneuploidy, two common features of cancer cells, frequently observed together. However, the impact of centrosome clustering on chromosome missegregation is still relatively high, potentially posing a high burden on cell viability. More importantly, supernumerary centrosomes are only one aspect of the spectrum of centrosomal abnormalities observed in cancer. This mechanism does not rule out other factors by which centrosome abnormalities could induce CIN. Moreover, the centrosome clustering process was derived from the analysis of CIN in cell lines and it would be important to address whether the validity of this and other models can be extended to primary human cancers *in vivo*.

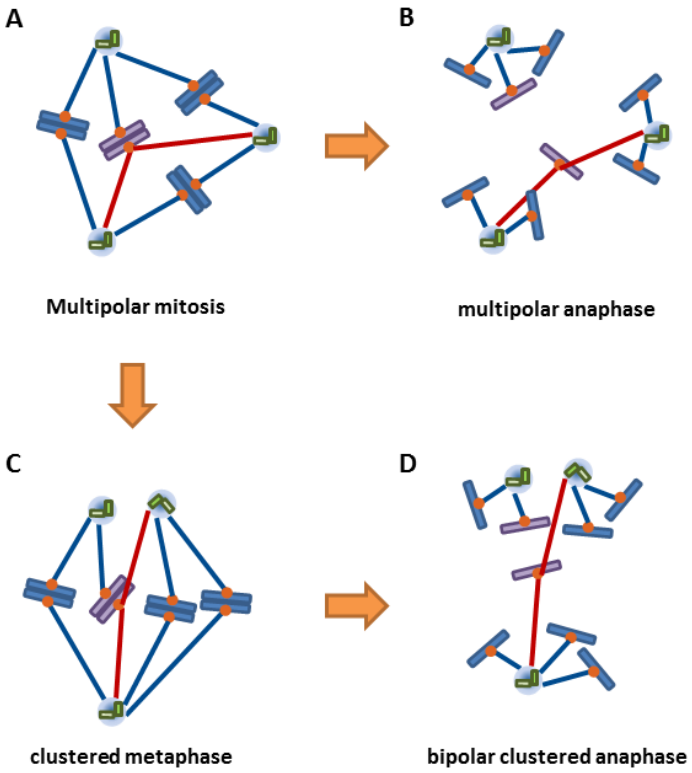

Figure 11 – Multipolar mitosis and chromosome instability

Extra centrosomes establish supernumerary spindle poles, leading to multipolar mitosis. Multipolar mitoses have an increased risk of forming merotelic attachments, here depicted in red for the purple chromosome (**A**). Resolution of multipolar mitoses in a multipolar anaphase causes extensive chromosome missegregation. Resulting nuclei will be severely aneuploid (**B**). Spindle poles can group on two sides of the chromosome mass, forming a clustered metaphase (**C**). Clustered metaphases result in bipolar anaphases. However, if merotelic attachments formed earlier in mitosis persist, missegregation events can still occur. In this case, merotelic attachments result in the generation of anaphase lagging chromosomes **(D**).

1.4 RESEARCH OBJECTIVES

CIN is a hallmark of cancer and plays an important role in enabling tumorigenesis. Several clinical studies have reported centrosome abnormalities in tumors and have shown a correlation with aneuploidy, proposing extra centrosomes as a source of CIN. Despite recent advances in describing how supernumerary centrosomes can impact on chromosome segregation fidelity via centrosome clustering, we are still far from having a complete picture. The wide spectrum of centrosome abnormalities leaves open the possibility that additional centrosome-associated sources of CIN might exist, other than centrosome clustering. Moreover, the specific mechanisms by which centrosome abnormalities originate in human cancers are poorly defined. Therefore, a better understanding of how centrosome abnormalities impact on mitosis progression and CIN is of paramount importance to exploit these mechanisms for cancer diagnosis and therapy.

The aim of this study is to more accurately characterize the relationship between centriole overproduction and CIN and, especially, to explore the possible role of centriole rosettes in the generation of chromosome missegregation. A possible mechanistic link between centriole rosettes and CIN will be investigated and their relevance in vivo will be addressed.

For this purpose, two cell lines with inducible overexpression of centriolar proteins will be characterized with regard to centriole overproduction and emergence of CIN markers. In addition, the impact of centriole overduplication on microtubule assembly will be addressed using quantitative fluorescence microscopy methods and specific assays to measure centrosome nucleation ability.

Next, the anaphase lagging chromosome frequency and specific chromosome missegregation rate will be assessed. The CIN phenotype will characterized with a focus on lagging chromosomes and spindle pole features. Mitosis progression will be examined by live-cell imaging, and SAC activation and interkinetochore tension will be studied, with the extensive use of digital image analysis and fluorescence signal quantification techniques. Furthermore, the possibility of rescuing the CIN phenotype will be explored via overexpression of proteins controlling kinetochore-microtubule attachment error correction.

Another part of this work will focus on investigating the relative contribution of centriole rosettes and centrosome clustering to the generation of CIN. For that, features of centriole overproduction over time will be examined. Moreover, the consequences of continuous centriole overproduction on cell proliferation will be analyzed, with the help of protein biochemistry methods and flow cytometry. Finally, the relevance of centriole overduplication as a source of CIN in vivo will be examined, with specific focus on the features of centrosome amplification in primary human cancers.

CHAPTER 2

RESULTS

2.1 SUPERNUMERARY CENTROSOMES IMPACT ON MICROTUBULE ASSEMBLY

2.1.1 INDUCIBLE CELL LINE MODELS OF CENTRIOLE OVERPRODUCTION

In order to study the effect of centriole overproduction on generation of CIN, two isogenic cell line models were chosen. These *in vitro* models were previously established in our group and are based on a U2OS-T-REx inducible system: addition of tetracycline allows conditional expression eGFP-PLK4, the master regulatory kinase for centriole duplication[27] or eGFP-STIL, a putative component of the cartwheel structure[31].

STIL and PLK4 overexpression has previously been shown to cause centriole amplification that accumulates over time. Overduplication occurs via the formation of procentriole rosettes around parental centrioles, followed by the formation of supernumerary mature centrosomes in the subsequent cell cycle[27,31,79].

For the purpose of this thesis, U2OS-eGFP-PLK4 and U2OS-eGFP-STIL cells were compared in relation to their centrosome amplification pattern following transgene induction.

Cells were grown on coverslips and induced for 15 hours. Coverslips were PHEM-extracted to remove cytoplasmic background, fixed in 4% paraformaldehyde and processed for immunofluorescence. Centrosome amplification patterns were investigated via anti-centrin and anti-PCNT antibodies to visualize centrioles and PCM, respectively.

Microscopic observation revealed that eGFP-PLK4 overexpression was highly efficient in the generation of centriole rosettes. Counting of centrioles in rosettes showed that they can reach as many as nine centrioles engaged to the parents (**Fig. 12A**), in accordance with the described role of PLK4 as master regulator of centriole replication. EGFP- STIL overexpression, on the other hand, induced formation of only one or two supernumerary centrioles per cell (**Fig. 12B**).

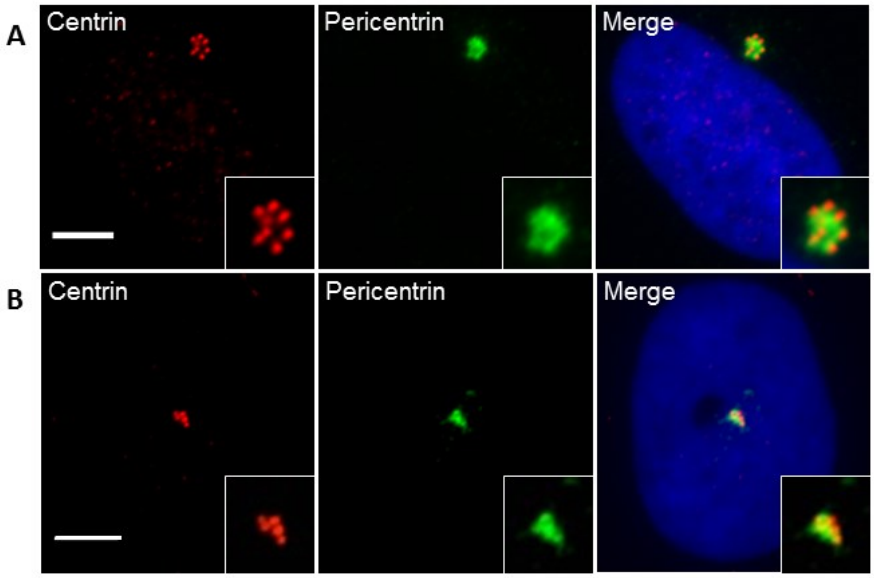

Figure 12 – Centriole number in eGFP-PLK4 and eGFP-STIL overexpressing cells

(**A**) U2OS-eGFP-PLK4 and (**B**) U2OS-eGFP-STIL cells were plated on coverslips and induced for 15 hours with tetracycline. Coverslips were then fixed and processed for immunofluorescence. Centrin (red) and PCNT (green) were stained with specific antibodies; nuclei were counterstained with Hoechst 33342 (blue). Scale bar: 5 μm.

Transgene induction for 15 hours is sufficient to induce centriole overduplication in 71.15% of cells, in case of eGFP-PLK4 overexpression, but only in 31.12% of the cells in the case of eGFP-STIL. The distribution of the number of centrioles per cell was assessed. Distribution following eGFP-PLK4 overexpression was skewed toward larger numbers of procentrioles as compared to eGFP-STIL overexpression (**Fig. 13**).

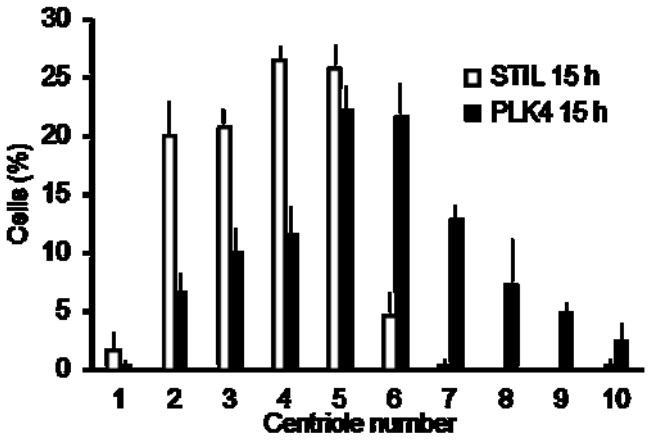

Figure 13 – Centriole number distribution after 15 hours induction

U2OS-eGFP-STIL (*white bars*) and U2OS-eGFP-PLK4 (*black bars*) were induced for 15 hours. Centriole number was scored in interphase nuclei by centrin immunofluorescence staining; bars represent percentages of cells with a defined centriole number. The chart shows results of 3 independent experiments, at least 100 cells were scored for each experiment. Error bars: standard error of the mean (s.e.m.).

To test whether the lower centriole number, in case of STIL overexpression, is caused by too short induction, cells were analyzed at later time points. U2OS-eGFP-STIL cells were induced for 3 days and daily samples were collected and stained with anti-γ-tubulin antibodies to detect amplified centrosomes. Centrosome amplification after STIL overexpression accumulated over time and eventually reached higher levels (**Fig. 14**).

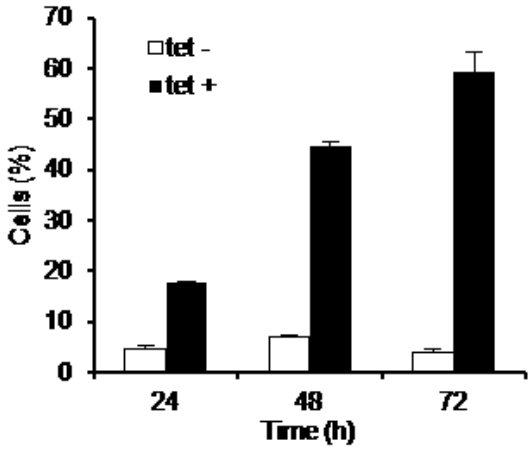

Figure 14 – Centrosome amplification following eGFP-STIL induction

U2OS-eGFP-STIL were grown on coverslips over a period of three days with (*black bars*) or without (*white bars*) tetracycline. Centrosome amplification was scored by γ-tubulin immunofluorescence staining. More than two signals were classified as amplified centrosome content. Bars represent percentages of cells harboring amplified centrosomes. The chart shows results of 3 independent experiments. At least 100 cells were scored for each experiment. Error bars: s.e.m.

Following these results, centriole number distribution was re-evaluated at 72 hours after tetracycline addition in both cell lines. Analysis of centriole content showed a distribution skewed toward higher numbers in case of eGFP-STIL overexpression; however, it did not reach the same of amplification as in the case of PLK4 overexpression (**Fig. 15**).

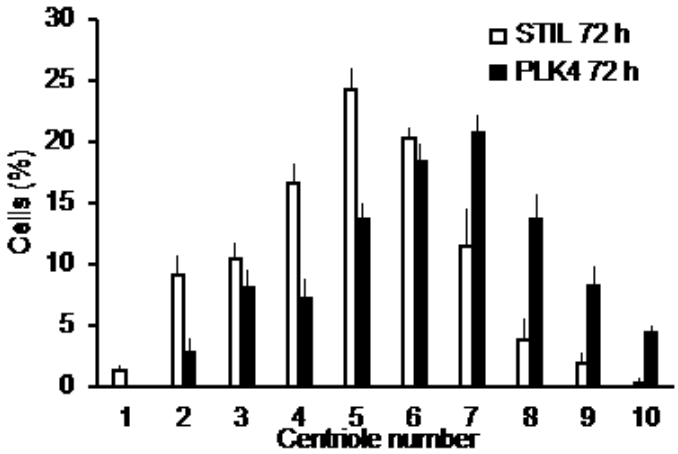

Figure 15 – Centriole number distribution after 72 hours induction

U2OS-eGFP-STIL (*white bars*) and U2OS-eGFP-PLK4 (*black bars*) were induced for 72 hours. Centriole number was scored in interphase cells by centrin immunofluorescence staining; bars represent percentages of cells with a defined

centriole number. The chart shows results of 3 independent experiments. At least 100 cells were scored for each experiment. Error bars: s.e.m.

Taken together, these results show that eGFP-STIL and eGFP-PLK4 inducible cell lines are both able to induce supernumerary centrioles. In contrast to PLK4, STIL overexpression is less efficient in inducing centriole overduplication; however, at later time points centrosome amplification reaches comparably high levels of approximately 70% in both systems.

2.1.2 CENTROSOME AMPLIFICATION INCREASES CELLULAR MICROTUBULE POLYMER AMOUNT

Centrosomes are the main microtubule nucleators in the cell. This ability relies on the capacity of mother centrioles to recruit PCM[12]. A previous study claimed that extra centrosomes produce increased numbers of microtubule fibers, however a quantitative analysis was not performed [82].

To determine whether centrosome amplification has an impact on microtubule assembly, U2OS-eGFP-STIL cells were induced for 72 hours to obtain a high level of extra centrosomes per cell. Microtubule polymer intensity was quantified and compared to that of non-induced cells.

Before fixation, the soluble monomeric fraction of microtubules was extracted via PHEM buffer washing. Then the remaining fibrous fraction was stained with an anti-α-tubulin antibody; centrioles were visualized by co-staining with an anti-CP110 antibody. Staining was performed in collaboration with Annik Roßberg.

Z-stack series encompassing whole interphase cells were collected. Background noise was subtracted via a rolling ball algorithm. Total fluorescence intensity of the cells was digitally quantified on sum-intensity projections.

It was observed that the total α-tubulin fluorescence intensity was increased in cells overexpressing eGFP-STIL (**Fig. 16A**), indicating that cells bearing supernumerary centrioles contain larger amounts of microtubule polymer. Importantly, this effect was not dependent on morphological changes of the cell, as there was no significant difference in the cell area between induced and non-induced cells (**Fig. 16B**).

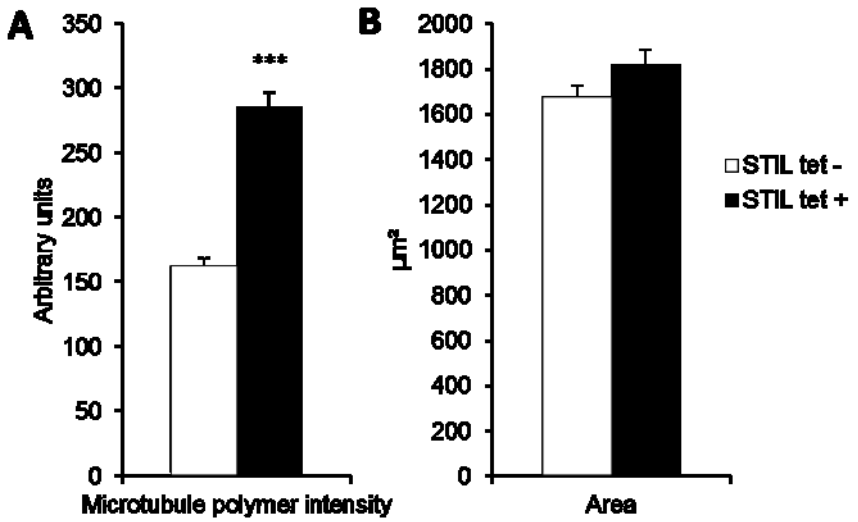

Figure 16 – Microtubule polymer intensity in eGFP-STIL expressing cells

U2OS-eGFP-STIL cells were grown on coverslips with (*black bars*) or without (*white bars*) addition of tetracycline. Cells were stained for CP110 and α-tubulin.
(**A**) Digital images across different coverslips were acquired with identical acquisition settings. Z-stack pictures were processed to remove background and obtain sum-intensity projections. Microtubule polymer intensity was expressed as the sum of total pixel intensity values of regions of interest (ROI) containing whole cells. Bars represent average cellular microtubule polymer intensity in arbitrary units. At least 50 cells were measured per condition. Error bars: s.e.m.
(**B**) Bars represent average area of ROIs used to calculate microtubule polymer intensity. Error bars: s.e.m.

2.1.3 SUPERNUMERARY CENTROSOMES INCREASE THE AMOUNT OF EB1 COMETS

To further confirm these results, EB1 dots were quantified on microtubules. EB1 belongs to a family of proteins tracking the plus-end of growing microtubules[83]. Therefore, by counting the number of EB1 dots, it is possible to infer the number of microtubule fibers in the cell. This provided an independent way of quantifying the amount of microtubules per cell.

U2OS-eGFP-STIL cells were induced for 72 hours, PHEM-extracted and stained with anti-EB1, anti-α-tubulin and anti-CP110 antibodies. Z-stacks of interphase cells were collected; after background subtraction, maximum intensity projections were produced and EB1 dots were automatically counted.

Results from this analysis pointed in the same direction as microtubule polymer intensity measurement described above. EB1 dots were more numerous in induced cells, indicating an increased amount of plus-ends and thus microtubule fibers (**Fig. 17**).

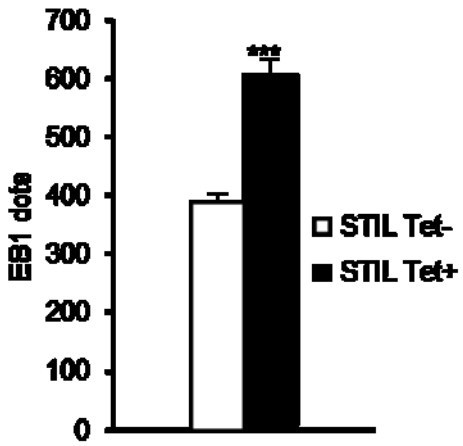

Figure 17 – EB1 dot counts in eGFP-STIL overexpressing cells

U2OS-eGFP-STIL cells were grown on coverslips with (*black bars*) or without (*white bars*) addition of tetracycline. Coverslips were stained for CP110, α-tubulin and EB1. Digital images across different coverslips were acquired with identical acquisition settings. Z-stack pictures were processed to remove background and obtain maximum intensity projections. EB1 dots were counted via a "find maxima algorithm" in ROIs containing whole cells. The same threshold was applied across all images. Bars represent average EB1 dot numbers. At least 50 cells were analyzed in each condition. Error bars: s.e.m.

2.1.4 AMPLIFIED CENTROSOMES ANCHOR INCREASED MICROTUBULE NUMBERS

To determine whether the observed increase in microtubule polymer mass, which followed eGFP-STIL induction, was correlated with an increased microtubule nucleation capacity at the centrosome, U2OS-eGFP-STIL cells were challenged in a microtubule regrowth assay.

Microtubule stability is highly temperature sensitive, and exposure to low temperature causes the complete disruption of the microtubule cytoskeleton. Rewarming allows microtubule repolymerization within few minutes and reconstitution of the cytoskeleton, with most fibers nucleated at the centrosome. Previous work has shown that cells with supernumerary centrioles, challenged with a microtubule regrowth assay, display increased microtubule nucleation at the centrosome[82].

U2OS-eGFP-STIL cells were induced for 72 hours. Then, cells were incubated with ice-cold PBS for one hour, which led to the complete solubilization of microtubule polymers (**Fig. 18A**). After 30 seconds incubation in warm medium, cells were snap fixed in methanol, stained with anti- α-tubulin and anti-centrin antibodies, and analyzed in collaboration with Annik Roßberg. Microtubule polymerization was visible at centrosomes in cells allowed to repolymerize, but not in control cells, which were not allowed to repolymerize. Individual fibers were manually counted and centriole status was assessed by centrin staining.

After rewarming, microtubule regrowth was evident in both non-induced and induced conditions (**Fig. 18A**). Regrowth time was strongly affecting the numbers of fibers regrowing, thus causing large inter-experimental variability. However, quantification of microtubule fibers emanating from the centrosome showed that induced cells consistently nucleated higher numbers of microtubule fibers in all independent replicates (**Fig. 18B**). Moreover, a linear correlation was found between the centrosomal microtubule number and the centriole number in the cells ($\rho = 0.90; p < 0.001$) (**Fig. 18C**).

There results indicate that the observed increase in microtubule polymer correlates with an increased capacity of centrosomes to anchor microtubules. Moreover, the number of centrosomal microtubules was found to linearly increase with the amount of centrioles present at the centrosome. However, due to the late time point examined, supernumerary centrioles had the time to undergo several cell cycles and mature into parents. Therefore, it was not possible to distinguish whether all centrioles or only parental centrioles contributed to increased microtubule nucleation.

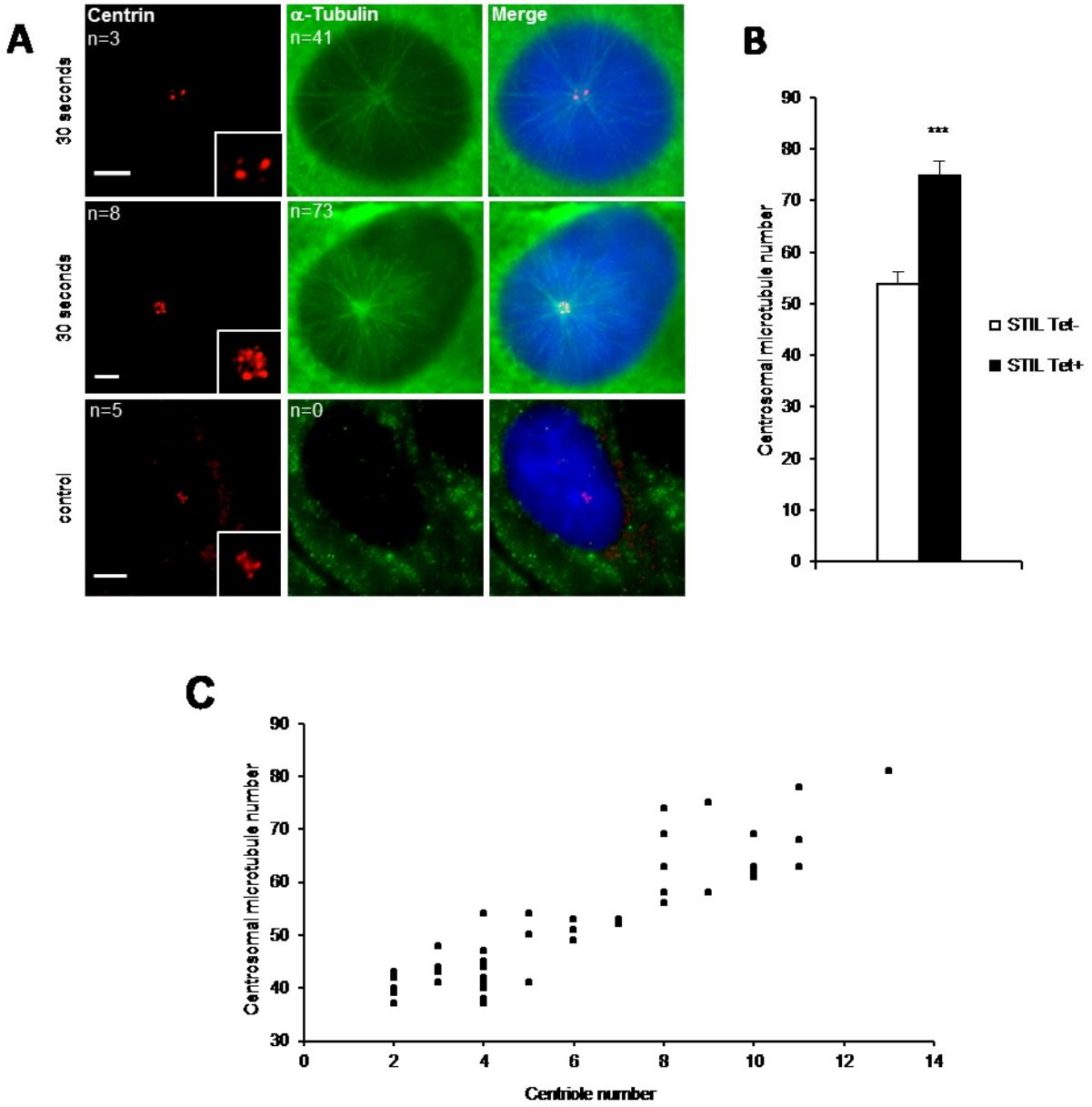

Figure 18 – Microtubule regrowth assay in eGFP-STIL overexpressing cells

(**A**) U2OS-eGFP-STIL cells were grown on coverslips and induced for 72 hours. Medium was removed and replaced with ice-cold PBS. Cells were incubated on ice for 1 hour. PBS was removed and microtubules were allowed to repolymerize in medium at 37°C for 30 seconds. Cells were then fixed and immunostained. Control cells were fixed without the repolymerization step. (**B**) Z-stack pictures were collected and centrosomal microtubule numbers were assessed in at least 40 cells for each condition. Experiments were performed in triplicate. Results from a representative experiment are presented. Error bars: s.e.m. (**C**) Correlation between centriole number and centrosomal microtubule number from a representative experiment.

2.1.5 PERICENTRIN INTENSITY CORRELATES WITH THE CENTRIOLE NUMBER IN INTERPHASE CELLS

To determine whether centriole rosettes and, in particular, immature procentrioles still engaged to parent centrioles, are able to influence microtubule assembly, the amount of PCM was quantified after short-term PLK4 overexpression. In this setting, supernumerary centrioles are induced at high numbers, in cells that have undergone only one cell cycle. Therefore, the centrin clusters observed, represent *bona fide* centriole rosettes[79].

PCNT was chosen as an indirect marker to measure centrosome nucleation capacity. Indeed, PCNT is an essential scaffolding protein that is required for recruitment and anchoring of other proteins to the PCM[84]. Moreover, the PCNT amount at centrosomes is largely responsible for their increased microtubule nucleation capacity at mitosis. Among the proteins recruited by PCNT is γ-tubulin, which promotes minus-end stabilization and microtubule nucleation from the centrosome together. PCNT intensity correlates with the capacity of centrosomes to nucleate microtubules[85].

U2OS-eGFP-PLK4 cells were induced for 15 hours, to obtain large numbers of cells with centriole rosettes. Cells were fixed, PHEM-extracted, and stained with anti-centrin and anti-PCNT antibodies to visualize centrioles and PCM, respectively. Immunofluorescence was performed in collaboration with Annik Roßberg.

Pericentrin intensity displayed a clear correlation with centriole numbers at the centrosomes ($\rho = 0.856$; $p < 0.001$). This result suggests that daughter centrioles within rosettes, and not only parental centrioles, are able to influence microtubule assembly (**Fig. 19**).

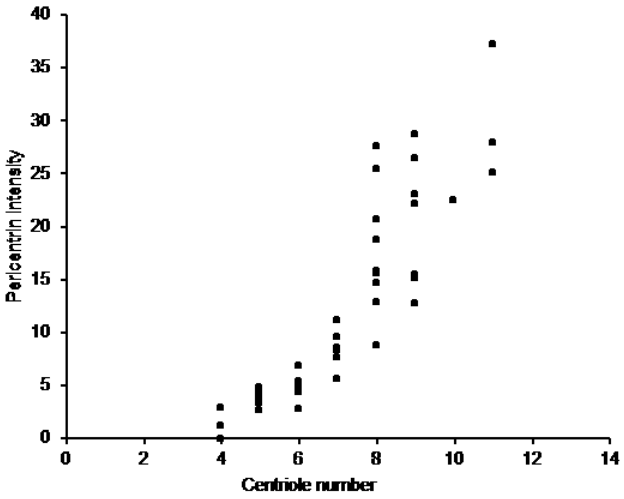

Figure 19 – Pericentrin signal intensity following eGFP-PLK4 overexpression

U2OS-eGFP-PLK4 cells were grown on coverslips and induced for 15 hours. Cells were then fixed and immunostained. Z-stack pictures were collected and PCNT signal intensity was quantified on sum-intensity projections in a ROI containing the whole signal. Intensity was assessed in at least 40 cells for each condition. Results from a representative experiment are presented.

2.2 CENTRIOLE OVERDUPLICATION IS ASSOCIATED WITH CHROMOSOME INSTABILITY

2.2.1 STIL OVEREXPRESSION INCREASES THE FREQUENCY OF MICRONUCLEI CONTAINING KINETOCHORES

To determine whether the observed production of supernumerary centrosomes can induce chromosome missegregation, micronuclei frequency was assessed after STIL overexpression.

Micronuclei (MNi) constitute a surrogate marker for CIN (see chapter 1.3.2). Merotelic attachments constitute an indicator of chromosome missegregation, and when a balanced merotelic attachment occurs, the affected kinetochore does not move during anaphase, forming a lagging chromosome. If the merotelic attachment is not resolved, then the isolated chromatid will decondense away from the main nucleus forming a micronucleus (MN)[53,86]. Therefore, MNi constitute a strong sign for the presence of merotelic attachments.

However, chromosome fragments or kinetochore defects can also induce the formation of MNi. Indeed, a fragment of chromatin, that is lacking the kinetochore, is not competent for segregation. Therefore, at anaphase onset, the fragment unavoidably forms an anaphase lagging chromosome, because it misses attachment to the spindle fibers[86].

Since the causes of MNi formation in these two cases are different, it is important to distinguish between them. It is widely accepted that this can be done by staining kinetochores or centromeres. If a lagging chromatid bears a kinetochore signal, it means that it had the possibility to connect to spindle fibers and being segregated; therefore, only MNi which are positive for a kinetochore signal are a true sign of numerical CIN[86].

U2OS-eGFP-STIL cells were induced for 72 hours and the frequency of micronuclei was assessed by immunofluorescence. As an additional *in vitro* model, another inducible cell line was used, that expresses eGFP-SAS6. SAS6 is an additional structural cartwheel protein. Finally, a U2OS-eGFP cell line constituted a negative control. Centromeres of chromosomes were visualized with human anti-centromere antibodies (CREST) and DNA was counterstained with 4',6-diamidino-2-phenylindole (DAPI).

After induction, the frequency of MNi almost doubled. Importantly, a similar result was obtained when SAS6 expression was induced. On the other hand, GFP expression caused no increase in the MNi frequency (**Fig. 20A**). When CREST signals were taken into account, eGFP-STIL- and eGFP-SAS6-induced cells showed a selective increase in the number of MNi positive for CREST (**Fig. 20B**).

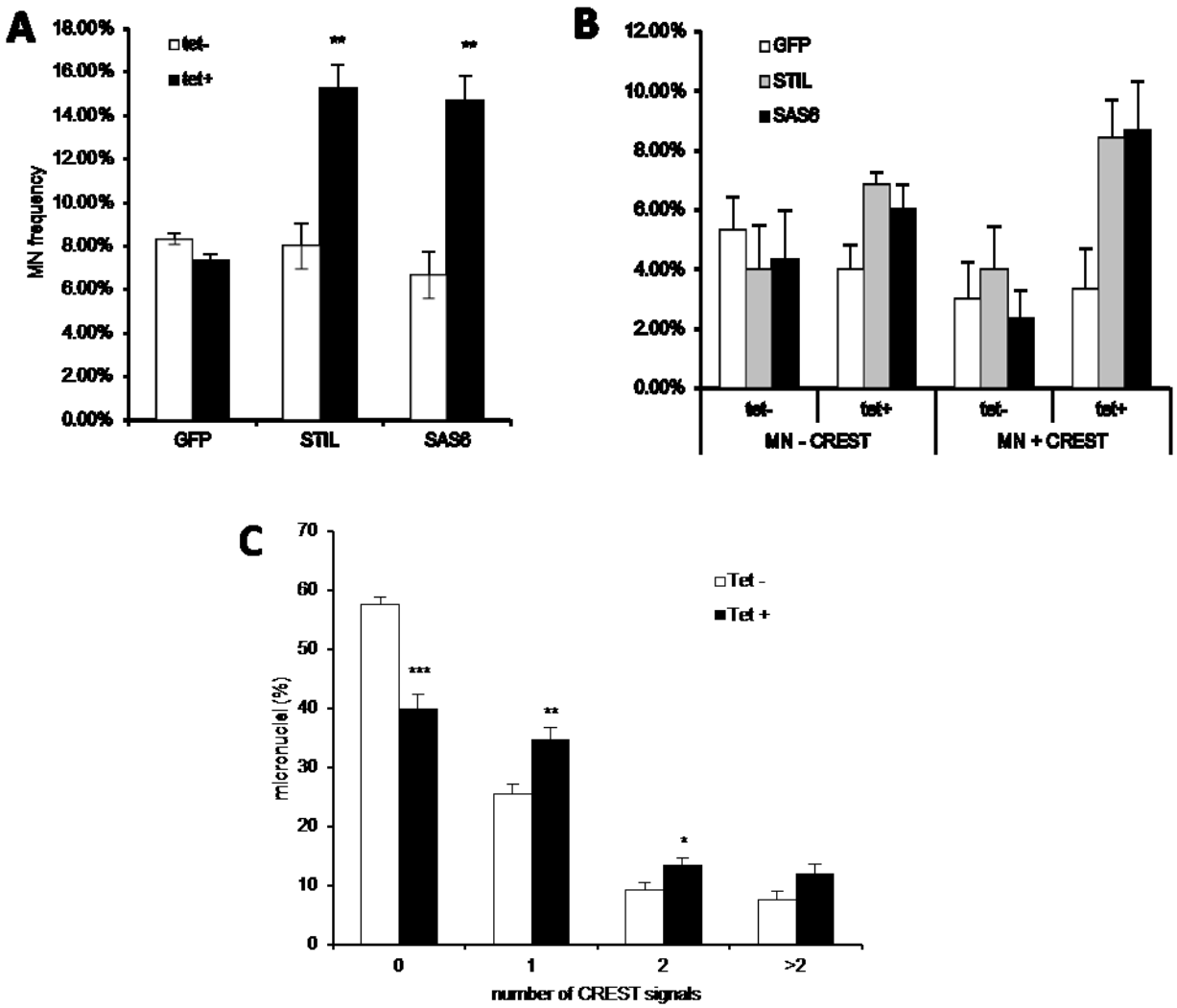

Figure 20 – Micronucleus frequency in eGFP-STIL and eGFP-SAS6 overexpressing cells

U2OS-eGFP, U2OS-eGFP-STIL and U2OS-eGFP-SAS6 cells were grown on coverslips and induced for 72 hours. Cells were then fixed and immunostained. At least three independent experiments were performed; 100 cells were counted in each replicate. (**A**) Total MN frequency was measured in induced (*black bars*) and non-induced (*white bars*) cells. (**B**) MN frequency in relation to the presence of at least one kinetochore signal in the MN. (**C**) Kinetochore signal distribution in micronuclei of U2OS-eGFP-STIL cells induced for 72 hours (*black bars*) or non-induced controls (*white bars*). MN: micronucleus; MN - CREST: micronucleus without CREST signal; MN + CREST: micronucleus with at least one CREST signal.

In addition, the distribution of CREST signals was assessed in the U2OS-eGFP-STIL cell line. The MNi frequency was increased regardless of the number of CREST signals present, however, the most significant increase was observed in the case of micronuclei containing one or two centromeres (**Fig. 20C**).

2.2.2 MICRONUCLEI CONTAINING KINETOCHORES ARE ASSOCIATED WITH THE PRESENCE OF AMPLIFIED CENTROSOMES

If amplified centrosomes are responsible for chromosome missegregation events, then it can be hypothesized that kinetochore-containing MNi will be more frequently present in cells harboring extra centrosomes.

To determine whether the presence of CREST-positive MNi was directly correlated with centrosome amplification, U2OS-eGFP-STIL cells were induced for 72 hours and stained with anti-γ-tubulin and CREST antibodies.

It was observed that MNi containing at least one CREST signal were more frequently present in cells displaying amplified centrosomes. On the other hand, this association was absent for CREST-negative MNi (**Fig. 21C**). These results suggest that supernumerary centrioles are strongly associated with the production of MNi containing whole chromosomes.

2.2.3 STIL-INDUCED MICRONUCLEI DO NOT CONTAIN CHROMOSOMAL FRAGMENTS

Previous studies have shown that another way of excluding the presence of chromosome fragments within the micronuclei is to stain for a double-strand break marker. Indeed, if a chromosome fragment is formed, then it necessarily originates from chromosome breakage. Since DNA repair pathways are disabled at mitosis, the breakage can be fixed only in the following cell cycle[87]. Therefore, if a MN contains a chromosome fragment, then it recruits DNA double-strand break proteins during interphase.

U2OS-eGFP-STIL cells were stained with CREST and an anti-phopsho-γ-H2A.X antibody, which stains a histone modification needed for activation of the double strand break repair system[87].

Phopsho-γ-H2A.X stainings gave a faint but specific signal. Example figures are given in panel **Fig. 21A**. MNi devoid of a CREST signal, and therefore containing fragments, showed phopsho-γ-H2A.X positivity in about 70% of cases in both induced and non-induced cells (**Fig. 21B**). When a CREST signal was present in the MN, cells showed a significantly decreased frequency of phopsho-γ-H2A.X positivity, further arguing in favor of the presence of whole chromosomes within them (**Fig. 21B**).

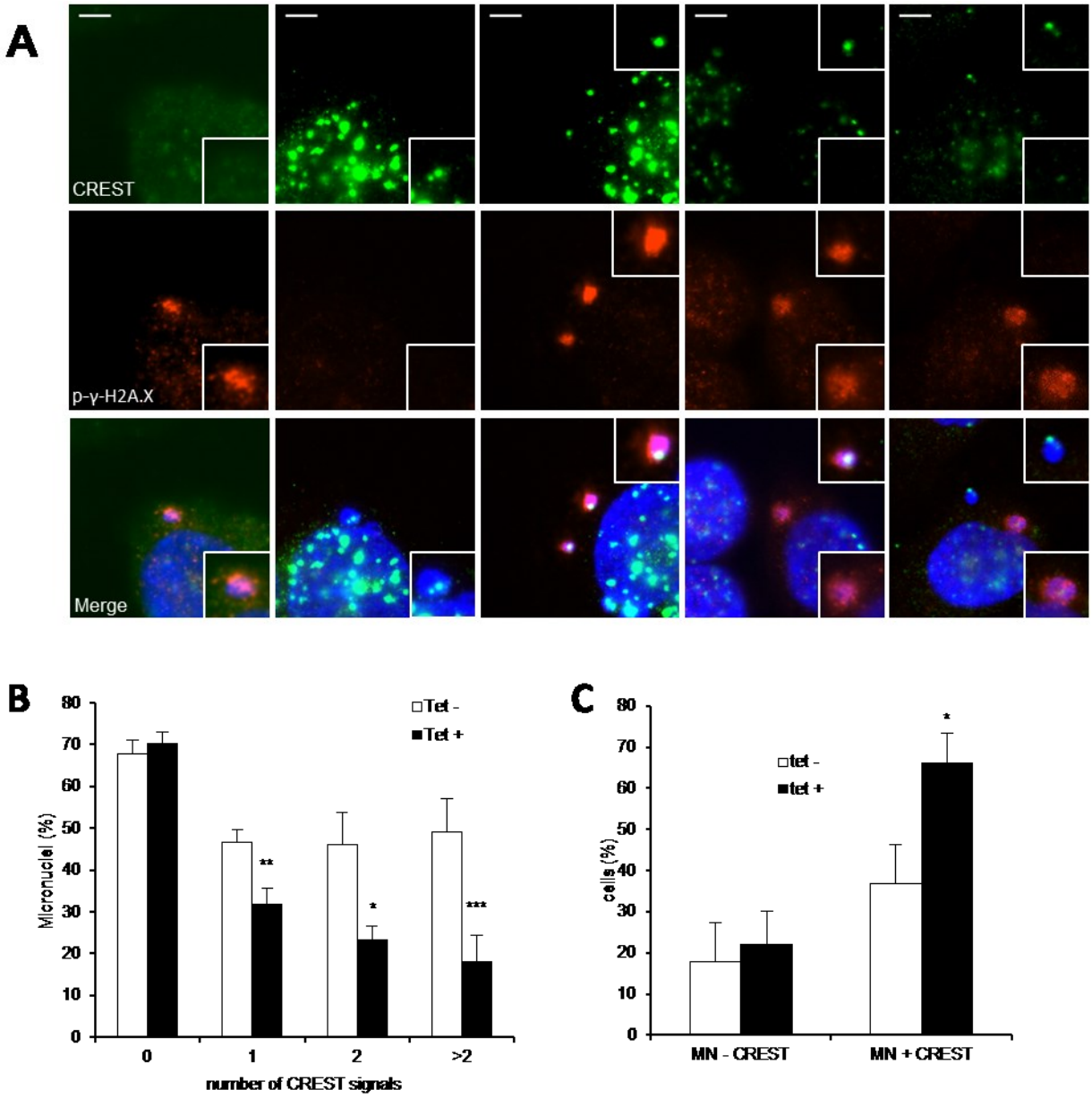

Figure 21 – phospho-γ-H2A.X staining of micronuclei in eGFP-STIL overexpressing cells

(**A**) U2OS-eGFP-STIL cells were grown on coverslips and induced for 72 hours. Cells were then fixed and immunostained for kinetochores (green), p-γ-H2A.X (red) and DNA was counterstained with DAPI (blue). Example images are presented, where micronuclei are showing different combinations of CREST and phospho-γ-H2A.X stainings. Scale bar: 5 μm. (**B**) Percentage of MN-positive for phospho-γ-H2A.X was measured in induced (*black bars*) and non-induced (*white bars*) cells. Three independent experiments were performed; at least 100 micronuclei were counted in each replicate. Error bars: s.e.m. (**C**) U2OS-eGFP-STIL cells were grown on coverslips and induced for 72 hours. Cells were then fixed and immunostained for kinetochores and γ-tubulin. MN frequency was assessed in relation to the presence of at least one kinetochore signal in cells with amplified centrosomes. Three independent experiments were performed; at least 100 micronuclei were counted in each replicate. Error bars: s.e.m. p-γ-H2A.X: phospho-γ-H2A.X; MN: micronucleus; MN - CREST: micronucleus without CREST signal; MN + CREST: micronucleus with at least one CREST signal.

2.2.4 STIL OVEREXPRESSION INCREASES KARYOTYPE HETEROGENEITY

Cancer cell lines display highly aberrant karyotypes and a basal level of cell-to-cell variability, with many non-clonal chromosome aneuploidies. Usually their karyotype is expressed as “modal karyotype”, meaning that only the most frequent aberrations are listed, without specifying their frequency or presence of subclones[88].

Accordingly, when analyzing a specific chromosome numbers within a cell line, a distribution across different chromosome numbers is obtained with one major peak. This peak represents the modal chromosome number and corresponds to the chromosome number most frequently observed within the cell line population. The fraction of cells deviating from the mode (deviant fraction) is an indicator of population heterogeneity[37].

Following the induction of CIN, sustained and elevated chromosome missegregation rates will produce aneuploidy. This affects chromosome number distribution. Specifically, deviant fractions increase as karyotype heterogeneity increases within the population[37].

Analysis of the chromosome deviant fraction constitutes one of the most direct methods for assessing CIN[38].

To test whether the observed increase in MNi frequency is resulting in a parallel increase of CIN, cell-to-cell karyotype heterogeneity was measured following STIL and SAS6 overexpression.

U2OS-eGFP-STIL cells were induced and population samples were collected at daily time points. Cells were then fixed in ice-cold methanol. Coverslips were processed for fluorescence in situ hybridization (FISH) with a panel of centromere-specific probes. Deviant fractions were determined at each time point.

Chromosomes displayed different basal deviant fractions; however, following eGFP-STIL induction, chromosome heterogeneity gradually accumulated over time. On the other hand, non-induced cells displayed no particular trend over time (**Fig. 22A**). Similar results were obtained when eGFP-SAS6 was overexpressed for 72 hours (**Fig. 22B**), while eGFP overexpression did not cause any change in the deviant fraction (**Fig. 22C**).

These results confirmed that the observed increase in cell-to-cell karyotype heterogeneity is caused by the induction of amplified centrosomes.

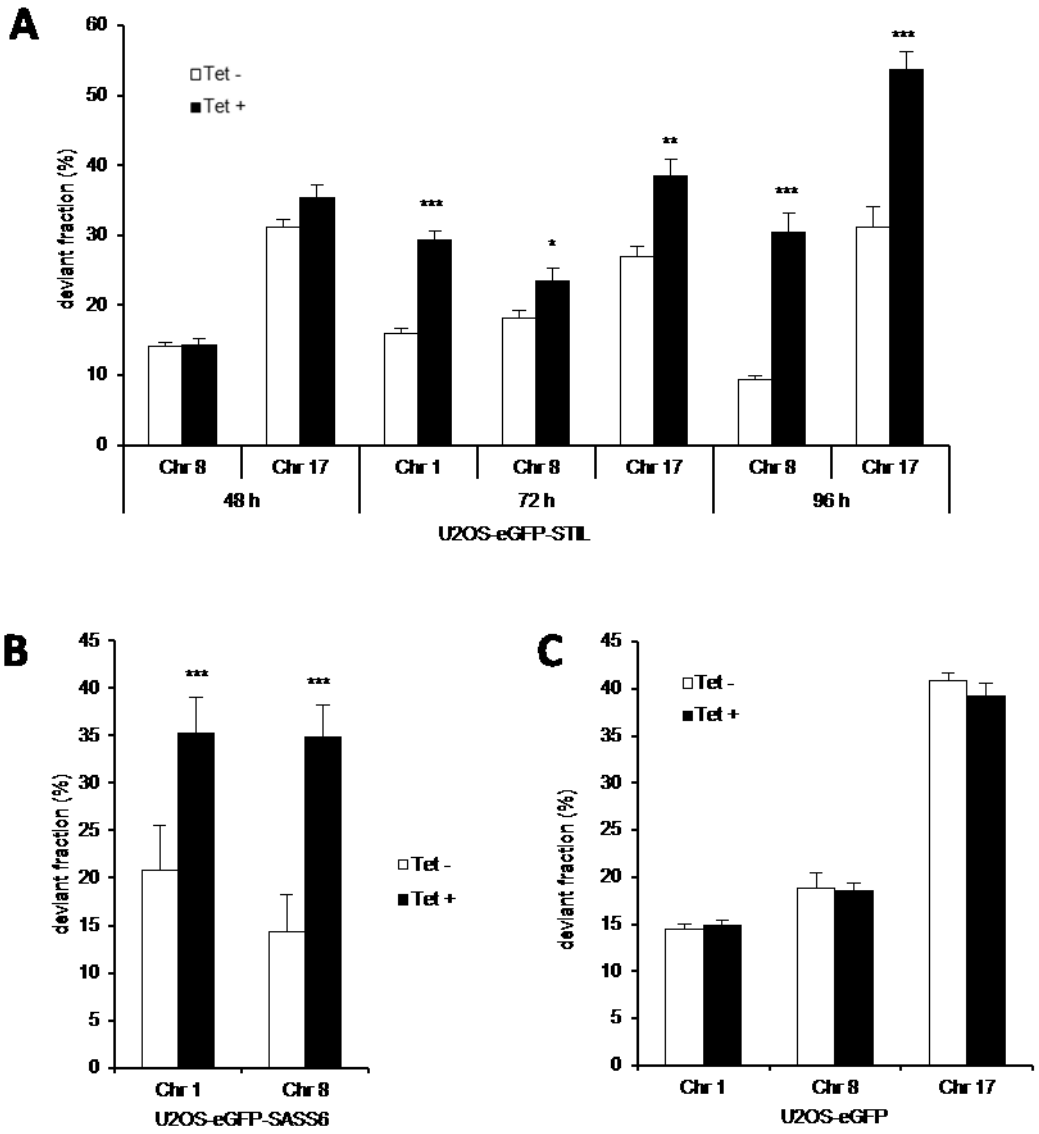

Figure 22 – Chromosomal mode deviant fractions following eGFP-STIL, eGFP-SAS6 and eGFP overexpression

(**A**) U2OS-eGFP-STIL cells were grown on coverslips and induced for 96h. At the time points described, cells were fixed and FISH was performed with centromere-specific probes. Chromosome modal number was defined as the number of signals presents in the majority of cells. The deviant fraction represents the percentage of cells that harbored a different number of signals. The fraction was assessed in cells overexpressing STIL (black bars) and non-induced controls (white bars). Experiments were performed in triplicate. At least 300 cells were counted for each condition. Error bars: standard deviation (SD). (**B**) U2OS-eGFP-SAS6 and (**C**) U2OS-eGFP cells were induced for 72 hours and analysis was performed as described above. Experiments were performed in triplicate. At least 300 cells were counted for each condition. Error bars: SD. Chr: chromosome.

2.3 BIPOLAR MITOSES WITH CENTRIOLE ROSETTES ARE A MAJOR CAUSE OF CIN

2.3.1 CENTRIOLE ROSETTES AND CENTROSOME AMPLIFICATION AT MITOSIS

It has been previously reported that when centriole overduplication occurs around a pair of parental centrioles (**Fig. 23A**), in the following mitosis supernumerary centrioles are still engaged to their parents. The spindle is bipolar with two poles, which display centriole rosettes (**Fig. 23B**), and chromosomes are segregated between two sister cells[27,79].
During this mitosis PLK1 activity disengages the multiple daughters and licenses them for reduplication. Thus, in the subsequent cell cycle, multiple parents are present (**Fig. 23B**), and by the next mitosis they reach full maturation and form multiple spindle poles (**Fig. 23C**).

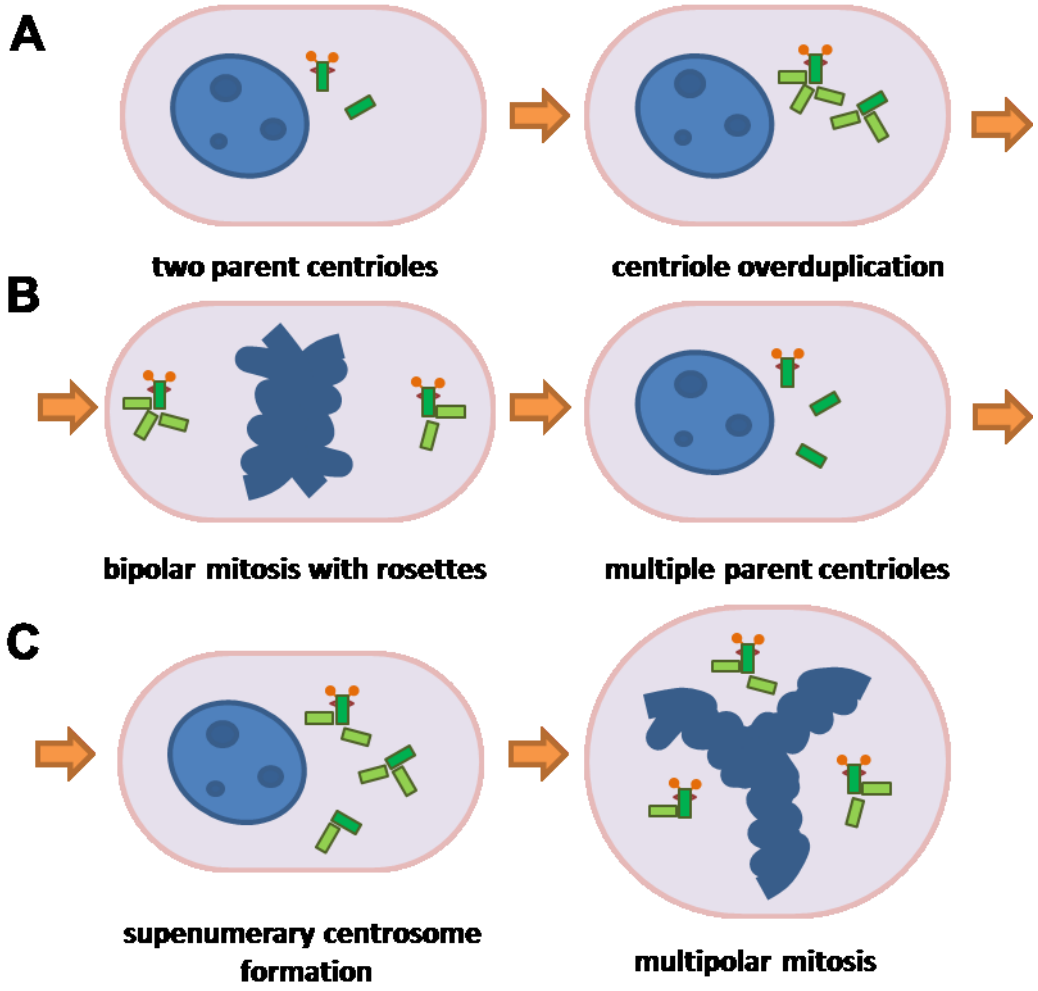

Figure 23 – Centrosome amplification stages

(**A**) A cell with normal centriole content has two parent centrioles, one of which is decorated with appendages. Overduplicated centrioles form around the parental centrioles. (**B**) Daughter centrioles stay engaged to their parents during mitosis. Therefore, two spindle poles are present. However, following cell division, cells inherit multiple centrioles. (**C**) Each of the new parental centrioles duplicates again. The second mitosis has as many spindle poles as the centrioles inherited from the first mitosis.

In an attempt to determine the relative contribution of these different types of mitoses to the origin of CIN in eGFP-STIL-overexpressing cells, mitosis progression was imaged and the types of mitosis were classified according to their centrosome status. U2OS-eGFP-STIL cells were induced for 72 hours and stained with anti-centrin and anti-PCNT antibodies to visualize centriole amount and spindle poles, respectively.

Four types of mitoses were classified according to their centriole status and spindle pole number (**Fig. 24**):

- Normal bipolar mitosis
- Bipolar mitosis with centriole rosettes
- Mitosis with multiple spindle poles
- Mitosis with clustered spindle poles

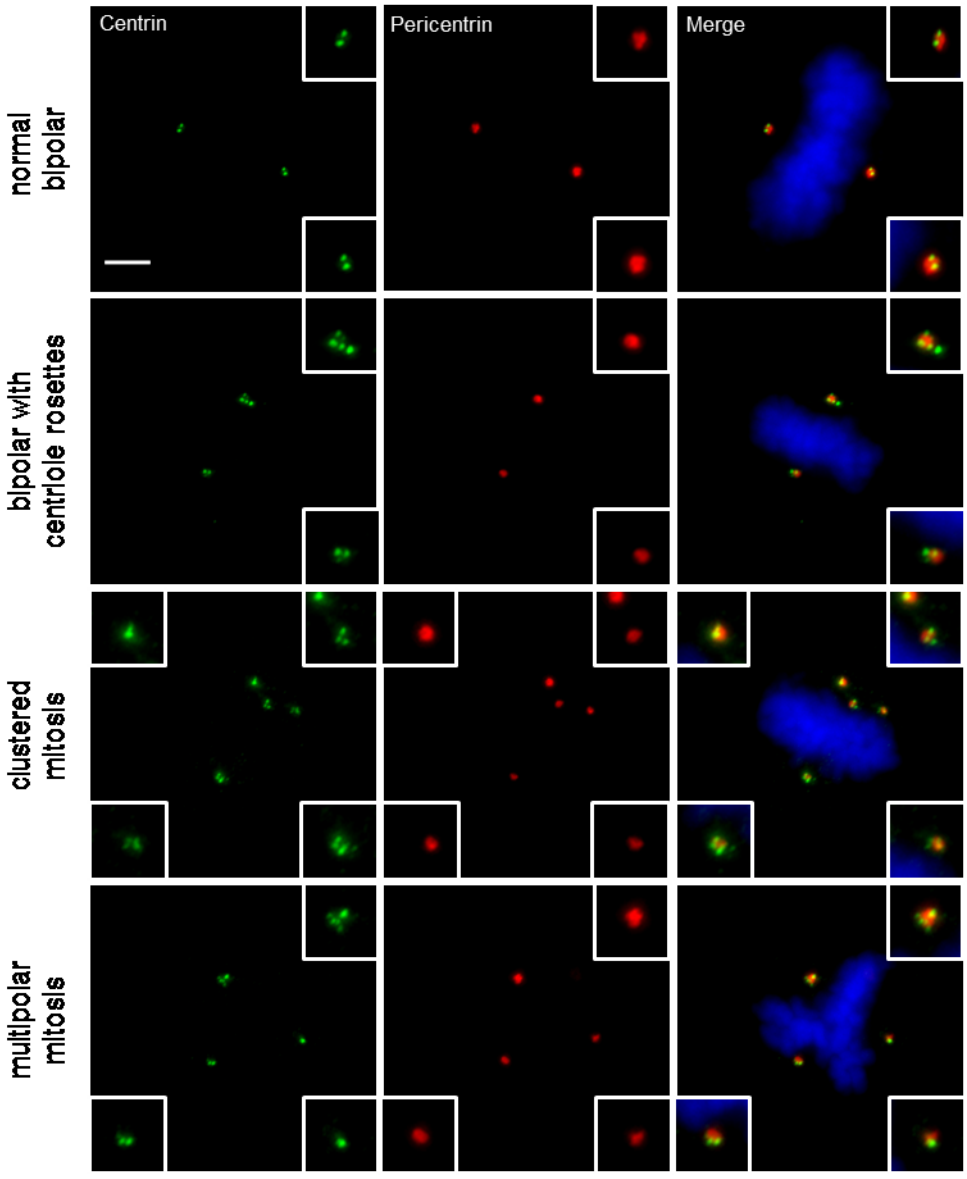

Figure 24 – Mitosis types following eGFP-STIL overexpression

U2OS-eGFP-STIL cells were plated on coverslips and induced for 72 hours with tetracycline. Specimens were then fixed and processed for immunofluorescence. Centrin (green) and PCNT (red) were stained with specific antibodies; DNA was counterstained with Hoechst 33342 (blue). Scale bar: 5 µm.

The “bipolar mitosis with rosette type” is expected to occur during the first cycle of centrosome amplification, while multipolar and clustered mitoses are expected to be more prominent at later time points, as they require at least 2 generations to develop.

Careful classification of mitosis types showed that, as late as 72 hours after induction, more than 80% of mitoses in STIL overexpressing cells displayed an abnormal centriole content. However, only 44% of mitoses were actually harboring multiple spindle poles. There were, instead, still 40% of bipolar mitoses with centriole rosettes (**Fig. 25**). Together with the fact that an increase in karyotype heterogeneity is already detectable at earlier time points (see chapter 2.2.4), this suggested that centriole rosettes might also contribute to CIN through an unknown mechanism.

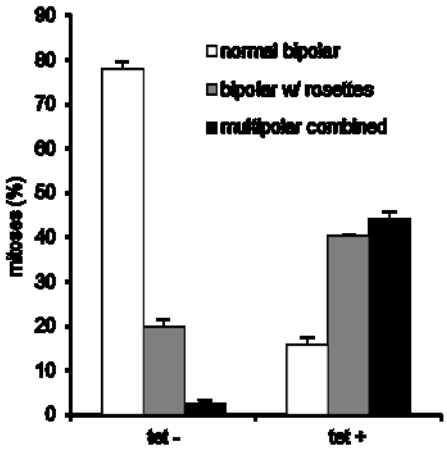

Figure 25 – Mitosis types distribution following eGFP-STIL overexpression

U2OS-eGFP-STIL cells were plated on coverslips and induced for 72 hours with tetracycline. Metaphase cells were classified according to spindle pole number and centriole content. Experiment was performed in triplicate. Error bars: s.e.m.

2.3.2 CENTRIOLE ROSETTES INDUCE ANAPHASE LAGGING CHROMOSOMES

To determine whether the presence of centriole rosettes has an impact on chromosome segregation fidelity, the frequency of anaphase lagging chromosomes was assessed specifically in bipolar mitoses with centriole rosettes. For this purpose, U2OS-eGFP-STIL and U2OS-eGFP-PLK4 cells were used to test the influence of centriole rosettes on lagging chromosome formation both during the first, as well as subsequent mitoses.

The U2OS-eGFP-PLK4 cell line was induced and analyzed after 15 hours. Indeed, while STIL overexpressing cells formed 40% of bipolar mitosis with centriole rosettes 72 hours after induction, 15 hours of PLK4 overexpression were already sufficient to get up to 70% of mitoses of this specific class (**Fig. 26B**). Furthermore, induced U2OS-eGFP-PLK4 cells often displayed centriole rosettes with high numbers of daughter centrioles (**Fig. 26A**).

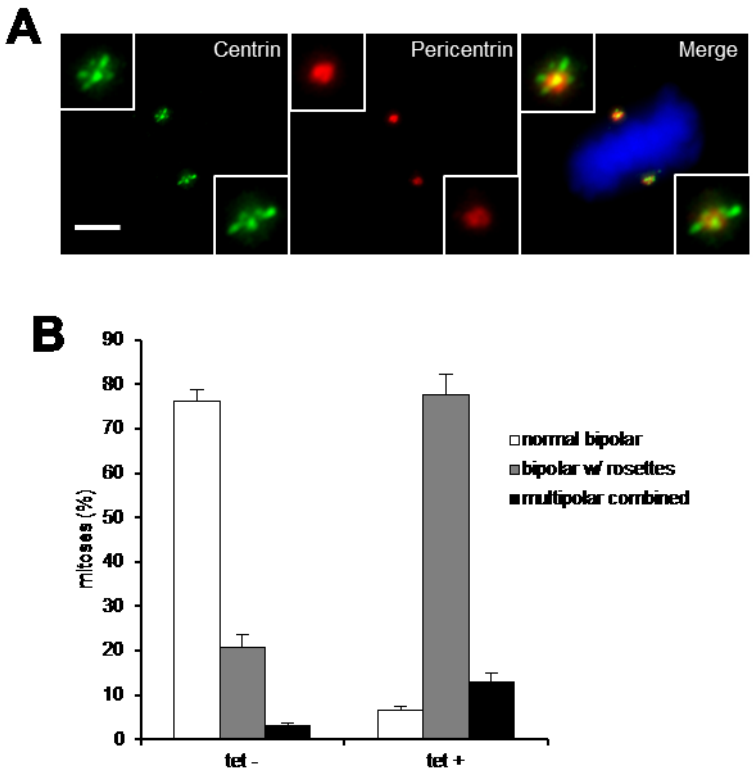

Figure 26 – Mitosis type distribution following eGFP-PLK4 overexpression

(**A**) U2OS-eGFP-PLK4 cells were plated on coverslips and induced for 15 hours with tetracycline. Centrin (green) and PCNT (red) were stained with specific antibodies; DNA was counterstained with Hoechst 33342 (blue). (**B**) Mitotic cells were classified according to spindle pole number and centriole content. Experiment was performed in triplicate. Error bars: s.e.m.

Following PHEM extraction and fixation, coverslips were stained for immunofluorescence microscopy with anti-centrin, anti-PCNT and CREST antibodies. Spindle pole number was determined by PCNT staining; rosettes were identified by counting the number of centrin signals at spindle poles. Assessing the exact number of spindle poles was of particular importance in this experiment. Indeed, when a clustered mitosis enters anaphase, the spindle poles collapse to a small region. Because of this, anaphases containing clustered spindle poles could be mistaken for bipolar anaphases with rosettes. PCNT staining helped to discriminate these phenotypes, as it produces a ring-shaped signal around parental centrioles. Only anaphases, where a single ring signal was present at each side of the spindle, were analyzed (**Fig. 27**). Anaphase lagging chromosomes were defined as bodies of chromatin, stained with DAPI, isolated from the main chromosome masses at anaphase. Only anaphase lagging chromosomes bearing a CREST signal were taken into consideration, to avoid the confounding effect of chromosomal fragments that likely arise through a mechanism completely unrelated to the one being object of this thesis (**Fig. 27**).

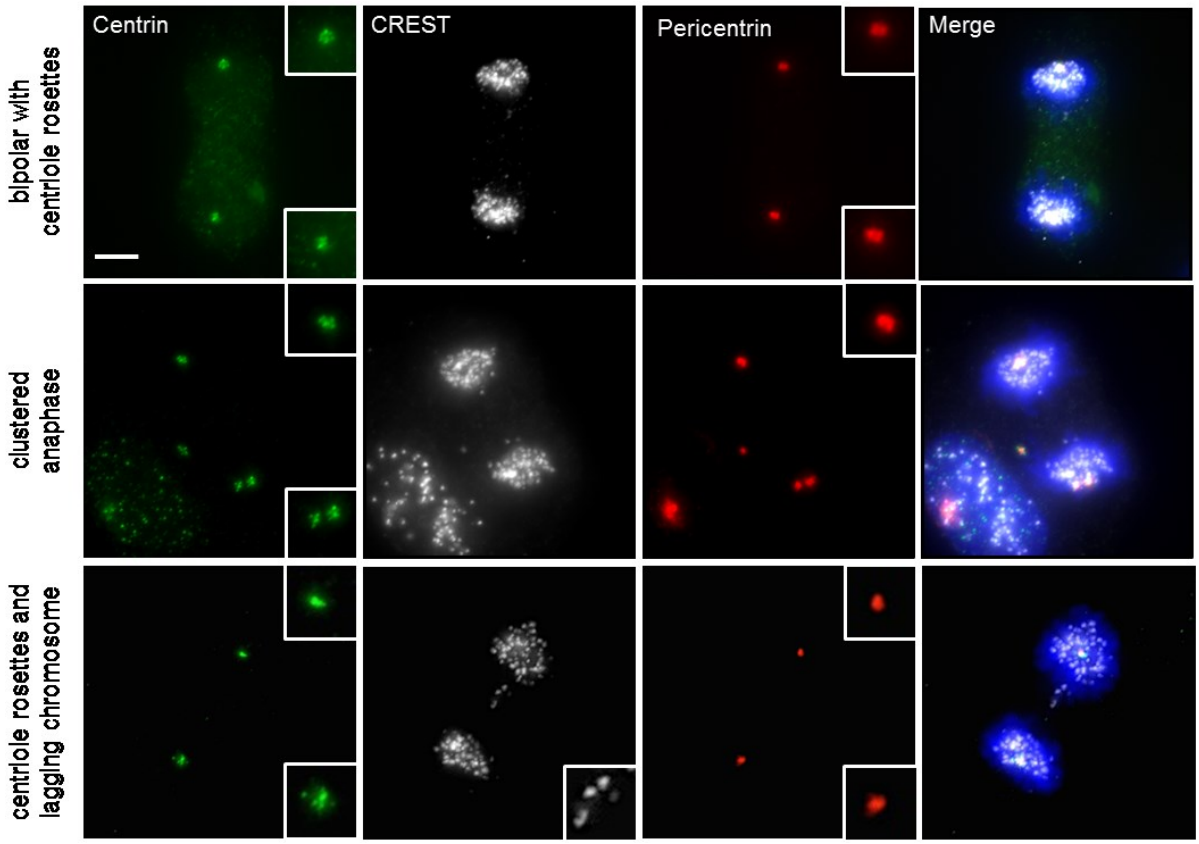

Figure 27 – Anaphase types and lagging chromosomes following eGFP-PLK4 overexpression

U2OS-eGFP-PLK4 cells were plated on coverslips and induced for 15 hours with tetracycline. Centrin (green), CREST (white) and PCNT (red) were stained with specific antibodies, DNA was counterstained with Hoechst 33342 (blue). Scale bar: 5 µm.

When the mitosis type was taken into account, the difference in the anaphase lagging chromosome frequency between bipolar mitoses with normal centrioles or centriole rosettes was striking. In both eGFP-STIL and eGFP-PLK4 cell lines, the presence of centriole rosettes in bipolar mitoses increased the chance of containing anaphase lagging chromosomes around 2-fold (**Fig. 28**). Moreover, in non-induced cells, the basal level of centriole rosettes in mitosis had an analogous impact on anaphase lagging chromosome frequency.

To further confirm this result, the anaphase lagging chromosome frequency in bipolar mitoses with centriole rosettes was analyzed in a panel of cancer cell lines. The cell lines were chosen due to their high basal frequency of centrosome amplification and included MDA-MB-231 (breast cancer), DU-145 (prostate cancer) and PC-3 (prostate cancer) cells.

Cells were processed and stained as described for eGFP-STIL and eGFP-PLK4 overexpressing cells. Similarly to what was already observed, these cell lines also showed an increased rate of anaphase lagging chromosomes when centriole rosettes were present at spindle poles (**Fig. 28**).

These results strongly suggest that centriole rosettes are able to contribute to the CIN phenotype.

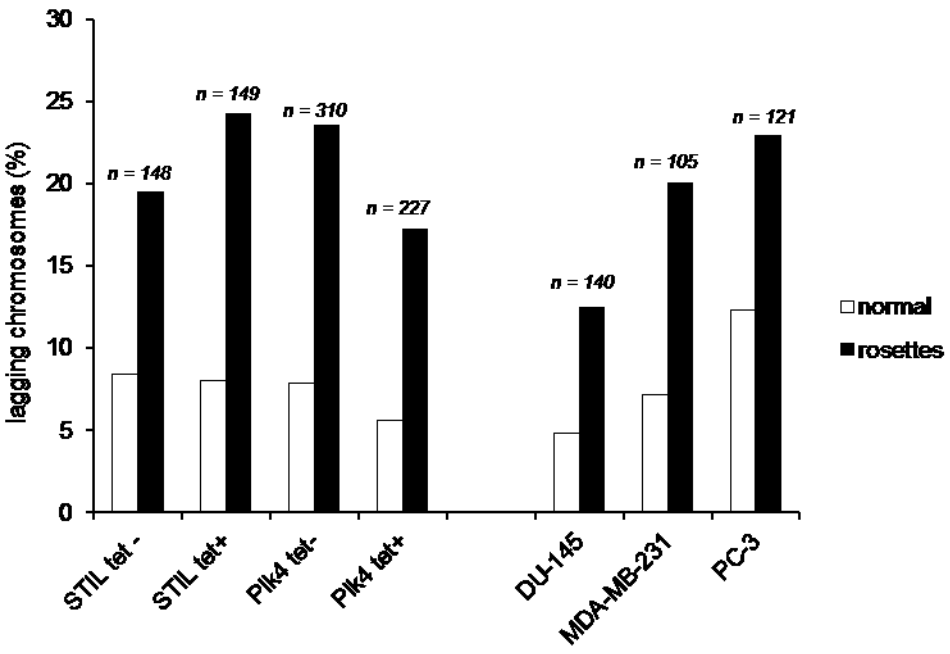

Figure 28 – Anaphase lagging chromosome frequency in bipolar mitoses with centriole rosettes

Cell lines were grown on coverslips, fixed and stained for immunofluorescence microscopy. U2OS-eGFP-STIL and U2OS-eGFP-PLK4 cells were induced for 72 and 15 hours, respectively. Centrin, kinetochores and PCNT were stained with specific antibodies; DNA was counterstained with Hoechst 33342. The total number of anaphases analyzed in every cell line is reported.

2.3.3 ABSOLUTE NUMBERS OF CENTRIOLE SIGNALS PRESENT AT SPINDLE POLES DO NOT INFLUENCE THE LAGGING CHROMOSOME FREQUENCY

Both PLK4 and STIL overexpression impacted on anaphase lagging chromosome frequency with remarkable similarity (**Fig. 28**). However, as described in chapter 2.1.1, STIL and PLK4 have a very different efficiency in inducing the formation of new centrioles. Therefore, the number of centrioles at each spindle pole and their impact on anaphase lagging chromosomes was assessed. Image analysis was performed in collaboration with Annik Roßberg.

U2OS-eGFP-STIL and U2OS-eGFP-PLK4 were plated on coverslips and induced for 15 and 72 hours, respectively. Coverslips were stained for immunofluorescence microscopy with anti-centrin and anti-PCNT antibodies. Spindle pole number was detected by PCNT; then the number of centrin signals was counted.

Distribution of centriole numbers per spindle pole showed that eGFP-STIL overexpressing cells accumulated less centrin signals per spindle pole both at 15 and 72 hours (**Fig. 29A-B**), reflecting the results obtained on interphase cells.

Spontaneously occurring centriole rosettes in MDA-MB-231, DU-145 and PC-3 cells were also characterized by low numbers of supernumerary centrioles per spindle pole (**Fig. 30**).

These results indicate that the number of centrioles in rosettes does not correlate with anaphase lagging chromosome frequency at anaphase.

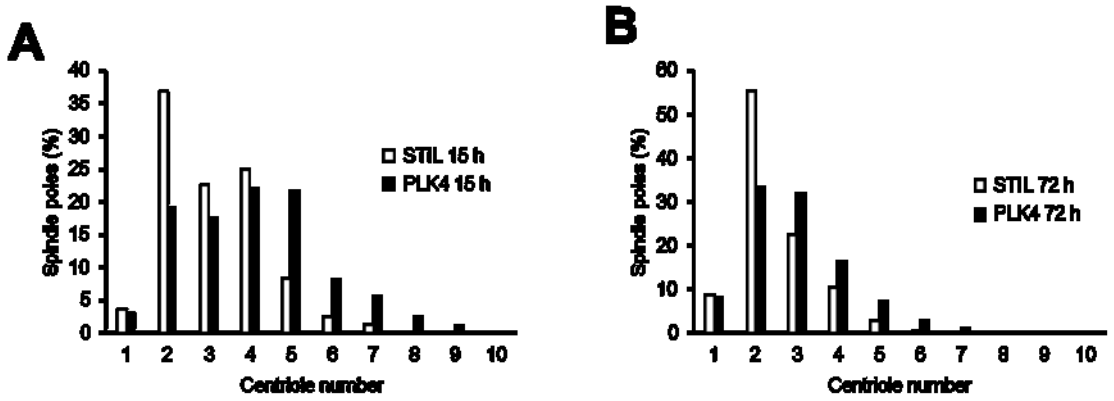

Figure 29 – Centriole number distribution per spindle pole following eGFP-STIL and eGFP-PLK4 overexpression

U2OS-eGFP-STIL and U2OS-eGFP-PLK4 cells were plated on coverslips and induced for 15 hours (**A**) and 72 hours (**B**), respectively. Coverslips were fixed and stained for immunofluorescence microscopy. Centrin, CREST and PCNT were stained with specific antibodies; DNA was counterstained with Hoechst 33342. Centriole number was scored at each spindle pole. The chart shows a representative experiment; at least 100 cells were scored.

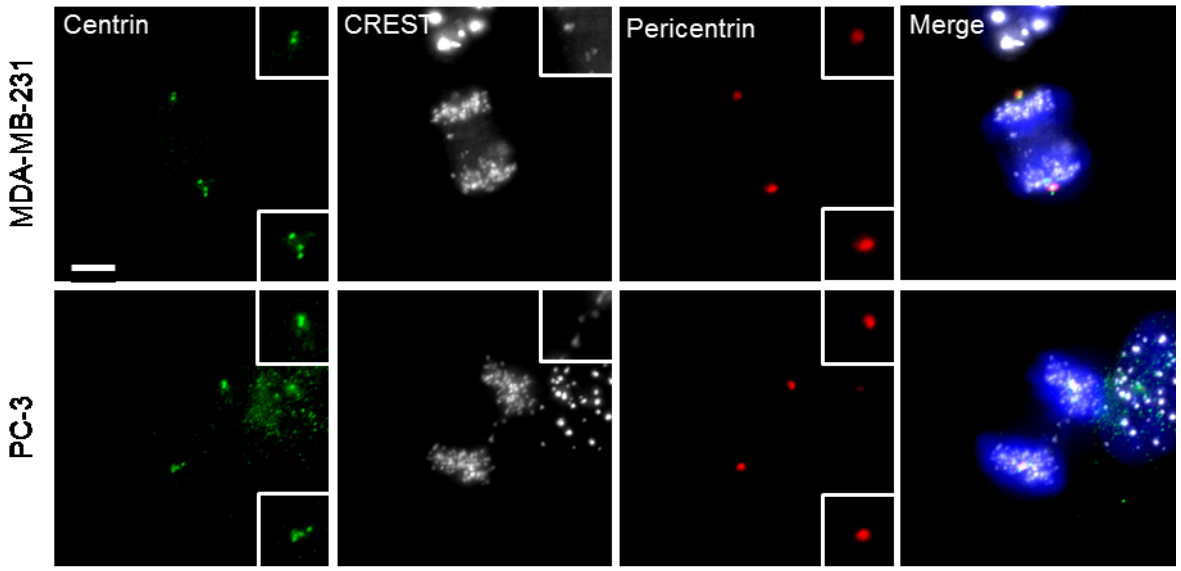

Figure 30 – Spontaneous bipolar anaphases with centriole rosettes in cancer cell lines

Cell lines were grown on coverslips, fixed and stained for immunofluorescence microscopy. Centrin (green), CREST (white) and PCNT (red) were stained with specific antibodies, DNA was counterstained with Hoechst 33342 (blue).

2.3.4 ASYMMETRIC NUMBERS OF CENTRIOLES AT SPINDLE POLES ARE MORE FREQUENTLY ASSOCIATED WITH ANAPHASE LAGGING CHROMOSOMES

To test whether the disruption of symmetric number of centrioles at spindle poles was correlated with the generation of merotelic attachments, centriole numbers at spindle poles were specifically analyzed in relation to the generation of anaphase lagging chromosomes.

The images generated to produce the data summarized in **Fig. 28** were analyzed. Centrin signals were visually counted at each spindle pole and the anaphases were classified into those with symmetric and asymmetric numbers, respectively (**Fig. 31C**). A normal mitosis bears only two centrioles at each pole; in case of centriole overduplication this number is increased. However, due to the stochastic process of formation of centriole duplication origins, the percentage of mitoses with asymmetric centriole numbers at the poles accounted for more than 80% of all cases (**Fig. 31A**).

When the frequency of anaphase lagging chromosomes is compared in mitoses with symmetric or asymmetric numbers of centrin signals at spindle poles, asymmetric anaphases have an increased likelihood of displaying a lagging chromosome (**Fig. 31B**).

This finding suggests that centriole rosettes generate anaphase lagging chromosomes through the disruption of centriole number symmetry at the spindle poles.

2.3.5 ANAPHASE LAGGING CHROMOSOMES INDUCED BY CENTRIOLE ROSETTES ARE OFTEN FOUND IN PAIRS

It was previously described that anaphase lagging chromosomes can, in some instances, be found in pairs. A possible mechanism explaining this phenomenon is that a merotelically attached kinetochore can promote merotelic attachment of its sister[89].
Merotelic attached kinetochores often display a distorted, elongated geometry. Distortion occurs because the kinetochore is contacting microtubule fibers coming from two different spindle poles and therefore it is stretched in opposite direction[51,89,90]. In addition, pulling forces cause the sister kinetochore pair to rotate and lose alignment to the spindle axis. Thereby the other sister kinetochore is turned at an angle that exposes it to contact with fibers from the opposite pole as well. In some cases, the sister kinetochore can also stabilize a merotelic attachment and the two chromatids will both lag behind at anaphase[89].

To determine whether the promotion of merotelic attachments of sister kinetochores was favored in mitoses with bipolar rosettes, the occurrence of anaphase lagging chromosome pairs was assessed.

Z-stacks of mitoses collected for experiment in chapter 2.3.2 were re-examined for the presence of anaphase lagging chromosome pairs in the presence of centriole rosettes. An example of anaphase lagging chromosomes constituted by a sister kinetochore pair is depicted in **Fig. 32A**.

In non-induced cells, about 30% of anaphase lagging chromosomes were present as paired signals. In induced cells this percentage was significantly increased to about 50% (**Fig. 32B**).

A higher frequency of anaphase lagging chromosomes observed as pairs suggests that centriole rosettes are increasing the chance of spreading the merotelic attachments across sister kinetochores.

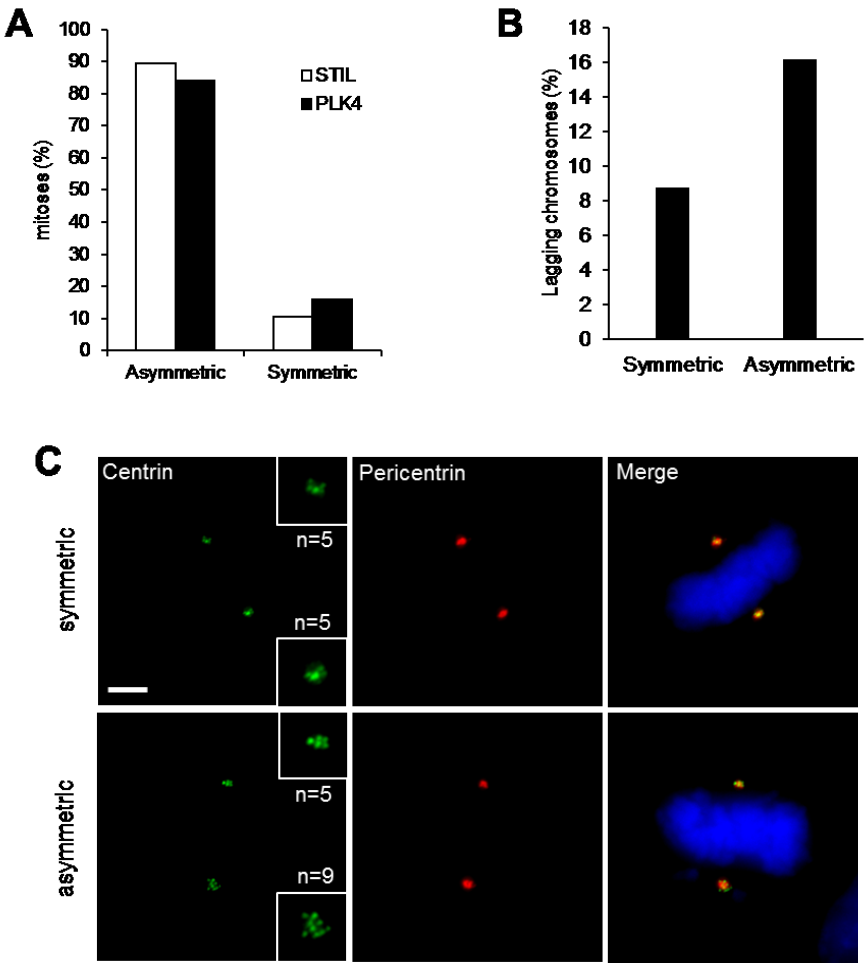

Figure 31 – Centriole number asymmetry at spindle poles following eGFP-STIL and eGFP-PLK4 overexpression

Cell lines were grown on coverslips, fixed and stained for immunofluorescence microscopy. U2OS-eGFP-STIL and U2OS-eGFP-PLK4 cells were induced for 72 and 15 hours, respectively. Cells were fixed and immunofluorescence microscopy was performed. Centriole number at the two spindle poles was compared and the anaphase was classified accordingly (**A**). The anaphase lagging chromosome frequency is shown in relation to the spindle pole symmetry in U2OS-eGFP-PLK4 cells (**B**). Example images of metaphases with symmetric and asymmetric centriole number at spindle poles. Centrin (green) and PCNT (red) were stained with specific antibodies, DNA was counterstained with Hoechst 33342 (blue). Scale bar: 5 μm (**C**).

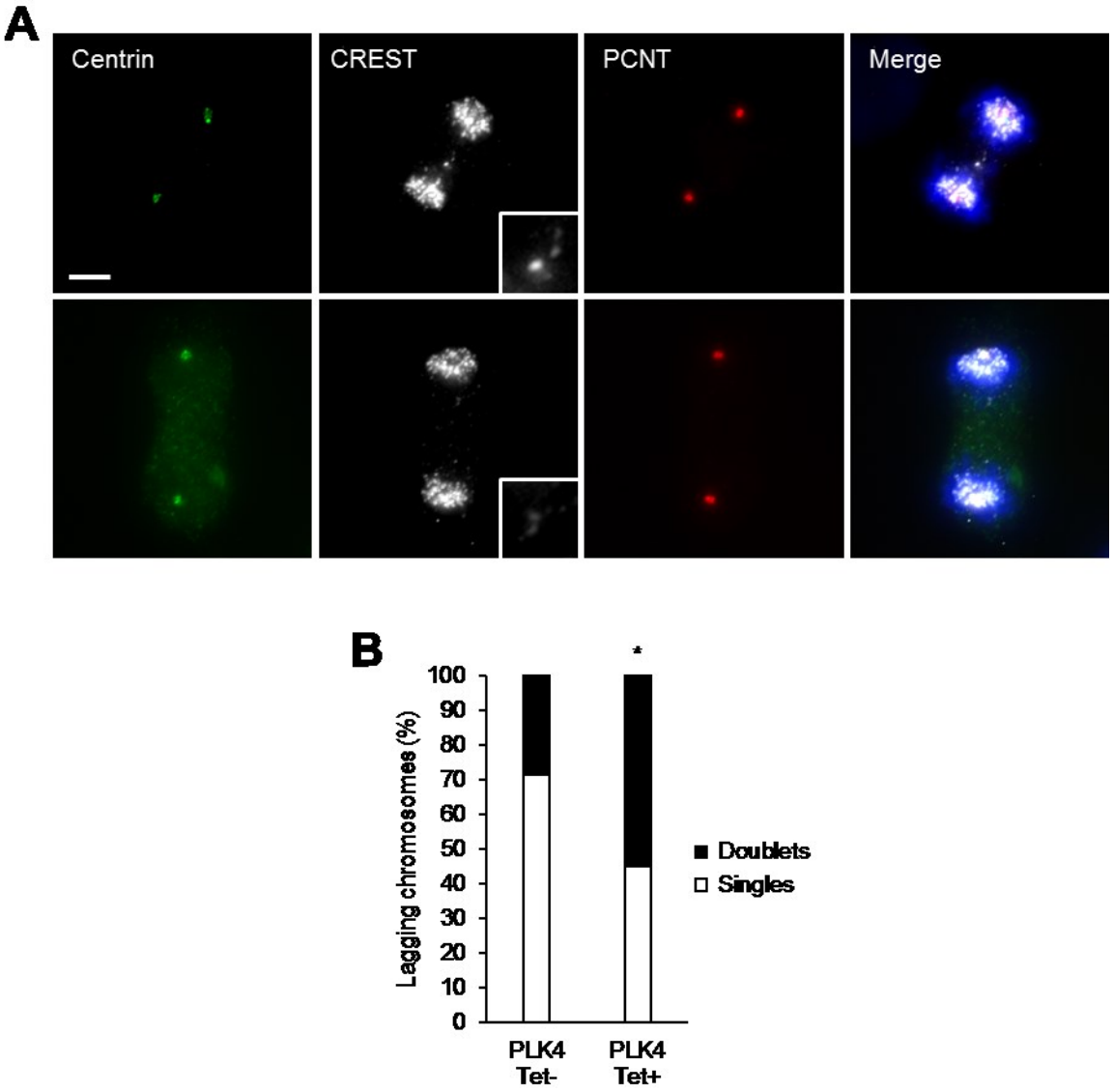

Figure 32 – Anaphase lagging kinetochore pairs following eGFP-PLK4 overexpression

U2OS-eGFP-PLK4 cells were grown on coverslips and induced 15 hours. Cells were fixed and immunofluorescence staining was performed. Centrin (green), CREST (white) and PCNT (red) were stained with specific antibodies, DNA was counterstained with Hoechst 33342 (blue). Anaphase lagging chromosomes were measured in at least three independent experiments for each condition. At least 60 anaphases were analyzed per replicate. Error bars: s.e.m.

2.3.6 THE PRESENCE OF CENTRIOLE ROSETTES INCREASES CHROMOSOME MISSEGREGATION RATE

Anaphase lagging chromosomes are an indirect marker of CIN. A study revealed that they are still being segregated to the correct sister nucleus and that most missegregation events occur without overt lagging[91]. Therefore, to test whether the observed increase in lagging chromosomes indeed leads to CIN, the chromosome missegregation rate resulting from centriole rosettes was measured.

FISH for centromere-specific probes was used to determine the chromosome number in sister nuclei. Cells were blocked with the cytokinesis inhibitor cytochalasin B. Cytochalasin B inhibits actin polymerization; when cells are exposed to it at low concentration, the formation of the contractile actin ring at the cytokinesis furrow is inhibited[86]. This results in cytokinesis abortion, and the two sister nuclei are retained within one cytoplasm, forming a binucleated cell. This offers a way to recognize the cells that have divided during cytochalasin incubation. By counting the number of signals and how they are distributed within these binucleated cells it is possible to measure the missegregation rate of a specific chromosome. This approach is independent of chromosome modal number and cell-to-cell heterogeneity, as each pair of sister nuclei is considered separately.

U2OS-eGFP-PLK4 cells were chosen for this analysis. It was already shown in chapter 2.1.1 that 15 hours after induction of PLK4 overexpression about 70% of the cells contain centriole rosettes. Therefore, it was safe to assume that the cells observed were mainly resulting from bipolar divisions with centriole rosettes and that the confounding influence of normal and multipolar mitoses would be negligible.

U2OS-eGFP-PLK4 cells were induced for 15 hours and exposed for the same time with 4.5 µg/mL of cytochalasin B. The short exposure time ensured that cells divided only once during cytochalasin B incubation. Cells were plated on coverslips at low density, so that binucleated cells could be easily distinguished. Coverslips were fixed in methanol. FISH was performed with centromere-specific probes for chromosomes 2 and 3.

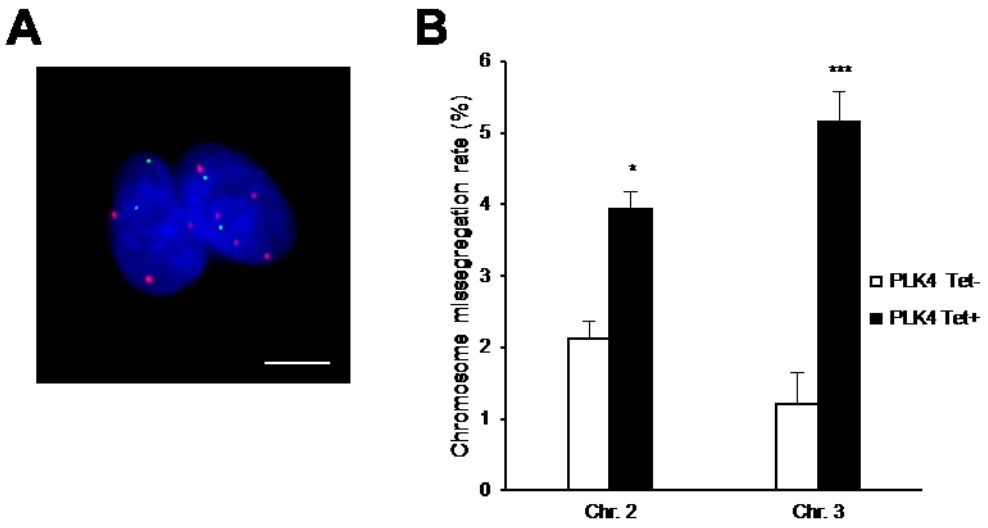

Figure 33 – Chromosome missegregation following short-term eGFP-PLK4 overexpression

(**A**) U2OS-eGFP-PLK4 cells were grown on coverslips and exposed for 15 hours to tetracycline and cytochalasin B. Cells were fixed and FISH was performed with centromere-specific probes for chromosome 2 (green) and 3 (red). Chromosome missegregation events were scored by counting the number of signals in sister nuclei. An example of cells with chromosome missegregation is shown. Scale bar: 20 µM. (**B**) Only binucleated cells with an even total number of signals were taken into account. The chromosome missegregation rate was assessed in cells overexpressing PLK4 (black bars) and non-induced controls (white bars). Experiments were performed in triplicate. At least 100 cells were counted for each condition. Error bars: s.e.m.

Binucleated cells were clearly identifiable. However, as a further measure to avoid misclassification, only paired nuclei with even total numbers of signals were considered. As chromosomes are composed of two chromatids, at anaphase completion the total number of chromatids has always to be an even number.

Binucleated cells were then scored for analysis. A missegregation event was counted when the number of signals in the two sister nuclei was different as depicted in **Fig. 33A**.

Induced U2OS-eGFP-PLK4 cells showed a significant increase in chromosome missegregation as compared to non-induced controls (**Fig. 33B**). The missegregation rate for chromosome 2 almost doubled; for chromosome 3 the effect was even more prominent.

Around 70% of cells that have divided under cytochalasin B exposure are *bona fide* bipolar mitoses with centriole rosettes (see chapter 2.1.1). These results strongly indicate that the presence of centriole rosettes increases chromosome missegregation rates and therefore centriole rosettes are sufficient to induce CIN.

2.3.7 CENTRIOLE ROSETTES DO NOT INFLUENCE THE DURATION OF MITOSIS

In order to investigate the cause of kinetochore-microtubule malattachments in bipolar mitoses with centriole rosettes, live-cell imaging of mitotic cells was performed.

An extension of mitosis length is an important predictor of kinetochore-microtubule malattachments. Cells exposed to taxol or nocodazole, which affect microtubule dynamic instability, enter anaphase with a delay and display high levels of chromosome missegregation[92,93].

Centrosomes are the major site of microtubule nucleation at mitosis. Many microtubule regulatory proteins localize at the centrosome during mitosis[94]. The presence of multiple spindle poles has been shown to elongate mitosis time[95]. Whether the presence of supernumerary centrioles has an impact on mitosis time and microtubule dynamics regulation is not known.

U2OS-eGFP-PLK4 cells were plated on glass bottomed petri dishes. A vector encoding H2B-mCherry, a fusion protein of a histone subunit and a red fluorescent protein, was transfected to visualize chromosome movements during mitosis. Cells were allowed to recover for 24 hours after transfection. Culture medium was changed and cells were induced for 15 hours. Then, live-cell imaging was started for additional 15 hours in a controlled atmosphere at 37°C and 5% CO_2 pressure. Frames were acquired at 5 minute intervals.

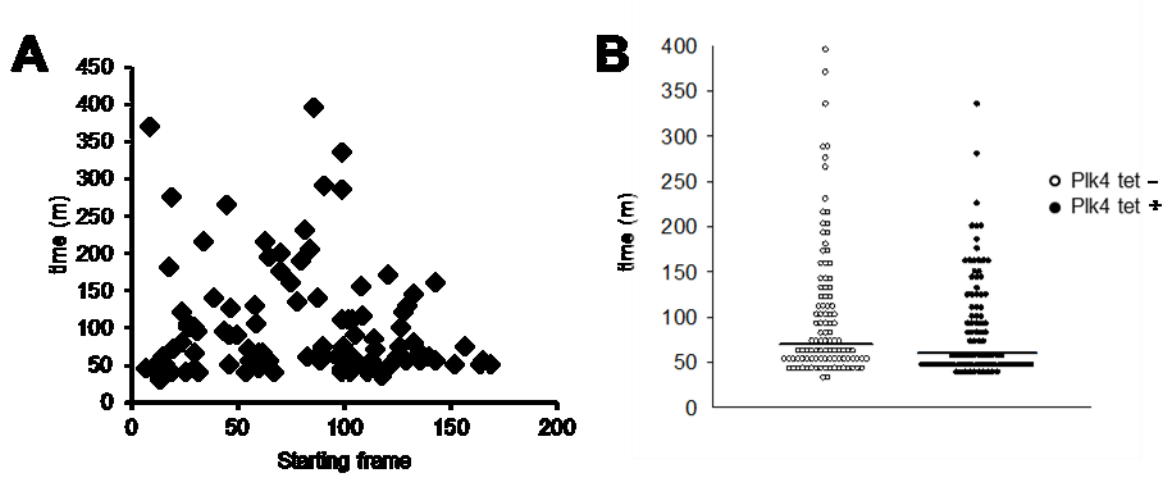

Figure 34 – Mitosis time following eGFP-PLK4 induction

U2OS-eGFP-PLK4 cells were plated on coverslips and transfected with H2B-mCherry. 24 hours after transfection, cells were exposed for 15 hours to tetracycline. Then live-cell imaging was started, images were acquired every 5 minutes for additional 15 hours. Mitosis duration was measured from chromosome condensation to telophase. (**A**) Mitosis duration is plotted against the starting frame in U2OS-eGFP-PLK4 cells. (**B**) Mitosis duration following eGFP-PLK4 overexpression (*black circles*) and in non-induced controls (*white circles*). The plot displays data from 3 independent experiments for each condition. Lines represent the median.

Long term live-cell imaging with fluorescent light can be toxic to cells and alter mitosis length. The longer cells are exposed to light, the longer mitosis will be. Therefore, a simple way to check for the presence of phototoxicity is to plot mitosis length against starting time of mitosis. If a linear correlation is found, then cells are experiencing significant phototoxicity[93]. As can be observed in **Fig. 34A**, no phototoxicity was observed during the experiment.

No significant difference was observed in mitotic morphology or duration between induced and non-induced U2OS-eGFP-PLK4 cells (**Fig. 34B**). In addition, anaphase lagging chromosome count revealed that the analysis on fixed cells greatly underestimated their actual frequency. Induced cells showed lagging chromosomes in around 49% of mitoses, while non-induced controls only in around 29%.

These results indicate that the presence of centriole rosettes does not have an impact on mitosis time or morphology.

2.3.8 CENTRIOLE ROSETTES DO NOT AFFECT KINETOCHORE FIBER STABILIZATION

Correction of merotelic attachments relies on microtubule turnover at kinetochores (see chapter 1.3.2). Microtubule turnover is carefully regulated during mitosis. At prometaphase kinetochore fibers have a half-life of about 2 minutes. This high rate allows for several rounds of capture and release. During metaphase, chromosomes are correctly bi-oriented and kinetochore fiber half-life increases 2-3 fold[59].

Mature kinetochore fibers are resistant to short term cold treatment. Fluorescence measurement of cold-stable kinetochore fibers is a simple way of detecting the presence of kinetochore-microtubule attachment deregulation in dividing cells[92].

In an attempt to study the influence of centriole rosettes and extra centrosomes on kinetochore fiber stabilization, quantification of cold-stable kinetochore fibers was performed.

U2OS-eGFP-STIL cells were induced for 72 hours to obtain a mixed population of cells bearing centriole rosettes and multiple centrosomes. Medium was replaced with ice-cold PBS and cells were incubated on ice for 15 minutes. The microtubule fraction was extracted by PHEM buffer washing at 4°C. Cells were fixed. The intensity of cold-resistant microtubule fibers was detected with anti-α-tubulin antibodies by immunofluorescence. Sum-intensity projections encompassing mitotic cells were collected and fluorescence intensity was digitally quantified.

Mitotic cells contained increasing levels of stabilized fibers from prophase to metaphase, according to the expected turnover shift during mitosis progression. In general, cold-stable fibers were visible in both non-induced and induced cells, and in the presence of extra centrosomes (**Fig. 35A**).

Quantification of cold-stable kinetochore fibers showed that metaphase cells contained increased levels of stabilized fibers, as compared to prometaphase cells (**Fig. 35B**). However, no significant difference was observed when induced and non-induced cells were compared within specific mitotic phases (**Fig. 35B**). This result suggests that proper kinetochore functioning is not affected by the presence of centriole rosettes nor by the presence of multiple spindle poles.

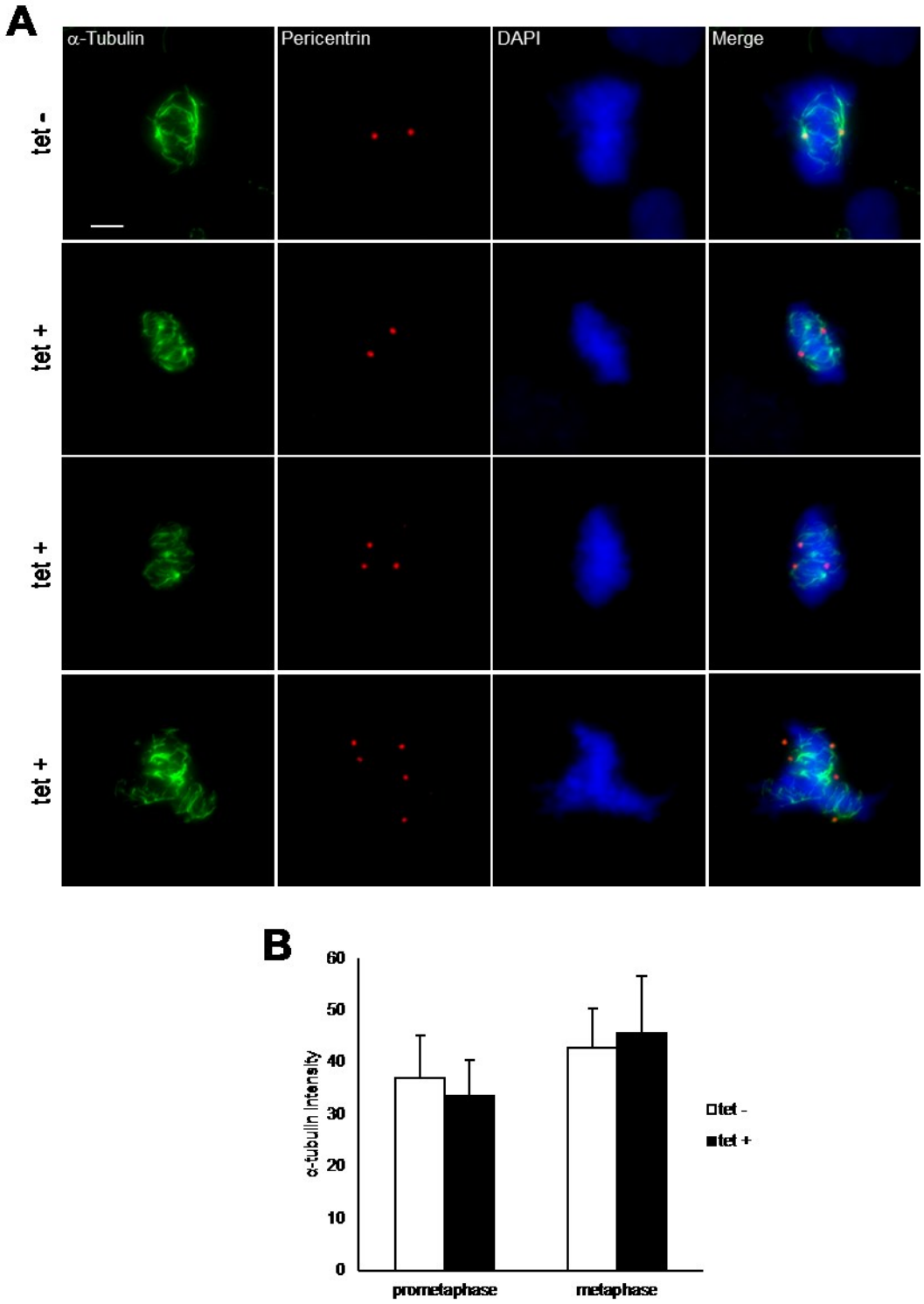

Figure 35 – Cold-stable kinetochore fiber quantification following eGFP-STIL induction

U2OS-eGFP-STIL cells were grown on coverslips and induced for 72 hours. Cells were fixed and immunofluorescence staining was performed with anti-α-tubulin (green) and PCNT (red) antibodies, DNA was counterstained with Hoechst 33342 (blue). (**A**) Example figures represent z-stack sum-intensity projections of mitotic cells. Similar kinetochore fibers can be observed in both induced cells and isogenic control. (**B**) The presence of multiple spindle poles does not affect fiber stabilization. Microtubule polymer intensity was expressed as the sum of total pixel intensity values in a circular ROI containing the spindle. Background was calculated from a larger area centered in the ROI and subtracted from the intensity value. Bar represents average corrected intensity values in arbitrary units; at least 50 cells were measured for each condition. Error bars: s.e.m.

2.3.9 THE SPINDLE ASSEMBLY CHECKPOINT IS NOT ACTIVATED IN CELLS WITH CENTRIOLE ROSETTES

In order to track the origin of CIN induced by centriole rosettes, SAC activation in these cells was investigated.

A functional SAC is essential for survival of cells with extra centrosomes. A defective SAC induces anaphase onset before clustering has occurred. The resulting multipolar mitosis produces severely aneuploid cells, which are not likely to survive[79,81,96].

BubR1 is an important player in SAC signal generation. BubR1 is localized on both unoccupied kinetochores and kinetochores lacking tension[97]. It was previously shown that multipolar mitoses recruit high levels of BubR1 on kinetochores, however a quantitative analysis was not performed [98].

If centriole rosettes are causing activation of the SAC as well, high levels of BubR1 should be detectable at kinetochores.

For this purpose, U2OS-eGFP-STIL cells were induced for 72 hours, PHEM-extracted, fixed and processed for immunofluorescence microscopy. Anti-PCNT antibodies were used to detect spindle pole numbers and CREST to visualize kinetochores; moreover, an anti-BubR1 antibody was used to probe SAC activation.

BubR1 intensity progressively dropped as cells reached metaphase. Furthermore, unaligned chromosomes consistently recruited high levels of BubR1 at their kinetochores (**Fig. 36A**).

Fluorescence quantification of BubR1 signals showed a clear decrease in intensity as cells were approaching metaphase. However, no significant difference was observed between non-induced cells and induced cells (**Fig. 36B**), suggesting that centriole rosettes do not activate the SAC, despite formation of kinetochore-microtubule attachment errors.

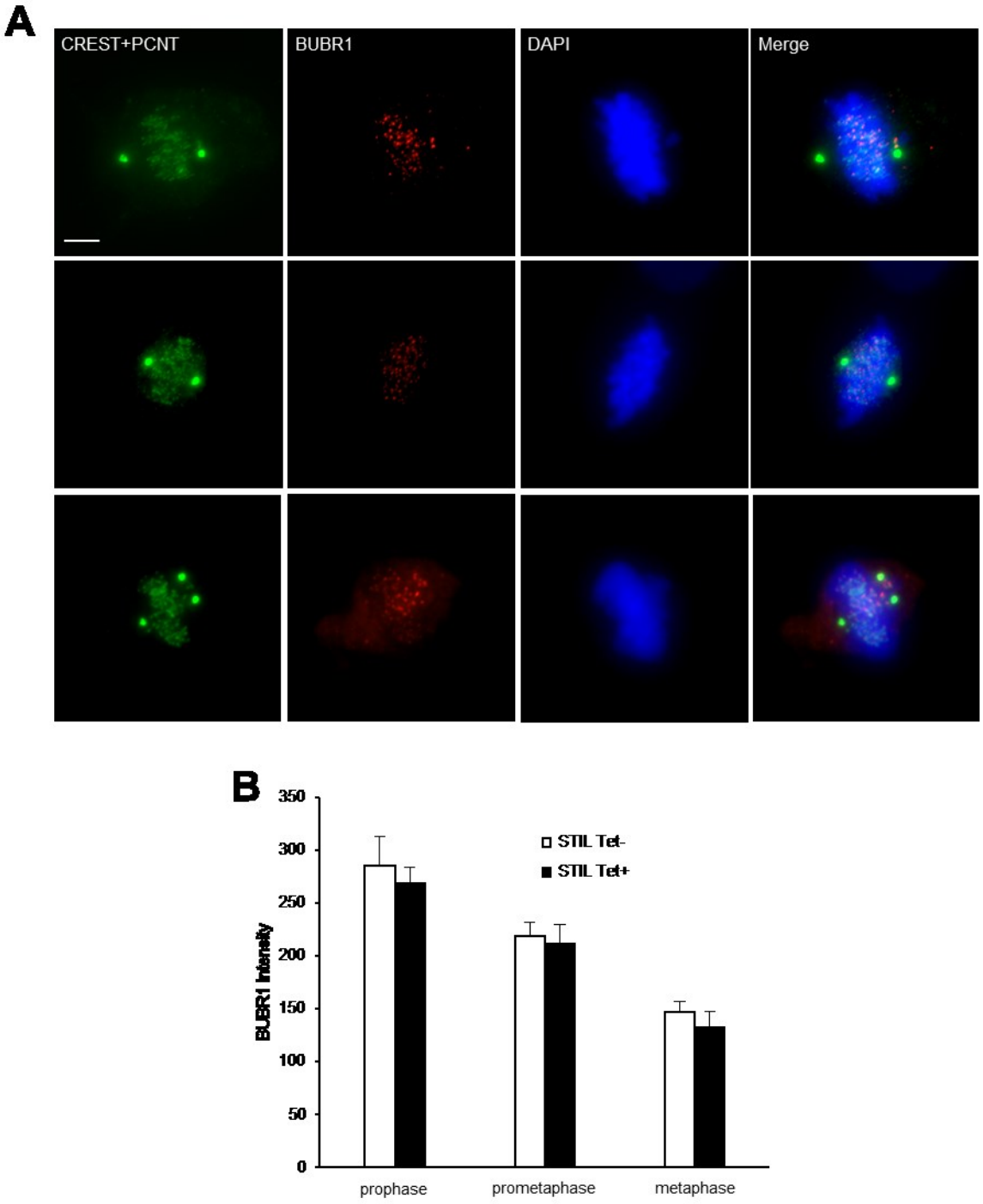

Figure 36 – BubR1 signal intensity quantification following eGFP-STIL induction

U2OS-eGFP-STIL cells were grown on coverslips and induced for 72 hours. Cells were fixed and immunofluorescence staining was performed with anti-PCNT, CREST (green) and BubR1 (red) antibodies, DNA was counterstained with Hoechst 33342 (blue). (**A**) Example figures represent z-stack maximum-intensity projections of mitotic cells. BubR1 signals are located on kinetochores that have not congressed. (**B**) BubR1 signal intensity was quantified at its best-of-focus in a ROI containing the whole signal. Background was calculated from a larger area centered in the ROI and subtracted from the intensity value. All distinguishable kinetochores were analyzed. Bars represent average corrected intensity values in arbitrary units; at least 40 cells were measured for each condition. Error bars: s.e.m.

2.3.10 CENTRIOLE ROSETTES DECREASE THE INTERKINETOCHORE STRETCH AT METAPHASE

To further investigate the influence of centriole rosettes on mitosis, interkinetochore stretch was determined, as an indirect measure of kinetochore bi-orientation.

Interkinetochore stretch is generated at sister kinetochores when bi-orientation is achieved. Microtubule-kinetochore attachments that do not promote tension engage the error correction machinery regulated by Aurora B, which destabilizes them creating a new chance for microtubule capture[46,52,90,99]. Kinetochore fiber stabilization plays an important role in establishing bi-orientation. Stable fibers impose strong pushing/pulling forces on kinetochores. Therefore, the more stabilization, the higher is the tension at kinetochore pairs[100,101].

Interkinetochore tension can be measured by determining the distance across sister kinetochore pairs. This distance steadily increases from prophase to metaphase. Distance at prophase is short and is defined as a "resting distance": at this stage kinetochores are unoccupied and therefore experience no tension. Distance at metaphase is maximal: kinetochores are fully occupied and fibers stabilized.

It was previously reported that extra centrosomes can impact on interkinetochore distance[98]. Whether centriole rosettes in bipolar mitoses can influence interkinetochore stretch has not been examined.

U2OS-eGFP-PLK4 and U2OS-eGFP-STIL cell lines were induced for 15 and 72 hours respectively. Cells were PHEM-extracted and processed for immunofluorescence microscopy. To distinguish the various mitosis types, cells were stained with anti-PCNT and anti-centrin antibodies. Sister kinetochore pairs were detected with CREST antibody. Notably, CREST staining allows reliable identification of sister kinetochore pairs as the two main signals are connected by a thin string.

Cells were classified according to their mitotic stage and centriole content. To obtain accurate measurements of interkinetochore distances, Z-stacks were acquired and kinetochore position was recorded in three dimensions. All visible kinetochore pairs were taken into account for analysis. Average interkinetochore distance per cell was calculated and these measurements were averaged accordingly for each condition.

In U2OS cells, sister kinetochores had a resting distance of 0.83 µm. Interkinetochore distance increased at prometaphase and was maximal in metaphase cells reaching around 1.42 µm in non-induced cells (**Fig. 37A**). Moreover, average interkinetochore distance and average BubR1 intensity within the same cell were strongly correlated: as cell approached metaphase, kinetochores experienced tension and BubR1 was unloaded from them (**Fig. 37C**).

Metaphases bearing centriole rosettes had a significantly shorter interkinetochore distance and the presence of supernumerary centrosomes further shortened this distance (**Fig. 37A**). This result might reflect the activation of the kinetochore-microtubule error correction machinery or a delay in achieving bi-orientation.

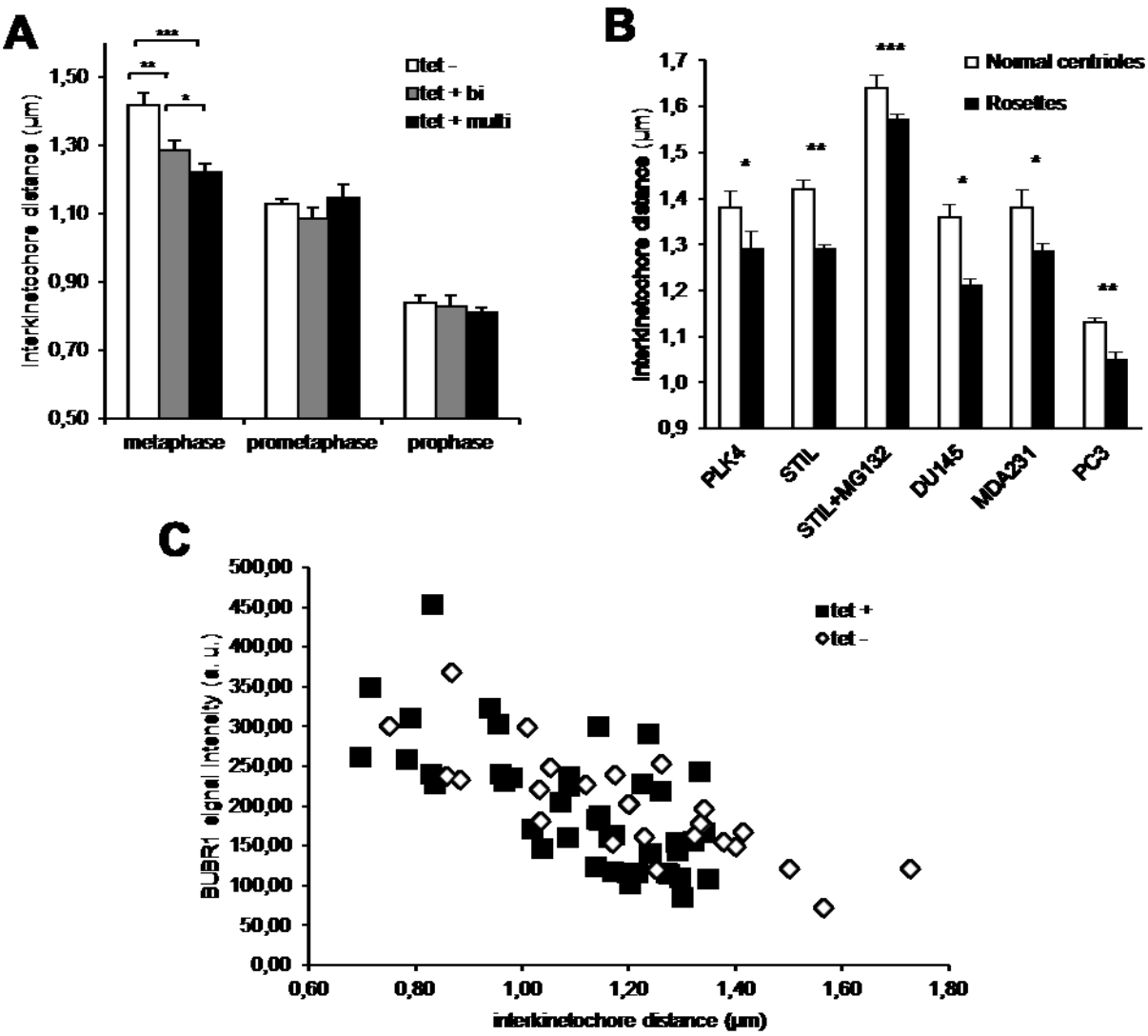

Figure 37 – Interkinetochore distance in bipolar metaphases with centriole rosettes

Cell lines were grown on coverslips, fixed and stained for immunofluorescence microscopy. U2OS-eGFP-STIL and U2OS-eGFP-PLK4 cells were induced for 72 and 15 hours, respectively. U2OS-eGFP-STIL cells were incubated with 20 µM MG-132 for three hours. Centrin, kinetochores and PCNT were stained with specific antibodies, DNA was counterstained with Hoechst 33342.
(**A**) Interkinetochore distance was measured on all detectable sister pairs visible in the mitotic cell. At least 50 cells were analyzed in each condition. Bars represent average interkinetochore distance within mitotic cells; error bars: s.e.m. Abbreviations: bi, bipolar; multi, multipolar.
(**B**) Interkinetochore distance comparison among cell lines. At least 10 mitotic cells were analyzed in each condition. Error bars: s.e.m. (**C**) Interkinetochore distance and BubR1 staining intensity correlation in U2OS-eGFP-STIL cells.

Due to the difficulty in clearly distinguishing metaphases from prometaphases in the presence of extra centrosomes, U2OS-eGFP-STIL cells were incubated for 3 hours in the presence of MG-132, a protease inhibitor. Incubation with MG-132 delays anaphase onset in mitotic cells, inducing accumulation of metaphases.

Incubation with MG-132 greatly enhanced interkinetochore tension, due to a hyper-stabilization of kinetochore fibers. However, it did not rescue the difference in interkinetochore distance between cells with and without centriole rosettes (**Fig. 37B**). Therefore, providing additional time for kinetochore-

microtubule attachment error correction was not sufficient to overcome the impairment induced by centriole rosettes and additional spindle poles.

Interkinetochore stretch reduction was confirmed when metaphases of U2OS-eGFP-PLK4 cells were analyzed. Importantly, a similar decrease was observed in other cancer cells lines with spontaneously occurring centriole rosettes (**Fig. 37B**). Interkinetochore distances at metaphase were largely comparable among cell lines and the presence of centriole rosettes caused a similar shortening. PC-3 cells constituted an exception: this cell line displayed a considerably shorter distance. However, the presence of centriole rosettes further reduced this distance.

Taken together, these results indicate that centriole rosettes impair kinetochore bi-orientation as measured by interkinetochore stretch reduction. This suggests an involvement of the kinetochore-microtubule attachment error correction mechanism. This phenotype occurs with spontaneously occurring centriole rosettes as well, independently from the cell line model examined.

2.3.11 ANAPHASE LAGGING CHROMOSOMES INDUCED BY CENTRIOLE ROSETTES ARE NOT RESCUED BY INCREASING MICROTUBULE TURNOVER

Correction of kinetochore-microtubule merotelic attachments depends on Aurora B kinase activity[99]. Effector proteins, responsible for error correction, are MCAK and KIF2B[57]. Error correction is accomplished by regulation of microtubule turnover at kinetochores. MCAK and KIF2B are microtubule motors that stimulate microtubule depolymerization. This promotes microtubule release from kinetochores that are subsequently free to capture new ones until bi-orientation is achieved [56,58,59]. MCAK and KIF2B transient transfection has been proven effective in lowering the frequency of anaphase lagging chromosomes in cancer cell lines[56,57].

Accordingly, the possibility that enhancement of the kinetochore-microtubule error correction capacity may rescue chromosome missegregation caused by centriole rosettes was tested. For this purpose, MCAK and KIF2B were transiently transfected and anaphase lagging chromosomes were counted.

U2OS-eGFP-PLK4 cells were plated on coverslips. EGFP-MCAK or eGFP-KIF2B vectors were transiently transfected. Cells were then allowed to recover for 24 hours and were subsequently induced for 15 hours to obtain high numbers of bipolar anaphases with centriole rosettes. PHEM extraction was avoided, as it caused loss of the eGFP signal from cells. On the other hand this did not allow for visualization of centrin signals. Therefore, coverslips were stained only with anti-PCNT and CREST antibody to detect spindle poles and kinetochores, respectively.

Analysis was restricted to anaphases displaying a specific eGFP-MCAK or eGFP-KIF2B signal. Following transient transfection, MCAK and KIF2B correctly localized on spindle poles and kinetochores. Moreover, a very strong signal could be observed on unaligned chromosomes at metaphase, as expected (**Fig. 38**).

Both eGFP-MCAK and eGFP-KIF2B transfection caused a reduction of anaphase lagging chromosomes in non-induced cells (**Fig. 40**). This constituted the proof of principle that microtubule turnover was efficiently enhanced, as previously described[57]. On the other hand, bipolar anaphases in induced cells, bearing *bona*

fide centriole rosettes, did not show any reduction in anaphase lagging chromosome frequency (**Fig. 39, 39**).

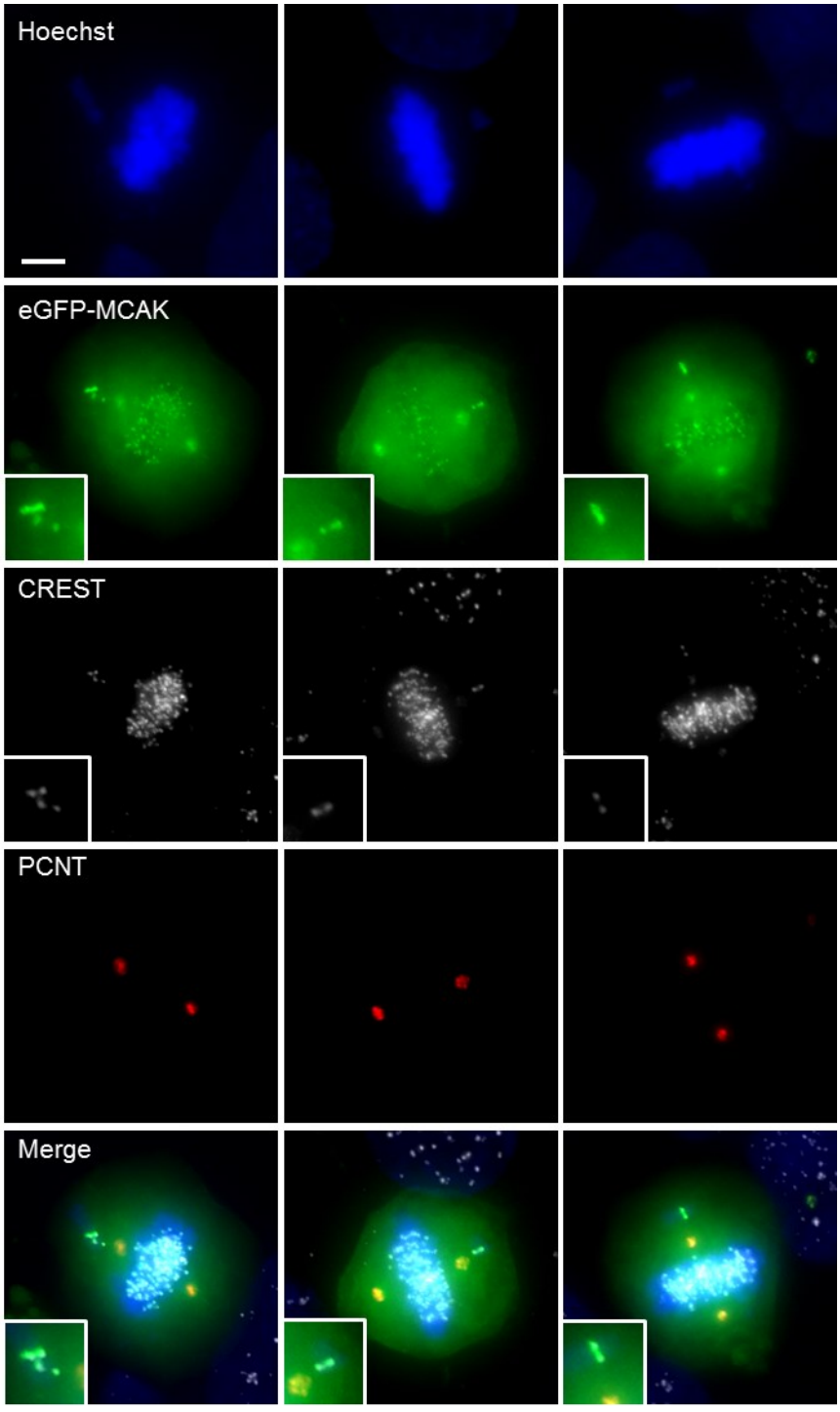

Figure 38 – eGFP-MCAK localization at kinetochores of unaligned chromosomes

U2OS-eGFP-PLK4 cells were grown on coverslips. EGFP-MCAK was transiently transfected and after one day cells were induced for 15 hours. Cells were fixed and immunofluorescence staining was performed with CREST (white) and PCNT (red) antibodies, DNA was counterstained with Hoechst 33342 (blue). Example figures represent z-stack maximum-intensity projections of mitotic cells. EGFP-MCAK protein accumulation can be observed on kinetochores of unaligned chromosomes. Scale bar: 5 μm.

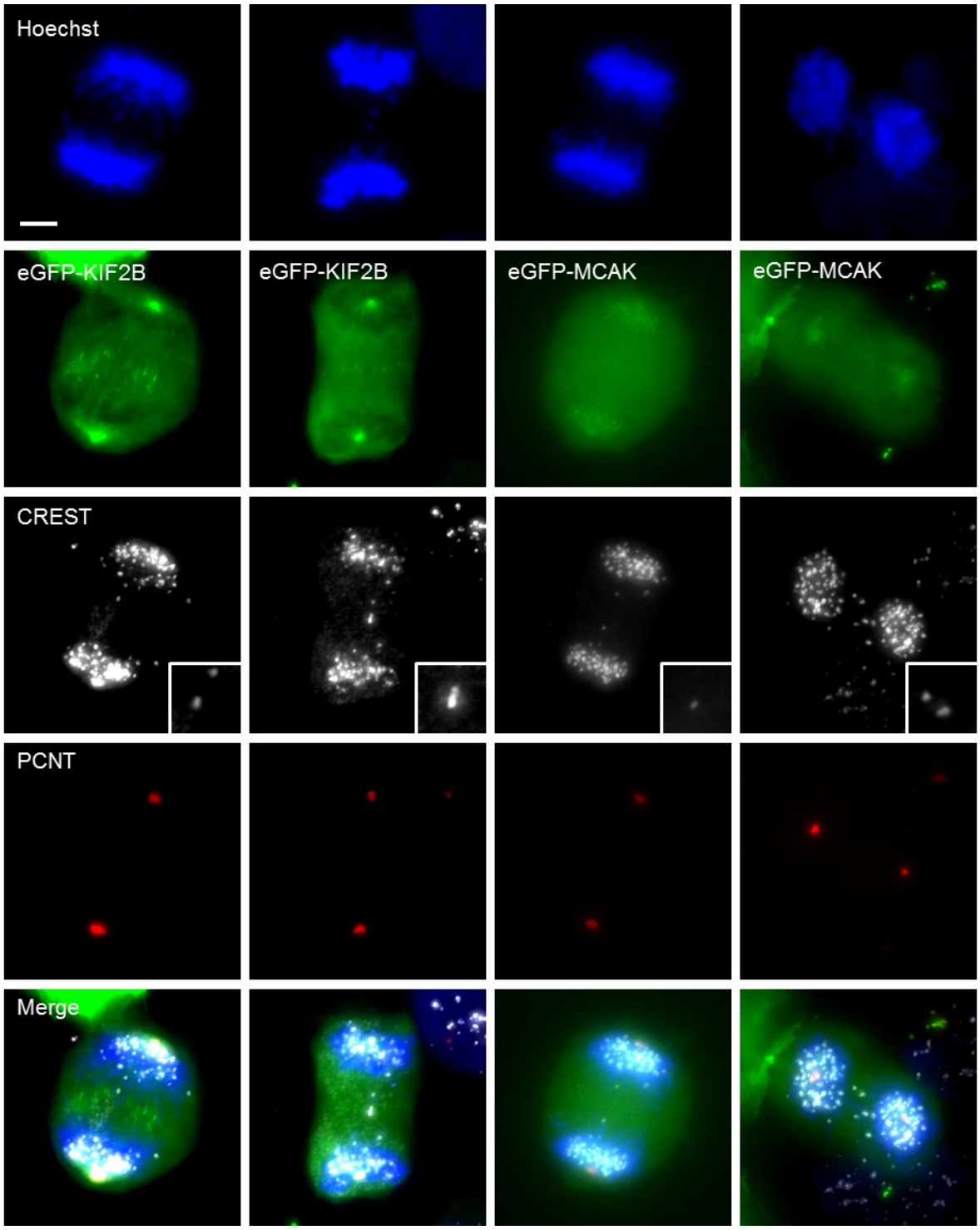

Figure 39 – Anaphase lagging chromosomes in eGFP-MCAK and eGFP-KIF2B transfected cells

U2OS-eGFP-PLK4 cells were grown on coverslips. EGFP-MCAK or eGFP-KIF2B were transiently transfected and after one day cells were induced for 15 hours. Cells were fixed and immunofluorescence staining was performed with CREST (white) and PCNT (red) antibodies, DNA was counterstained with Hoechst 33342 (blue). Example figures represent z-stack maximum-intensity projections of mitotic cells. Anaphase lagging chromosomes are present despite high expression level of transfected proteins. Scale bar: 5 μm.

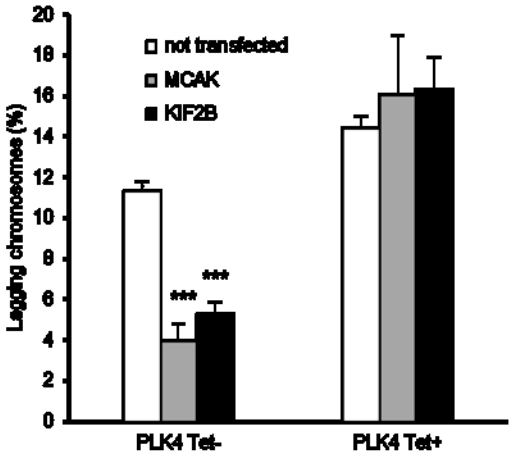

Figure 40 – Anaphase lagging chromosome frequency following eGFP-MCAK and eGFP-KIF2B transfection

U2OS-eGFP-PLK4 cells were grown on coverslips. EGFP-MCAK or eGFP-KIF2B were transiently transfected and after one day cells were induced for 15 hours. Cells were fixed and immunofluorescence staining was performed. Anaphase lagging chromosomes were quantified in at least three independent experiments for each condition. At least 60 anaphases were analyzed per replicate. Error bars: s.e.m.

These results clearly indicate that increasing the microtubule turnover through eGFP-MCAK or eGFP-KIF2B overexpression is not able to rescue anaphase lagging chromosome formation in PLK4 overexpressing cells. This finding is of particular importance, as it is the first reported cause of kinetochore-microtubule malattachment that cannot be overcome by stimulation of the spindle error correction machinery.

2.4 CENTRIOLE OVERDUPLICATION IMPACT ON CELL PROLIFERATION

2.4.1 PROGENY OF BIPOLAR MITOSES WITH CENTRIOLE ROSETTES CONSTITUTES THE MAJORITY OF THE GROWING CELL POPULATION

To test the relative contribution of the progeny of bipolar mitosis with rosettes to the growing cell population, their frequency was assessed at several time points under continuous transgene induction.

Both aneuploidy and centrosome amplification can negatively affect cell survival. Constitutive aneuploidy has been shown to have a detrimental effect on cells. Isogenic mammalian cells bearing one additional chromosome show slowed proliferation[40]. Centrosome amplification can also have a negative effect, as multipolar mitoses rarely produce viable progeny. Therefore, centrosome clustering has been proposed as a possible mechanism to allow survival of cells bearing extra centrosomes and generate aneuploidy[79]. Yet, whether the progeny of clustered mitosis or the one of bipolar mitoses with centriole rosettes is viable and contributes to growing cell populations, it is not known.

To distinguish among the progeny of different types of mitosis, cells were immunostained for an array of centriolar proteins: centrin, CEP152 and CEP170. Centrin was used to stain all centrioles. CEP152 is a marker for parental centrioles that are able to generate procentrioles during S phase[7]. CEP170 stains subdistal appendages, therefore is a late marker for centriole maturation[3].

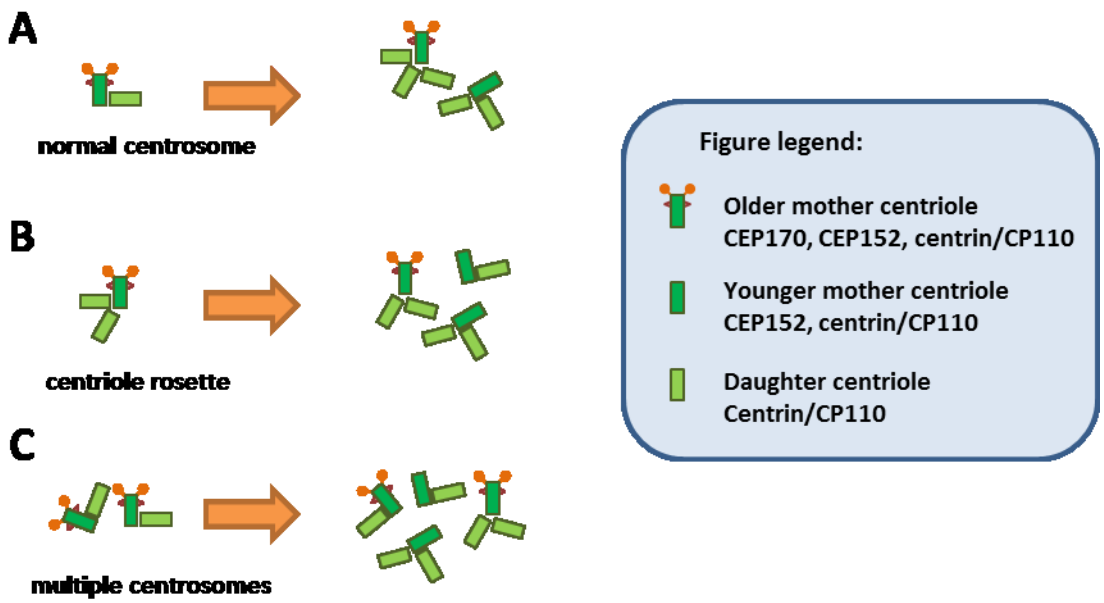

Figure 41 – Centrosome amplification patterns

(**A**) When centriole overproduction occurs in a cell with a normal centrosome complement, centriole rosettes are produced, with multiple procentrioles around a couple of parental centrioles, one of which harbors appendages. (**B**) If a cell has inherited a centriole rosette, centriole overproduction causes further rosettes formation. However, multiple parental centrioles are present. Of these, only one harbors appendages. (**C**) In clustered mitoses, a cell might inherit multiple mature centrosomes. Therefore, in this case, multiple fully mature centrosomes decorated with appendages are present.

In cells with centrosome amplification, different patterns could be recognized, depending on the specific generation that the cell is going through. Three different interdependent types are recognizable:

1st type – centriole overduplication in a cell with normal centriole content

Centriole overduplication occurs in a normal cell with two parental centrioles, both CEP152-positives, one of which is also CEP170-positive. In S phase multiple procentrioles are present, visible as more than 4 centrin signals (**Fig. 41A**).

2nd type – progeny of cells that have inherited a single centriole rosette

When a cell with two centriole rosettes enters mitosis, the daughter cells inherit one centriole rosette each. In the rosette, there is only a single CEP170-positive centriole. Presumably, all the centrioles in the rosettes are licensed for duplication and produce multiple (more than two) CEP152 signals. During S phase, each of the CEP152-positive centrioles produces multiple daughters (**Fig. 41B**).

3rd type – progeny of cells that have inherited multiple centrosomes

The progeny of the second type undergoes multipolar mitosis and if it progresses with a multipolar anaphase, each daughter cell will inherit a single centrosome (rosette). Depending on the number of daughters engaged, it can give rise to a cell of the first or second type. If mitosis is clustered, a single daughter cell inherits two or more mature centrosomes (rosettes), each of which has one centriole stained for CEP170. Therefore, if a cell arises from a clustered mitosis, it will bear multiple (more than one) CEP170 signals (**Fig. 41C**).

By assessing the frequency of these 3 different types, it is possible to calculate the relative contribution of normal mitoses, bipolar mitoses with centriole rosettes and clustered mitoses to the cell population.

U2OS-eGFP-PLK4 cells were induced over a period of 8 days. Each day a series of coverslips was fixed in methanol and processed for immunofluorescence microscopy. Two different sets of antibodies were used: anti-CEP170 plus anti-centrin, and anti-CEP152 plus anti-centrin. Image analysis was performed in collaboration with Anna Cazzola.

CEP170 staining produced a ring-shaped signal around a centriole (**Fig. 42A**). CEP152 gave a dot-like specific staining, colocalizing with centrin signals. In **Fig. 42A**, it can be appreciated how each CEP152-positive parental centriole is producing an array of daughter centrioles around it, forming a rosette.

EGFP-PLK4 induction quickly led to high levels of centrosome amplification that thereby remained above 70% for all time-points (**Fig. 42B**). Cells bearing extra CEP152 signals rapidly rose over the first three days, then starting to steadily decline again (**Fig. 42C**). On the other hand, the vast majority of cells showed a single CEP170 signal at all time-points (**Fig. 42C**).

These results imply that cells of the second type represent the majority of the cell population at each time point. Before the 48 hour time point, there is still a substantial fraction of cells belonging to the first type. Cells of the third type are accounting for less than 10% of the total cell population in all cases.

These results strongly suggest that the progeny of cells inheriting a single centriole rosette are the majority of cells in a population under continuous centrosome amplification. These cells are necessarily arising from bipolar mitoses with centriole rosettes. On the other hand, the progeny of clustered mitoses accounts only for a minority of growing cells.
Therefore, bipolar mitoses with centriole rosettes, but not clustered mitoses, are the main contributors to the growing cell population, in this setting.

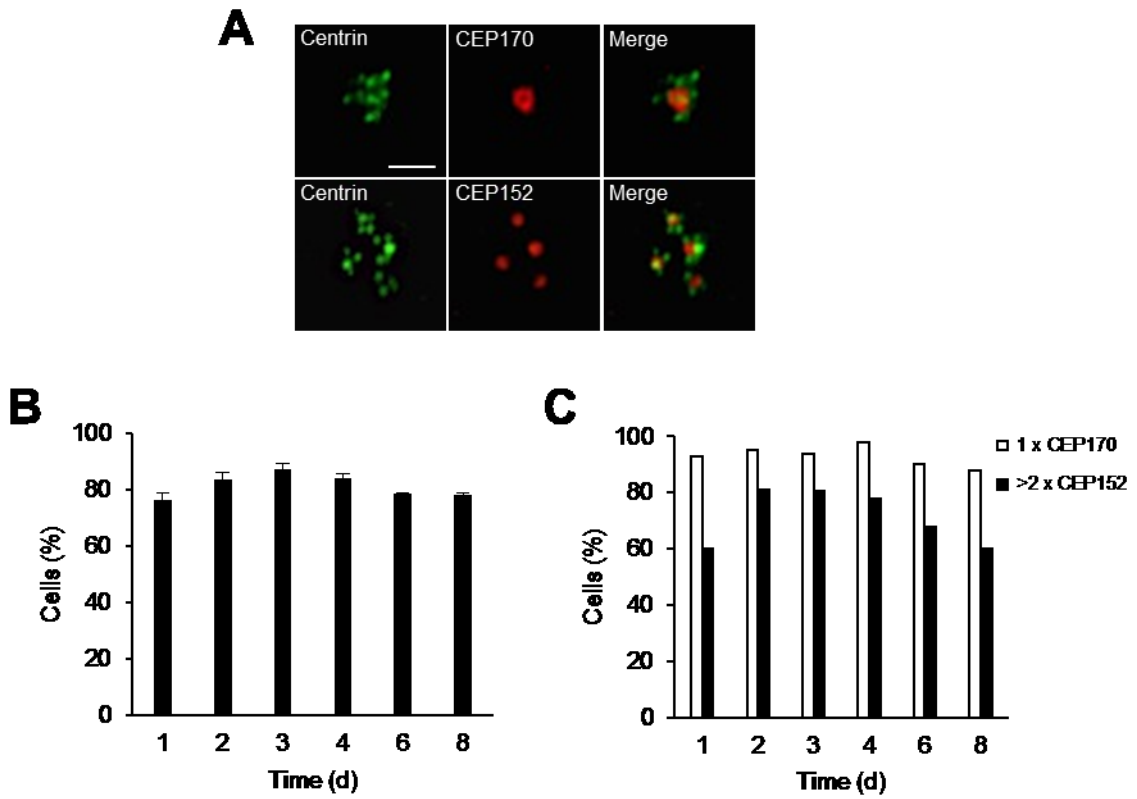

Figure 42 – Centrosome amplification pattern following continuous PLK4 expression

U2OS-eGFP-PLK4 cells were grown on coverslips and induced. Cells were fixed at different time points and stained for centrin (green) and CEP152 (red) or CEP170 (red) with specific antibodies. Nuclei were counterstained with Hoechst 33342 (blue). (**A**) CEP170 staining showed a ring-shaped signal around the older mother centriole. Anti-CEP152 stained all parental centrioles. (**B**) Centrosome amplification levels as detected by centriole number counting (>4 centrioles per cell). Error bars: SD. (**C**) CEP170 and CEP152 signal numbers in cells harboring amplified centrosomes. At least 100 cells were counted.

2.4.2 CENTRIOLE OVERDUPLICATION LEADS TO ACTIVATION OF THE p53 PATHWAY

It has been previously shown that centriole overduplication triggered by Plk4 overexpression leads to p53 stabilization and, as a consequence, to cell cycle arrest[102]. To independently confirm this effect, we investigated p53 pathway activation following eGFP-STIL overexpression.

Normally, p53 protein is kept at low levels through continuous degradation. However, in the presence of certain stressors, such as DNA damage, p53 becomes phosphorylated. This modification leads to p53 accumulation and activation of its transcriptional activity. Many genes transcribed by p53 are connected to cell cycle regulation. One of the most prominent transcriptional targets is p21, which acts as a cyclin/CDK inhibitor.

To test for p53 accumulation, U2OS-eGFP-STIL cells were induced for 72 hours and protein lysates were obtained. Additionally, another inducible cell line was used, that expresses eGFP-SAS6. A U2OS-GFP cell line constituted a negative control.

By immunoblot analysis we detected marked p53 stabilization after eGFP-STIL or eGFP-SAS6 overepression. On the other hand, p53 was present at low levels in non-induced cells or following eGFP expression (**Fig. 43A**). P21 protein levels mirrored the p53 results, consistent with its stabilization (**Fig. 43B**).

To further confirm that p53 activation resulted in cell cycle arrest, we investigated levels of two proteins that are present at high levels in mitotic cells, namely phopshorylated Eg-5 and Cyclin B1. In line with p53 activation and subsequent G1/S and G2/M phase arrest, we found a lower amount of these two mitotic markers (**Fig. 43C**).

These results confirmed that centriole overduplication is followed by p53 stabilization and that this phenotype does not depend on overexpression of a specific protein necessary for centriole amplification.

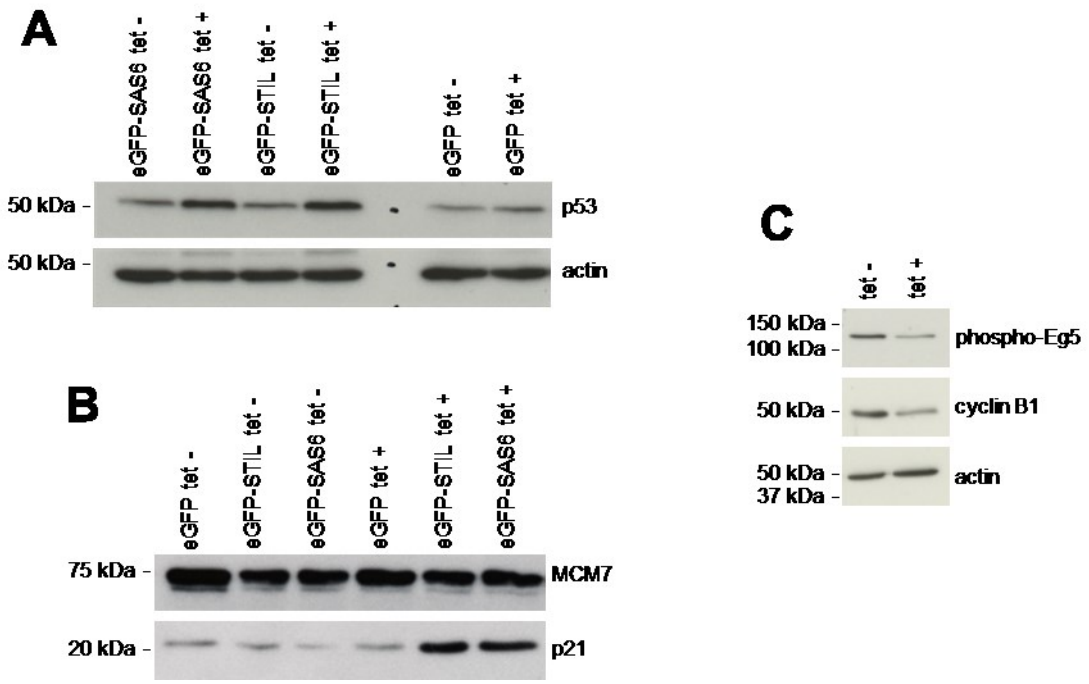

Figure 43 – p53 pathway activation following centriole overduplication

Cell lines were grown on coverslips, fixed and stained for immunofluorescence microscopy. U2OS-eGFP, U2OS-eGFP-STIL and U2OS-eGFP-SAS6 cells were induced for 72 hours. Protein lysates were obtained and analysis was performed by immunoblot with specific antibodies against p53, panel A; p21, panel B; phospho-Eg5 and cyclin B1, panel C. Actin or MCM7 were used as loading controls. Each experiment was repeated at least in triplicate. Representative immunoblots are shown.

2.4.3 CENTRIOLE OVERDUPLICATION RESULTS IN DECREASED CELL PROLIFERATION

To test whether p53 pathway activation following centriole overduplication results in cell cycle arrest, cell cycle profiling was performed by flow cytometry analysis.

For this purpose, U2OS-eGFP-STIL and U2OS-eGFP-SAS6 cells were induced for 72 hours to induce centriole overduplication. U2OS-eGFP cells were used as a negative control. Following induction, cells were harvested and fixed in methanol as cell suspension. Samples were permeabilized and stained with propidium iodide (PI), which binds stoichiometrically to DNA. At flow cytometry analysis, PI signal intensity linearly correlates to the DNA content of the cell. Two main peaks are shown corresponding to G1 and G2 phases.

After eGFP-STIL or eGFP-SAS6 induction, we observed a mild increase in the G1 phase peak of the cell cycle profile and a decrease in the S phase fraction. No change in the cell cycle profile was observed following eGFP overexpression as shown in **Fig. 44**.

This result suggests that p53 activation in cells harboring centriole overduplication leads to a mild proliferation block.

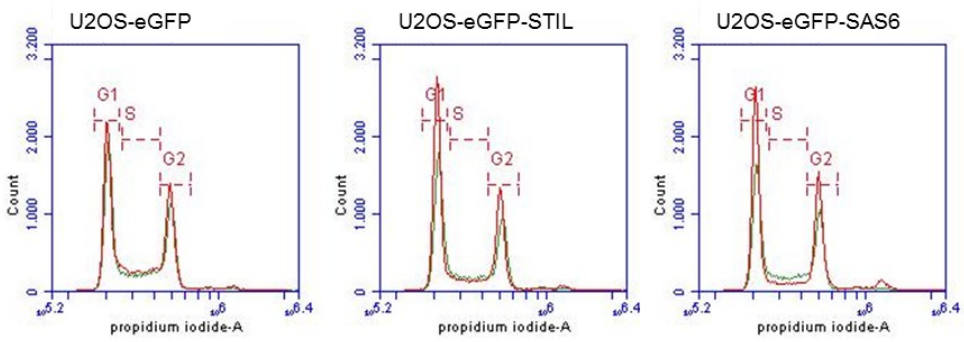

	G1 fraction	S fraction	G2 fraction
GFP tet -	45.33%	19.97%	31.13%
GFP tet +	43.83%	21.19%	30.95%
STIL tet -	46.88%	18.00%	30.77%
STIL tet+	52.72%	12.03%	30.57%
SAS6 tet -	44.57%	18.95%	32.03%
SAS6 tet +	50.29%	8.77%	33.93%

Figure 44 – Flow cytometry cell cycle profiling following centriole overduplication induction

U2OS-eGFP, U2OS-eGFP-STIL and U2OS-eGFP-SAS6 cells were induced for 72 hours. Cells were harvested and stained with PI for flow cytometry analysis. At least $3*10^4$ cells were measured per condition. Representative dot plots are shown. The cell cycle distribution was analyzed for induced (*red curve*) and non-induced cells (*green curve*). Values relative to the regions labeled as G1, S and G2 are reported in the table.

2.4.4 CENTRIOLE OVERDUPLICATION INDUCES A PERSISTENT PROLIFERATION ARREST

To further confirm the emergence of an anti-proliferative response following centriole overduplication, we measured the amount of proliferating cells by 5-bromo-2'-deoxyuridine (BrdU) incorporation assay.

BrdU is a nucleotide analog that can be incorporated instead of thymidine into the newly synthesized DNA strand during S-phase. The cells that have incorporated BrdU can be subsequently identified via immunofluorescence with BrdU-specific antibodies.

To determine the percentage of cells entering S-phase, U2OS-eGFP-STIL cells were induced for 72 hours and incubated with 100 µM BrdU the last 2 hours. The U2OS-eGFP cell line was used as a negative control. Cells were then fixed and DNA was denatured by 2N HCl incubation. Cells were stained for immunofluorescence. Replicating cells were identified with an anti-BrdU antibody.

Following eGFP-STIL overexpression, the percentage of BrdU negative cells increased roughly by 20%, suggesting that fewer cells are entering S phase at any time, further supporting a p53-driven cell cycle arrest (**Fig. 45A**).

To test whether the observed arrest was irreversible, we performed a long term BrdU incorporation assay. Following 72 hours induction, U2OS-eGFP-STIL cells were exposed to 10 µM BrdU for 48 hours in tetracycline-free medium, to detect the presence of quiescent cells.

In this situation, eGFP-STIL cells displayed a sharp increase in the percentage of BrdU-negative cells, indicating that these cells were viable but did not divide during the last 48 hours (**Fig. 45B**).

These results clearly indicate that a significant fraction of cells harboring centriole amplification experiences a permanent cell cycle arrest.

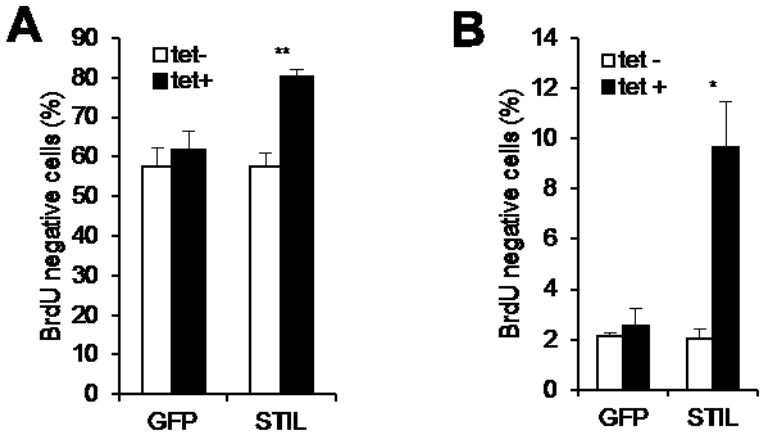

Figure 45 – Flow cytometry cell cycle profiling following centriole overduplication

U2OS-eGFP and U2OS-eGFP-STIL cells were grown on coverslips and induced for 72 hours. In addition cells were exposed to in 100 µM BrdU during the last 2 hours (**A**) or tetracycline was removed and cells were further grown for 48 hours with 10 µM BrdU (**B**). Cells were fixed and stained for immunofluorescence with anti-BrdU antibodies. The percentage of BrdU negative cells was assessed for induced (*black bars*) or non-induced cells (*white bars*).

2.5 CENTRIOLE ROSETTES IN PRIMARY HUMAN MALIGNANCIES

2.5.1 ROSETTES AROUND TWO PARENT CENTRIOLES CONSTITUTE A FREQUENT FINDING IN PRIMARY HUMAN MALIGNANCIES

To determine whether centriole rosettes are contributing to human malignancies *in vivo*, primary human leukemia samples were stained for an array of centriolar proteins.

Centrosome abnormalities have been described in leukemia and lymphomas, where in some instances they correlate with aneuploidy and disease aggressiveness[103]. A study showed that acute myeloid leukemia (AML) cells bearing high levels of centrosome amplification are associated with the adverse prognosis risk stratification group, suggesting that centrosome abnormalities might be involved in the development of karyotype alterations[104].
Moreover, many hematopoietic pre-malignant states, such as myelodysplastic syndromes and aplastic anemia, have an aneuploid karyotype. In these cases as well, karyotype is a predicting factor to assess the risk of evolution into AML. A study showed a correlation between supernumerary centrosomes and aneuploidy in these diseases[105].
However, a major drawback in these studies was the utilization of anti-PCNT or anti-γ-tubulin antibodies to score centrosome aberrations which is not accurate enough to detect centriole abnormalities.

To investigate the specific type of centriole amplification occurring in primary human malignancies, 35 acute myeloid leukemia and 9 acute lymphoblastic leukemia bone marrow samples were immunostained.

Mononucleated cells were isolated by gradient centrifugation. Cells were then placed on coverslips by cytospin centrifugation and fixed in methanol. This fixation method allowed obtaining satisfying staining conditions for the antibodies used. Then, cells were processed for immunofluorescence microscopy in collaboration with Anna Cazzola.

An array of antibodies against centriolar proteins was used:

- Centrin, all centrioles
- CP110, mature procentriole capping, all centrioles
- CEP170, subdistal appendages, older mother centriole
- CEP152, parental centrioles
- GT335, polyglutamylated tubulin, parental centrioles
- Centrobin, daughter centrioles

Centrosomes could be detected in the vast majority of cells. Example stainings are presented in **Fig. 46A**. Cells bearing centriole amplification could be observed alongside with cells having normal centriole content. To confirm that supernumerary centrin signals constituted actual centrioles and not centriole satellites (see chapter 1.3.4), samples were costained with CP110, a marker of mature procentrioles. Double staining showed centrin-CP110 colocalization, confirming, indeed, occurrence of centriole overduplication. CEP170 staining revealed the presence of a single ring-shaped signal in most of the cases. CEP152, GT335 and centrobin, which are parental centriole markers, showed two distinct signals in the majority of cells (**Fig. 46A**).

Taken together, these results show that, in hematological malignancies, supernumerary centrioles are often arranged around two parental centrioles, one of which is decorated with CEP170. This staining pattern is consistent with centriole overduplication occurring in a cell with normal centriole content. These cells are likely to form a bipolar spindle with centriole rosettes at their poles. However, whether this cell type is then undergoing mitosis is unknown, as mitotic figures are very rare in this kind of samples.

The images presented here constitute a very important result, as they are the first to describe the mode of centriole overduplication in primary human hematological malignancies.

To further confirm the occurrence of centriole overduplication in human malignancies, glioblastoma samples were investigated as well.

Glioblastoma is the most frequent brain cancer type in humans. Multipolar mitoses have been occasionally observed in glioblastoma cell lines and connected to amplified centrosomes. In glioblastoma, amplified centrosomes have been associated with high grade tumors and higher Aurora A expression[106].
In one study, a glioblastoma cell line was shown to undergo multipolar mitoses at high frequency. This was achieved by centrosome accumulation following cytokinesis abortion. Progeny of multipolar mitoses was reported to be viable, probably via ploidy reduction following multipolar mitosis[107].

Glioblastoma primary cell lines were provided by the Experimental Neurosurgery Division of the Neurosurgery Department of Heidelberg University from Prof. Christel Herold-Mende.

The cell lines used were registered with the following codes: NCH-149, NCH-342, NCH-343, NCH-354, NCH-357, and NCH-417. Cells at 2nd or 4th passage were grown on coverslips. After fixation in methanol, cells were processed for immunofluorescence microscopy.

Coverslips were stained for the same antibody panel used in for leukemia samples. Cells showed a remarkably similar centriole staining pattern to the one observed in hematological malignancies (**Fig. 46B**). Centrosome amplification was mostly constituted of a centrin cluster, with a single CEP170 signal and two CEP152 signals.
Importantly, these results confirmed the occurrence of centriole rosettes engaged to a single pair of parental centrioles in this type of solid tumor, as well.

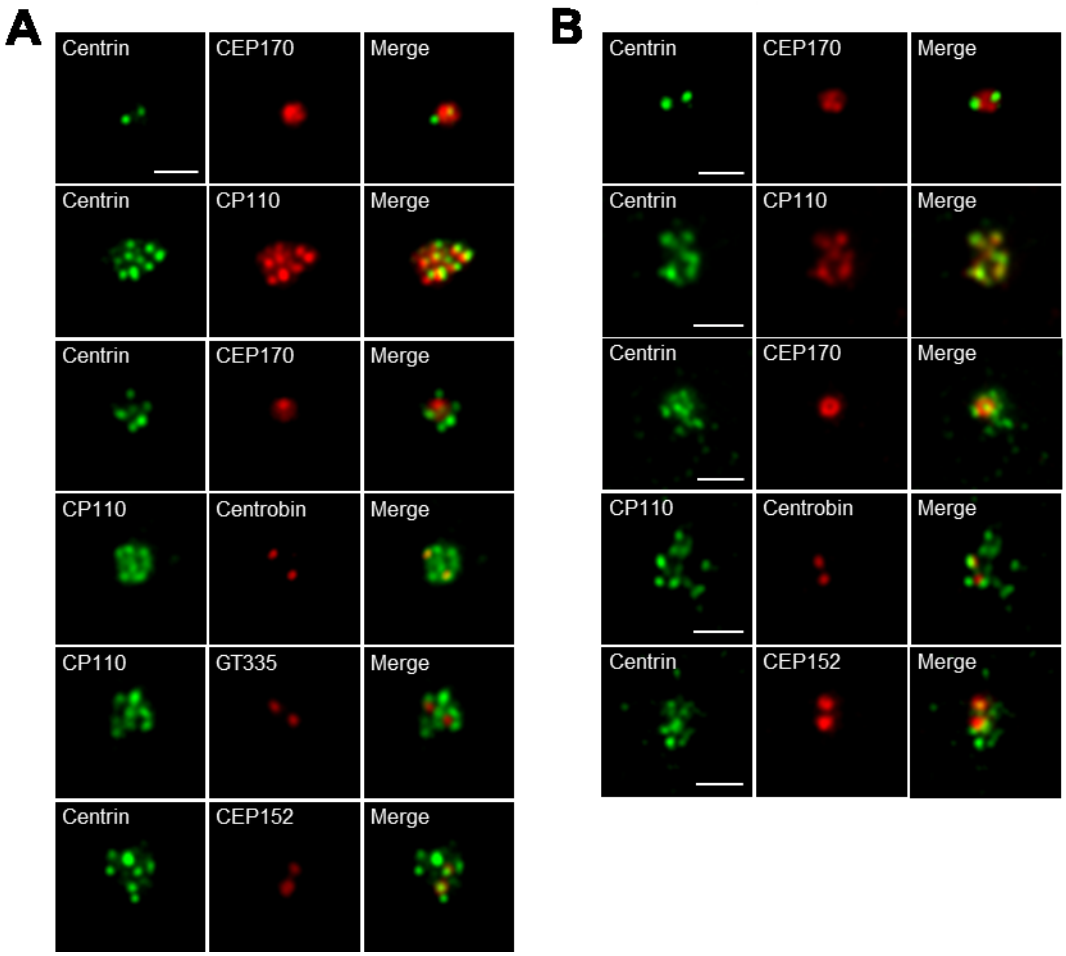

Figure 46 – Centrosome amplification features in primary human malignancies

Primary human samples of leukemia (**A**) and glioblastoma (**B**) were plated on coverslips and fixed. Immunofluorescence was performed with specific antibodies. Scale bar: 2 μm.

To determine the relative contribution of different centrosome amplification types in human malignancies, their frequency was assessed in primary leukemia samples and glioblastoma cell lines.

Quantification of signals revealed a very similar pattern among human malignancies.
Similarly to what reported in chapter 2.4.1, for the U2OS-eGFP-PLK4 cell line, in the vast majority of cases amplified centrosomes are constituted by a single fully mature centriole decorated with CEP170 in a parental centriole pair as shown by CEP152 (**Fig. 47**).
Polyglutamilated-tubulin staining (GT335) staining gave a satisfactory signal only in leukemia samples, but it further confirmed the presence of two parental centrioles.
Notably, glioblastoma samples showed a lower amount of cells with single CEP170 and double CEP152 staining suggesting a possible, although minor, role for clustered mitosis in this tumor (**Fig. 47**).

Taken together, these results strongly argue in favor of centriole overduplication, around a pair of parental centrioles, as the main mechanism of centrosome amplification in human malignancies.

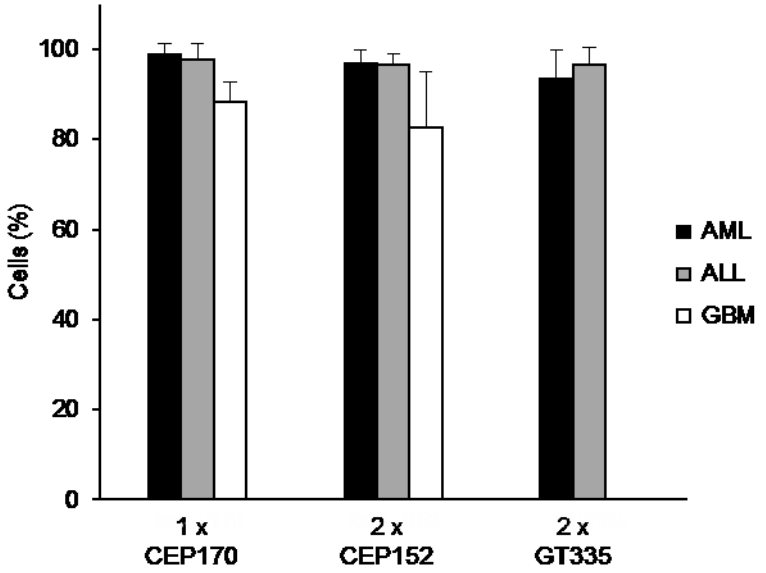

Figure 47 – Centrosome amplification patterns quantification in primary human malignancies

Leukemia bone marrow samples were cytospun on slides. Glioblastoma cell lines were grown on coverslips. Both types of samples were fixed in methanol-acetone and stained with specific antibodies. Nuclei were counterstained with Hoechst 33342. Sets of bars represent percentages of cell harboring a single CEP170 signal, two CEP152 signals or two GT335 signals. At least 100 cells were counted for each sample. Error bars: SD.

CHAPTER 3

DISCUSSION AND CONCLUSIONS

3.1 MECHANISM OF CHROMOSOMAL INSTABILITY INDUCTION BY ASYMMETRIC CENTRIOLE ROSETTES

3.1.1 BIPOLAR MITOSIS WITH CENTRIOLE ROSETTES AS A SOURCE OF CIN IN HUMAN MALIGNANCIES

Centrosome abnormalities are detected in a wide variety of tumors, both solid and hematological. The spectrum of such abnormalities encompasses both structural and numerical aberrations. Abnormal centrosome numbers are, by far, the most commonly reported finding and the most studied ones[61,108].

Supernumerary centrosomes are currently proposed to be an important source of CIN and aneuploidy in cancer. Recently, two studies have described a possible mechanism explaining this association. In the current view, supernumerary centrosomes assemble multipolar spindles in early mitosis and cluster into a bipolar arrangement before anaphase onset. The occurrence of transient multipolar intermediates promotes the formation of merotelic attachments and CIN[79,80]. Although this mechanism provides an explanation for the high rates of lagging chromosomes that are observed in some cancer cell lines, it does not rule out other types of centrosome abnormalities contributing to CIN.

The work presented here demonstrates for the first time that centriole rosettes, defined as multiple procentrioles engaged to a single parent, generate spindle asymmetry that promotes kinetochore-microtubule attachment errors and ultimately results in CIN. This mechanism is independent of the generation of multipolar mitoses and centrosome clustering. Importantly, the model presented here is complementary to the currently accepted hypothesis, as generation of centriole rosettes is a necessary stage preceding the appearance of supernumerary centrosomes.

Despite the evidence accumulated for the connection between centrosome abnormalities and CIN, the mechanisms underlying generation of supernumerary centrosomes in human cancer remains highly speculative[1,61]. In this work, we showed that centriole rosettes are a common finding in primary human malignancies. The detection of centriole rosettes provides, for the first time, strong evidence for the occurrence of centriole overduplication as one of the mechanisms of centrosome amplification *in vivo*. Furthermore, it suggests that spindle asymmetry induced by centriole rosettes may be a common cause for the generation of CIN in human cancer.

3.1.2 CENTRIOLE ROSETTES GENERATE ANAPHASE LAGGING CHROMOSOMES AND CIN

In this study, two cell line models conditionally expressing eGFP-STIL or eGFP-PLK4 were used to induce centriole overduplication and subsequently to investigate the influence of centrosome rosettes on chromosome segregation fidelity. Overexpression of eGFP-STIL and eGFP-PLK4 resulted in centriole overproduction and formation of centriole rosettes, which preceded the formation of supernumerary centrosomes.

Overexpression of eGFP-STIL resulted in the generation of CIN, similarly to what has been reported for PLK4[27,102]. Following eGFP-STIL overexpression, centrosome amplification accumulated over time and, simultaneously an increase in CIN markers such as micronuclei and karyotype heterogeneity were observed.

We believe that micronuclei features associated with eGFP-STIL overexpression were compatible with the generation of micronuclei from lagging chromosomes at anaphase, as they contained at least one kinetochore and were less likely to contain double strand breaks. Moreover, kinetochore-containing micronuclei were more often present in cells harboring centrosome amplification, suggesting a connection with CIN. In line, we detected a time-dependent increase in karyotype heterogeneity of the cell line following eGFP-STIL overexpression, indicating an increase of chromosome missegregation errors concomitant with the accumulation of centrosome aberrations.

Although in these assays we were not able to discriminate the relative contribution of centriole rosettes and extra centrosomes to the observed CIN, the early appearance of CIN markers suggested that centriole rosettes could constitute a source of chromosome missegregation.

In support of this hypothesis, immunofluorescence staining of spindle pole structure at mitosis revealed a high frequency of bipolar mitoses with asymmetric, increased numbers of centrioles at spindle poles, likely arising from cells with two centriole rosettes entering mitosis.

A crucial finding of this study is that bipolar mitoses with centriole rosettes displayed an increase in anaphase lagging chromosome frequency. Importantly, this observation was further confirmed in spontaneously occurring mitoses across several cancer cell lines, suggesting that lagging chromosomes are connected to centriole rosettes *per se* and not to STIL or PLK4 expression levels. We believe that the recurrence of this finding across different cell lines and tumor types is due to a common mechanism dependent on the presence of centriole rosettes.

A live-cell imaging study shows that GFP-tagged anaphase lagging chromosomes segregate to the correct nucleus without generating aneuploidy in most of the cases[91]. Notably, by measuring the missegregation rate of chromosome 2 and 3, we were able to demonstrate that, in our case, anaphase lagging chromosomes indicate the occurrence of segregation errors and thus CIN.

3.1.3 CENTRIOLE ROSETTES GENERATE CIN VIA MEROTELIC ATTACHMENT FORMATION

Another important finding of this study was the decreased interkinetochore tension in bipolar metaphases with centriole rosettes. We believe that it represents a partial defect in kinetochore bi-orientation at the base of the promotion of merotelic attachments in these cells.

Anaphase lagging chromosomes originate from kinetochore-microtubule merotelic attachments generated earlier during mitosis[47]. At metaphase, only correctly bi-oriented kinetochores display full tension across sister kinetochores. Merotelic attachments, instead, are characterized by partially reduced tension[109,110]. In line with this notion, the interkinetochore distance at metaphase was partially reduced following eGFP-STIL and eGFP-PLK4 overexpression. Reduced interkinetochore tension occurred in bipolar mitoses with centriole rosettes across all different cell lines analyzed and with spontaneously occurring rosettes as well. This observation mirrored what we observed in the case of lagging chromosomes and suggested that this bi-orientation defect might be casually related to the generation of CIN.

As merotelic attachments are not detected by the SAC, their presence results in CIN without delaying mitosis[99,111]. In agreement with this, mitosis duration was not extended in the presence of centriole rosettes. This was further confirmed by the finding that, following eGFP-STIL induction, no difference in the SAC activation level was observed, as measured by BubR1 quantification at kinetochores. Mitosis progressed normally without any significant differences in chromosome alignment and segregation, except for the occurrence of anaphase lagging chromosomes.

Taken together these results strongly argue for the generation merotelic attachments left uncorrected at the origin of the CIN observed in presence of pairs of centriole rosettes.

As mentioned above, multipolar mitoses also promote the formation of merotelic kinetochore-microtubule attachments and centrosome clustering is deemed responsible for CIN in cancer lines harboring centrosome amplification[79,80].

We propose that centriole rosettes constitute an additional source of merotelic attachment formation in addition to what was previously reported. The presence of only two spindle poles implies that, in our case, CIN originates from a mechanism different from clustering. However, given the intrinsic relation between centriole rosettes and formation of extra spindle poles, both mechanisms may operate in cancer cells depending on their specific centrosome amplification stage.

Merotelic attachment correction relies on the regulation of microtubule turnover at kinetochores[99]. It has been previously shown that in order to ensure SAC satisfaction and error correction, microtubule turnover is kept within a narrow range and even slight deregulation can have a significant impact on chromosome segregation fidelity[56,57]. Therefore, regulation of microtubule dynamics plays an important role in the promotion of chromosome bi-orientation[59].

Indeed, when cells are exposed to microtubule poisons the frequency of merotelic attachments dramatically increases. In these cases, the error correction machinery can become quickly saturated, resulting in anaphase entry with unresolved merotelic attachments. However, delaying anaphase onset provides extra time for error correction and merotelic attachments can be resolved, reducing chromosome missegregation[56].

The unchanged duration of mitosis and the absence of SAC activation in cells bearing centriole rosettes would support this view on error correction saturation, if merotelic attachments are promoted at a high rate. However, we observed that extending metaphase duration by addition of MG132 did not rescue the reduced interkinetochore tension in eGFP-STIL overexpressing cells.

We believe that this finding argues against a mere saturation of the error correction machinery. On the contrary, it suggests the possibility that the presence of centriole rosettes is interfering with the correction mechanism itself.

3.1.4 CENTRIOLE ROSETTES INTEFERE WITH THE CORRECTION OF KINETOCHORE-MICROTUBULE ATTACHMENTS

Correction of improperly attached kinetochores is based on a tension-dependent mechanism. If a kinetochore-microtubule attachment does not generate tension, as in the case of merotelic attachments, correction is achieved in two steps: microtubules are actively released from the kinetochores and new ones are captured[47,99]. It has long been known that detachment of improperly attached microtubule fibers constitutes the rate-limiting step in correction of abnormal attachments, while microtubule capture works efficiently on a broad angle[112].

Reduced interkinetochore tension in the presence of centriole rosettes suggests that kinetochores are engaging the error correction mechanism in this setting.

In our hands, stimulation of the detachment rate, by MCAK and KIF2B overexpression, decreased the frequency of anaphase lagging chromosomes in control cells. Importantly, lagging chromosomes were not rescued when PLK4 was overexpressed. We believe that the selective absence of an effect in PLK4-overexpressing cells may be explained by permanent interference of centriole rosettes with the correction machinery.

This result stands out as compared to findings reported by other groups, being the first report of chromosome missegregation that cannot be rescued by enhancement of the error correction machinery.

In one study by Bakhoum and collegues, it has been reported that cancer cells are characterized by harboring hyperstable kinetochore-microtubule attachments, slowing down detachment rates. This causes an increased frequency of anaphase lagging chromosomes in bipolar anaphases. However, their frequency decreases following MCAK and KIF2B overexpression[57]. In accordance with what was described in that study, we observed a selective decrease of the lagging chromosome frequency in isogenic controls, confirming that U2OS cells *per se* display a certain degree of hyperstable kinetochore-microtubule attachments. Nonetheless, such reduction was absent following PLK4 overexpression.

In another study by Ertych and collegues, increased microtubule assembly rates in bipolar mitoses have been proposed as a possible source of anaphase lagging chromosomes. Similarly to what has been described for hyperstable attachments, the alteration of microtubule dynamics ultimately results in a decreased turnover at kinetochores. Importantly, extending mitosis duration or restoring normal

microtubule dynamics also rescues anaphase lagging chromosome frequency[113]. Although being an appealing hypothesis, different from what reported in that study, we observed that kinetochore fiber stability was not affected following induction of centriole amplification. Moreover, as already mentioned, extension of metaphase duration did not rescue the reduction of interkinetochore tension.

The fundamental disagreement of our findings with those studies requires an alternative explanation for the generation of merotelic attachments and anaphase lagging chromosomes when centriole rosettes are present.

We believe that, following overexpression of PLK4, the presence of centriole rosettes overrides error correction without interfering with microtubule turnover. Taken together, our results support the existence of an alternative mechanism based on centriole rosettes that does not interfere with the detachment step of error correction, but rather alters the capture of new microtubules.

3.1.5 ASYMMETRIC CENTRIOLE ROSETTES ALTER THE CHANCE OF MICROTUBULE CAPTURE BY KINETOCHORES

Centrosome-nucleated microtubules probe the cytoplasmic space in search of kinetochores. This search and capture behavior is the predominant mechanism in mitosis to ensure bi-orientation. Other additional pathways integrate this mechanism to shorten the time of mitosis[114]. An intriguing hypothesis is that centriole rosettes may affect this search and capture mechanism.

Insight into how centriole rosettes induce CIN first came from the different efficiency of eGFP-STIL and eGFP-PLK in centriole overduplication, with higher numbers of centrioles per rosette in case of eGFP-PLK4, as compared to eGFP-STIL overexpression.

Both PLK4 and STIL overexpression were characterized by the occurrence of bipolar mitoses with centriole rosettes. However, the relative frequency of cells with centriole rosettes was different in the two cell lines, reflecting the higher efficiency of PLK4 in inducing centriole overduplication.

This difference was likely due to the higher number of daughter centrioles that were formed per parent centriole, as confirmed by the number of centrin signals per rosette both in interphase and mitosis. Accordingly, STIL overexpression required more time as compared to PLK4, to reach higher levels of centriole amplification.

Although the number of centrioles per rosette was different, their effect on the frequency of anaphase lagging chromosomes was remarkably similar. The results we obtained in other cancer cell lines pointed in the same direction, supporting the idea that the mere number of centrioles at spindle poles might not be causing CIN *per se*.

On the other hand, we observed that anaphase lagging chromosomes were more often found in mitoses with asymmetric numbers of centrioles in PLK4-overexpressing cells. This finding provided a satisfactory explanation about why cell lines with both large and small amounts of centrioles in rosettes display

comparable lagging chromosome frequencies. Furthermore, it suggested that centriole rosettes might interfere with the search-and-capture mechanism by disrupting spindle symmetry.

The data gathered on microtubule dynamics in interphase cells showed that supernumerary centrioles were associated with an increased microtubule numbers and microtubule polymer mass, similarly to what has been reported previously by Godinho and collegues[82]. This phenotype was likely due to an increase in the ability of centrosomes to recruit PCM, which could be detected by pericentrin quantification already after 15 hours of PLK4 overexpression. Moreover, the amount of PCM correlated with centriole numbers at the centrosome. Therefore, it is likely that supernumerary centrioles contribute to PCM recruitment.

We propose that a similar enhancement may occur during mitosis and, as a result, asymmetric centriole rosettes nucleate unequal numbers of microtubules. This imbalance would, in turn, interfere with the search and capture mechanism by skewing the probability of microtubule binding toward the prominent spindle pole. It remains to be determined how daughter centrioles influence PCM recruitment and microtubule numbers in mitosis.

Similar to this hypothesis, CPAP depletion has been shown to impair daughter centriole maturation and ultimately results in mitoses where spindle poles display asymmetric features. The younger mother centriole lacks centriolar appendages and recruits less PCM at the spindle pole. Importantly, these mitoses are characterized by a higher frequency of anaphase lagging chromosomes[115].

We noticed that anaphase lagging chromosomes occurred significantly more often as paired signals in the presence of centriole rosettes. Previous work has established that merotelic kinetochores often acquire an elongated, distorted morphology and in some instances the kinetochore signal can split. However, in this case the two signal domains have different size and intensity[47,116].

In our setting, the paired lagging signals showed similar size and intensity, therefore resembling couples of sister chromatids. Indeed, it has been previously proposed that, when a kinetochore attaches merotelically, this results in rotation of the kinetochore pair and exposure of the sister kinetochore to binding from both poles, increasing the likelihood for further merotelic attachment[111]. Therefore, we reasoned that the presence of spindle pole asymmetry would increase the frequency of these events: given equal exposure to both poles, kinetochore capture would still favor the pole associated with more microtubules, promoting spreading of merotelic attachments across sister kinetochores and resulting in paired lagging chromosomes.

We propose that the presence of asymmetric centriole rosettes at spindle poles disrupts the search and capture mechanism by producing an imbalanced amount of microtubules from the two half-spindles.

3.1.6 A MECHANISM LINKING SPINDLE ASYMMETRY AND CHROMOSOMAL INSTABILITY

Taken together, we demonstrated that centriole rosettes in bipolar mitoses generate CIN primarily by disruption of spindle pole symmetry. In this setting, asymmetry is created by an unequal number of daughter centrioles at poles, which affects microtubule anchoring and nucleation during mitosis, in a manner similar to what has been shown in interphase cells with supernumerary centrioles.

In asymmetric mitosis, the search and capture mechanism is biased toward binding from the prominent spindle pole. This causes an increased likelihood for kinetochores to interact with microtubules originating from a dominant centrosome, generating syntelic and merotelic attachments (**Fig. 48**).

We believe that the error correction machinery cannot resolve improper attachments in the presence of asymmetric rosettes, because increasing microtubule detachment rates cannot overcome the biased capture.

Under these conditions, kinetochore bi-orientation is impaired and cells enter anaphase with unresolved merotelic attachments. This is followed by generation of anaphase lagging chromosomes and segregation errors (**Fig. 48**).

In summary, the promotion of merotelic attachments in early mitosis by biased search and capture, together with interference with error correction provides an explanation for the CIN associated with asymmetric pairs of centriole rosettes.

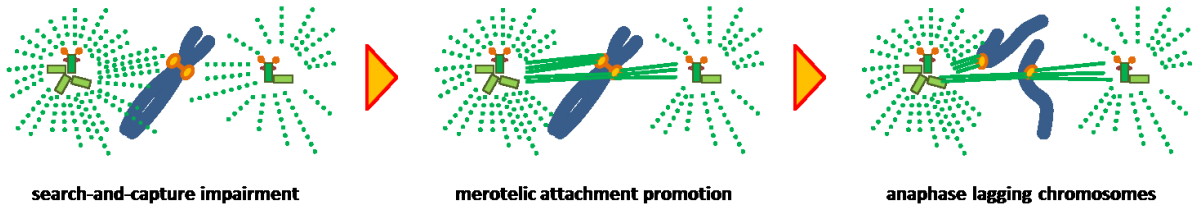

Figure 48 – Mechanism of CIN induction by asymmetric centriole rosettes

The presence of asymmetric centriole rosettes produces unequal numbers of microtubules emanating from the two spindle poles. This imbalance interferes with the search-and-capture mechanism as it increases the likelihood for kinetochores of capturing microtubules connected to the prominent spindle pole. As a result, merotelic attachment formation is promoted during early mitotic stages. In addition, this asymmetry irreversibly impairs the functioning of the kinetochore-microtubule attachment error correction mechanism, with merotelic attachments persisting unresolved. This ultimately results in anaphase lagging chromosome generation and chromosome missegregation.

The possibility that centrioles regulate microtubule numbers emanating from the centrosome is very appealing. It has been established that mitosis can be completed in the absence of centrioles[117]. In this case kinetochores produce microtubule fibers that are then focused in a bipolar arrangement. However, the spindle structure is disorganized and chromosomes are prone to missegregation[118]. On the other hand, when centrosomes are present, kinetochore-driven microtubule formation is less prominent and the search and capture mechanism is favored, as microtubule nucleation occurs mainly at centrosomes[119].

We propose that centriole duplication is carefully regulated because centriole numbers regulate the amount of microtubule fibers on half-spindles. Only the presence of equal microtubule numbers ensures the efficacy of the error correction mechanism and thus minimizes chromosome missegregation events.

3.2 RELEVANCE OF CENTRIOLE OVERDUPLICATION IN HUMAN CANCER

3.2.1 EXTRA CENTROSOMES ARE NEGATIVELY SELECTED

We examined the relative contribution of bipolar mitoses with centriole rosettes and multipolar mitoses to progeny formation under 8 days of continuous PLK4 overexpression. By assessing the number of parental centrioles and fully mature mothers in groups of supernumerary centrioles we were able to infer whether cells inherited a single rosette or a cluster of centrosomes. Unexpectedly, despite more than 70% of the cells harbored amplified centrosomes at all time points and even if cells underwent several divisions, we observed no increase in the fraction of cells arising from clustered mitoses. On the other hand, living cells were mainly derived from bipolar mitoses with rosettes including divisions at late time points. Although we cannot exclude the possibility that PLK4 overexpression alters the pattern of centrosome maturation, these findings suggested that centriole rosettes produced viable progeny while clustered mitoses did not.

In support of this hypothesis, we have produced evidence that, under continuous induction of centriole overduplication, a significant fraction of cells experience p53 pathway activation and persistent cell cycle arrest, in accordance to what previously reported following PLK4 overexpression[102]. We believe that the progeny of clustered mitoses could largely contribute to the fraction of cells undergoing proliferation arrest.

Other results further arguing in favor of negative selection for cells harboring extra centrosomes were collected by my colleague Dr. Gleb Konotop, who has investigated the fate of cells arising from bipolar, clustered and multipolar mitoses in HeLa cells overexpressing HA-PLK4 (**Fig. 49**). Bipolar mitoses produced progeny with more than 80% viability over two generations while multipolar mitoses did not produce any viable offspring, similar to what was previously described by Ganem and collegues[79]. However, clustered mitoses also showed a relatively poor viability with only 30% of cells surviving the first generation and of these, only around 25% surviving the second division.

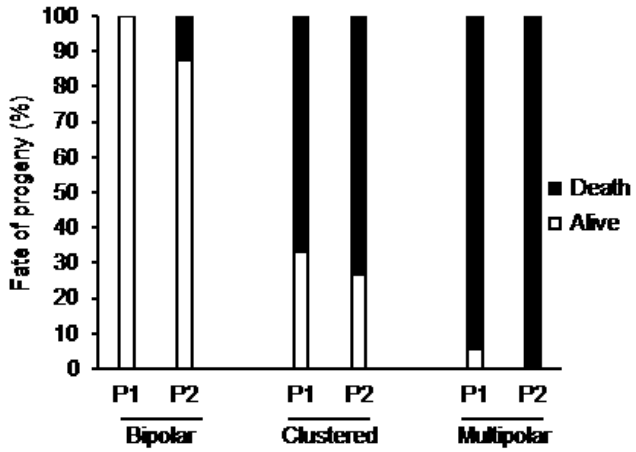

Figure 49 (*courtesy of* Dr. *Gleb Konotop*) – Fate of the progeny following PLK4 overexpression in HeLa-HA-PLK4-dendra-centrin2 cells

HeLa-HA-PLK4-dendra-centrin2 cells were induced for 48 hours with tetracycline and imaged for 72 hours. Mitotic cells were detected and the fate of the daughter cells arising from them was followed across several generations. The percentage of dead and alive cells within each generation is represented. P1: first generation; P2: second generation.

Taken together, these results strongly argued for the possibility of negative selection on the progeny of clustered mitoses. Several possibilities might explain this observation. The CIN generated by clustered mitosis may induce a high level of aneuploidy, which constitutes a burden on cell viability similarly to what happen to multipolar mitosis[79]. Alternatively, the delay imposed on mitosis by the clustering mechanism could elicit an apoptotic response[120]. Furthermore, as centrosome clustering is not completely efficient, the daughter cells would have a certain risk of undergoing a multipolar mitosis at each generation.

3.2.2 CENTRIOLE OVERDUPLICATION IS A COMMON CENTROSOME ABNORMALITY IN PRIMARY HUMAN MALIGNANCIES

An important point was to establish whether asymmetric centriole rosettes are a plausible mechanism generating CIN in primary malignancies.

It is commonly recognized that the collection of detailed data about centrosome amplification *in vivo* has been hampered by the intrinsic difficulties of producing a satisfactory immunostaining on paraffin-embedded histology sections and description of centrosome abnormalities has been limited to their morphological appearance[61,108]. To our knowledge, the vast majority of studies have relied on γ-tubulin and PCNT staining to detect both numerical and structural aberrations of centrosomes. Centriole content and especially maturation level has been poorly investigated so far.

We examined primary human malignancies for centrosome amplification features using immunofluorescence staining to distinguish mother and daughter centrioles. In order to obtain good quality staining we used freshly isolated cells, thereby avoiding the use of paraffin-embedding.

Another crucial finding of this study is that more than 80% of analyzed abnormal centrosomes consisted of supernumerary centrioles arranged around a single pair of parental centrioles, one of which was fully mature.

This result provides, for the first time, a clear insight on how centrosome amplification can occur in cancer. The presence of two parental centrioles, one of which is decorated with appendages is consistent with a normal centrosome complement before occurrence of overduplication[17]. Therefore, the presence of multiple centrin signals implies that all extra signals represented daughter centrioles produced during a single cell cycle. This pattern closely resembles what we observe after STIL or PLK4 overexpression, suggesting that centriole overduplication is the favored route to centrosome amplification *in vivo*.

Moreover, the presence of a single pair of parental centrioles is compatible with the formation of two spindle poles with asymmetric centriole rosettes in mitosis. This is supporting the hypothesis that CIN could be generated *in vivo* through the mechanism described in this thesis.

Given the small number of samples analyzed, we cannot exclude that extra centrosomes and clustered mitoses play a larger role in other types of cancer. Indeed, multipolar mitoses have been reported to be very frequent in some tumor types and extra centrosomes can be present in as much as 100% of cells in some cell lines[78,108]. Therefore, centriole rosettes and extra centrosomes constitute two distinct steps of the same process. Their relative prevalence might be dependent on the genetic background influencing overduplication as well as the tolerance and viability of clustered mitoses.

3.3 PERSPECTIVES

3.3.1 LOW LEVEL CENTRIOLE OVERDUPLICATION AS A VIABLE CIN PHENOTYPE

Centrosome amplification is associated with tumor aggressiveness and progression. It is detected at early stages of tumor development and in pre-malignant lesions, arguing for the involvement of this process in tumorigenesis[108]. Given the current evidence, centrosome amplification constitutes one of the major causes of CIN and aneuploidy in cancer[1]. In this regard, relative survival of bipolar, clustered and multipolar mitoses is a highly relevant question concerning centrosome amplification as a tumor-promoting mechanism.

While on one hand cells harboring extra centrosomes and multipolar mitoses are detected in tumor specimens, *in vitro* data showed that such cells are selected against. Moreover, our data on primary human malignancies indicated that the progeny of clustered mitoses did not contribute significantly to the spectrum of centrosome abnormalities observed, suggesting that extra centrosomes undergo negative selection *in vivo* as well. If the aneuploidy caused by clustered mitoses suppresses cell proliferation or viability, then the presence of supernumerary centrosomes would rather operate as a tumor suppressive mechanism.

On the other hand, the high frequency of centriole rosettes *in vivo* together with their ability to induce chromosome missegregation indicated that centriole rosettes might be the major centrosome defect causing CIN in human cancer.

We speculate that due to the intrinsic connection between centriole rosettes and extra centrosomes, centriole overduplication levels play a crucial role in ensuring a viable CIN phenotype.

In case of low level of centriole overduplication, the presence of centriole rosettes would not necessarily lead to extra centrosomes. In this situation, there is still a chance to produce asymmetric spindles, where one pole has a normal centriole content while the other does not. In many instances, we observed such cases as shown in **Fig. 30**. As a result, CIN would still be present, but one daughter cell would inherit a normal centrosome, avoiding the burden of extra centrosomes.

According to this model, centrosome amplification levels show tumor-promoting effects up to a certain threshold, which depends on both chromosome missegregation rate and aneuploidy tolerance. Above this threshold, the detrimental consequences of the aneuploidy generated overweigh the favorable ones with CIN becoming tumor-suppressive.

The existence of a threshold for the tumor-promoting potential of CIN is supported by several lines of investigation. Mouse model studies, where CIN was induced via disruption of the SAC, have shown contradictory results, with some models supporting a tumor promoting and other a tumor suppressive effect[121]. The double nature of CIN is also reflected in the clinical setting, where it is usually associated with several parameters and in particular with poor patient outcome. There are some studies showing that, on the other hand, a too high level of CIN is associated with a better outcome as compared to cases with lower levels of CIN[122].

The hypothesis that centrosome amplification levels might explain the double nature of CIN is appealing. Therefore, in depth analysis of the consequences of centrosome amplification on cell viability is of great importance and further studies are needed to address this question.

3.3.2 A CHANGE OF PARADIGM FOR CENTROSOME AMPLIFICATION AS A CANCER THERAPEUTIC TARGET

While supernumerary centrosomes are often present in cancer cells, they constitute a rare event in normal and benign tissues. Selective killing of cells harboring extra centrosomes has been investigated as a potential cancer therapy that would spare non-neoplastic cells. In particular, development of centrosome clustering inhibitors has been proposed as a strategy to kill cancer cells via induction of multipolar anaphases[123–125].

Several lines of evidence have shown the relative efficacy of substances like griseofulvin in inducing multipolar mitoses and cell death *in vitro*[126,127]. However, the therapeutic potential of clustering inhibition is questioned by the results of our study.

The hypothesis of clustering as druggable target is based on the fundamental assumption that this mechanism constitutes the only viable strategy for cancer cells to avoid the detrimental effect of supernumerary centrosomes[79]. In contrast to this, we showed that both clustered and multipolar mitoses experience negative selection and produced non-viable progeny. Moreover, in the primary samples analyzed we showed that centriole overduplication often occurs around a single pair of centriole parents. Therefore, the presence of supernumerary centrioles in cancer tissues does not always imply the presence of multiple centriole parents and the generation of multiple spindle poles.

If the spontaneous lethality of clustered mitoses is further confirmed, we believe that therapeutic targeting of centrosomes would require a change of paradigm. Given the detrimental effect of supernumerary centrosomes, one possible approach would be induction of centrosome amplification in cancer cells.

The virtual absence of centrosome abnormalities in healthy tissues is also connected to the intrinsic resistance of normal cells to centrosome amplification[17]. On the other hand, cancer cells seem susceptible to a broad array of stimuli, which result in production of supernumerary centrosomes[65,128]. Importantly, at least part of the efficacy of chemotherapeutic drugs and radiotherapy can be ascribed to induction of centrosome amplification in cancer cells, with subsequent generation of multipolar mitoses[129–131].

This difference opens the possibility of developing drugs that induce centrosome amplification selectively in cancer cells at a high level. Induction of centrosome amplification could represent an effective strategy to exploit the tumor-suppressive effect of CIN for killing cancer cells.

Another possibility would be promoting disengagement in centriole rosettes before mitosis onset. This strategy would allow the multiple daughter centrioles of a rosette to be released from the parental centriole and to possibly function as independent spindle poles. By that, a viable bipolar mitosis with centriole rosettes would be converted into a lethal multipolar mitosis.

3.4 OUTLOOK

The work presented here showed for the first time that centriole rosettes are causing CIN in bipolar mitoses. The mechanism underlying generation of chromosome missegregation by centriole rosettes was investigated. We concluded that asymmetric centriole rosettes produce unbalanced amounts of microtubule fibers, thereby promoting erroneous kinetochore-microtubule attachment formation. In addition, asymmetric centriole rosettes interfere with the correction of these erroneous attachments. Furthermore, we showed that centriole rosettes are a common finding in primary human malignancies, indicating that this mechanism can contribute to the generation of CIN *in vivo*. However, several open questions remain to be answered.

Further work is required to determine how daughter centrioles influence microtubule regulation at mitosis. We were able to detect a correlation between centriole numbers and microtubule mass in interphase cells. The possibility of measuring microtubule fibers at spindle poles was hampered by a 10-fold increased microtubule nucleation at mitosis. Therefore, regulation of centrosomal microtubule numbers at mitosis should be investigated in further detail.

DISCUSSION AND CONCLUSIONS

Centrosome clustering is proposed to represent a viable strategy for cells to cope with extra centrosomes and generate CIN. Contrary to this view, we have generated evidence that extra centrosomes might undergo negative selection regardless of the cell ability to cluster them at mitosis. Defining the impact of centrosome amplification on cell viability represents a crucial point to define its relationship to CIN.

We detected a relatively high frequency of centriole rosettes as compared to supernumerary centrosomes in primary human malignancies. Due to the small number of tumor samples analyzed we cannot exclude that centrosome clustering might play a prominent role in other cancer types or other patient subsets. Extending the analysis of centrosome amplification features to other malignancies represents an important issue for future research.

Our analysis of primary malignancies indicated centriole overduplication as a common route for the production of supernumerary centrosomes in human cancer. However we observed only rarely more advanced amplification stages, resulting from division of cells with centriole rosettes. Therefore, further work is required to determine whether cells with centriole rosettes are able to proliferate and produce viable progeny *in vivo*.

The role of centrosome amplification in tumorigenesis is still an unresolved question. Our results pointed out the importance of the severity of the CIN phenotype for the production of tumor-promoting effects. In this regard, more research should be focused on the generation of animal models with inducible centriole overduplication.

CHAPTER 4

MATERIALS AND METHODS

4.1 MATERIALS

4.1.1 REAGENTS

In this work, molecular biology grade or purest available reagents were used. All reagents including chemicals, antibodies and enzymes were obtained from the following companies: Abcam (Cambridge, UK), Biochrom (Berlin, Germany), Bio-Rad (Munich, Germany), BD Biosciences (Heidelberg, Germany), Carl Roth (Karlsruhe, Germany), Cell Signaling Technology (Danvers, USA), Exbio (Prague, Czech Republic), Dyomics (Jena, Germany), Eppendorf (Hamburg, Germany), GE Healthcare (Buckinghamshire, UK),Gibco (Eggenstein, Germany), Ibidi (Munich, Germany), Life Technologies (Darmstadt, Germany), Merck Millipore (Bedford, USA), New England Biolabs (Frankfurt, Germany), Progen (Heidelberg, Germany), Proteintech (Manchester, UK), Quiagen (Hagen, Germany), Roche (Basel, Switzerland), Roche Diagnostics (Mannheim, Germany), Santa Cruz (Heidelberg, Germany) Serva (Heidelberg, Germany), Sigma-Aldrich (Munich, Germany), Thermo Fisher Scientific (Lafayette, CO, USA) and Vector Laboratories (Burlingame, USA).

4.1.2 CONSUMABLES

For the purpose of this thesis, consumables from the following companies were employed: GE Healthcare (Buckinghamshire, UK), Starlab (Hamburg, Germany), Sarstedt (Nümbrecht, Germany), Eppendorf (Hamburg, Germany) and Whatman (Maidstone, UK).

4.1.3 PREPARATION OF SOLUTIONS

All solutions and media used for this work were prepared with double distilled water (ddH_2O) or Milli-Q water (Millipore, Bedford, USA). Solutions were sterilized by autoclaving them for 20 min at 121°C or by filtration through 0.22 µm filters (Millipore, Bedford, USA). Solutions were stored at room temperature unless otherwise stated. The pH was adjusted using a Seven Multi pH-meter (Mettler Toledo, Giessen, Germany). Centrifuges from the following companies were employed: Eppendorf (Hamburg, Germany), Heraeus (Hanau, Germany), Thermo Fisher Scientific (Lafayette, CO, USA).

4.2 MOLECULAR BIOLOGY METHODS

4.2.1 BACTERIA STRAIN

Plasmid DNA was cloned in *E. Coli* DHα strain F- ϕ80*lac*ZΔM15 Δ*(lac*ZYA-*arg*F)U169 *rec*A1 *end*A1 *hsd*R17(rK-, mK+) *pho*A *sup*E44 *thi*-1 *gyr*A96 *rel*A1 λ-.

4.2.2 EXPRESSION CONSTRUCTS

A complete list of the expression constructs used in this work is provided in Table 1.

Table 1 – Expression constructs used for mammalian cell transfections

Vector	Backbone	Tag	Resistance	Insert	Addgene ID
pYOY152	pEGFP-C1	eGFP	Kanamycin/Neomycin	MCAK	#29479
pMX230	pEGFP-C1	eGFP	Kanamycin/Neomycin	KIF2B	#13987
pH2B_mCherry_IRES_neo3	IRES_neo3	mCherry	Ampicillin/Neomycin	H2B	#21044

pYOY152 and pMX230 vectors were a kind gift from Dr. Bernardo Orr (Geisel School of Medicine at Dartmouth, Hanover, USA). pH2B_mCherry_IRES_neo3 vector was a kind gift from Dr. Linda Nötzold (DKFZ, Heidelberg, Germany).

4.2.3 HEAT SHOCK TRANSFORMATION OF BACTERIA

Transformation of competent *E. Coli* DHα bacteria was accomplished by heat shock transformation. Aliquots of deep frozen *E. Coli* DHα strain were thawed on ice for 10 minutes. 5 - 40 ng of plasmid DNA were added to 40 µL of competent bacteria and the mixture was incubated on ice for additional 30 minutes. Heat shock transformation was performed by exposing bacteria for 45 seconds to 42°C, quickly followed by 1 minute incubation on ice. Transformed bacteria were then transferred to 900 µL of SOC medium freshly supplemented with glucose, without antibiotics, and incubated for 90 minutes at 37°C under shaking. Bacteria were pelleted by centrifugation for 5 minutes at 600 x g, resuspended in about 100 µL of SOC medium and plated on LB-agar supplemented with an appropriate selection antibiotic.

SOC medium	
Trypton	2% w/v
Yeast extract	0.5% w/v
NaCl	0.05% w/v
KCl	2.5 mM
$MgCl_2$	10 mM
Glucose	20 mM
pH	*7.0*

4.2.4 CULTIVATION OF BACTERIA

E. Coli DHα were cultured in lysogeny broth (LB) or plated on LB-agar and grown at 37°C under continuous shaking. Bacteria were selected under appropriate antibiotics.

LB medium	
Trypton	1% w/v
yeast extract	0.5% w/v
NaCl	1% w/v
pH	*7.2*

LB-agar	
LB medium	
Agar	1.5% w/v
Stored at	*4°C*

4.2.5 ISOLATION OF PLASMID DNA

Transformed bacteria colonies were isolated and transferred to liquid cultures at 37°C in LB medium (see chapter 4.2.4). To obtain smaller amounts of plasmid, 5mL of liquid culture were incubated for 8 hours; while, for larger amounts of DNA 1 mL of small liquid culture was then transferred to 100 mL liquid culture and incubated overnight.

Plasmid DNA was purified from small liquid culture using QIAprep Spin Miniprep Kit (Qiagen, Hilden, Germany) according to manufacturer's instruction. For larger cultures, the QIAGEN Plamid Maxi Kit (Qiagen, Hilden, Germany) was employed.

Concentration of the obtained DNA was determined by measuring the 260/280 nm absorbance ratio using a NanoDrop 2000 spectrophotometer (PeqLab Biotechnologie, Erlangen, Germany).

4.2.6 AGAROSE GEL ELECTROPHORESIS

For analysis and quality control purposes, size separation of DNA fragments by agarose gel electrophoresis was performed. 0.6% - 1.5% agarose gels were prepared and supplemented with 0.1 µL/mL ethidium-

bromide. Samples were mixed with 6X loading dye and were run in an electrophoresis chamber (Bio-Rad Laboratories, Hercules, USA) filled with TAE buffer. Separated bands were visualized by UV light in a gel documentation system.

6x DNA loading dye

Tris/HCl ph 7.5	100 mM
EDTA	200 mM
Bromophenol Blue	0.01% w/v
Xylencyanol	0.01% w/v
Glycerol	30% v/v

TAE buffer

Tris/HCl ph 8.0	40 mM
Acetic acid	0.12% v/v
EDTA	1 mM

4.3 CELL BIOLOGY METHODS

4.3.1 BONE MARROW SAMPLE PREPARATION

Bone marrow mononucleated cells (BMNC) were isolated from aspirates by density gradient centrifugation. Bone marrow aspirates were diluted with PBS without calcium and magnesium and 35 mL of cell suspension was layered on 15 mL of Biocoll separating solution (Biochrom, Berlin, Germany). The solution was centrifuged for 30 minutes at 400 x g in a swinging-bucket rotor without brake. After centrifugation the mononuclear cells were isolated from the interphase between Biocoll and serum. Cells were washed in PBS twice and red blood cells were lysed with erythrocyte lysis buffer when needed.

$4x10^5$ cells were diluted in PBS, and loaded in a cytospin funnel (Fisher Thermo Scientific, Lafayette, CO, USA). Cells were centrifuged on slides at 600 rpm for 6 minutes and fixed in ice-cold methanol for 10 minutes.

PBS

NaCl	137 mM
KCl	2.7 mM
Na_2HPO_4	10 mM
KH_2PO_4	1.7 mM
pH	*7,4*

Erythrocite lysis buffer 10X

NH_4Cl	8.26 gr
$NaHCO_3$	1.19 gr
EDTA 0.5 M	200 µL
ddH_2O	Bring to 100 mL
pH	*7.3*

4.3.2 CELL CULTURES

A complete list of the cell lines employed in this work is provided in Table 2 and Table 3.

Table 2 – Secondary cancer cell lines

Cell line	Description	Reference and source
U2OS-eGFP	Human osteosarcoma cells with inducible eGFP expression	Pontén J and Saksela E[132] Clinic Cooperation Unit Molecular Hematology/Oncology, DKFZ, Heidelberg
U2OS-eGFP-STIL		
U2OS-eGFP-PLK4		
U2OS-eGFP-SAS6		
DU-145	Human prostate carcinoma cells	Stone KR et al.[133]
PC-3	Human prostate carcinoma cells	Kaighn ME et al.[134]
MDA-MB-231	Human breast carcinoma cells	Cailleau R et al.[135]

Table 3 – Primary glioblastoma cell lines

Cell line	Description	Reference and source
NCH-149	Human glioblastoma cells	Prof. Christel Herold-Mende Experimental Neurosurgery Division - Neurosurgery Department Heidelberg University
NCH-342		
NCH-343		
NCH-354		
NCH-357		
NCH-417		

All cell lines were maintained at 37°C with 5% CO_2 atmosphere. Cells were cultured in cell culture flasks or dishes with appropriate growth medium as described in Table 4.

Table 4 – Cell culture media and supplements

Medium	Supplements	Selection antibiotics	Cell line
DMEM	10% tetracycline-free FCS 100 IU/mL Penicillin 100 µg/mL Streptomycin 2mM L-Glutamine	100 µg/mL Hygromycin B 1.5 µg/mL Puromycin	U2OS-eGFP
			U2OS-eGFP-STIL
			U2OS-eGFP-PLK4
			U2OS-eGFP-SAS6
RPMI		None	DU-145
			PC-3
			MDA-MB-231
DMEM		None	NCH-149
			NCH-342
			NCH-343
			NCH-354
			NCH-357
			NCH-417

Growth media were stored at 4°C.

Cells were passaged upon reaching 80% - 90% confluency. For this purpose, growth medium was removed and cells were rinsed with PBS-EDTA. Adherent cells were then incubated with trypsin-EDTA solution to be detached from the culture vessel. Fresh medium was added to inhibit trypsin activity. Cells were split at 1:5 or 1:10 ratio and seeded in a new vessel.

To store cells, cell cultures were harvested and centrifuged for 5 minutes at 800 x g. Growth medium was removed and cells were resuspended in ice-cold freezing medium (90% FCS and 10% DMSO) at $1*10^6$ cells/mL. 1 mL aliquots were transferred to cryovials. Cryovials were transferred to -80°C overnight and then moved to liquid nitrogen.

PBS-EDTA	
PBS	
EDTA	2 mM

Trypsin-EDTA	
PBS	
EDTA	2 mM
Trypsin	0.25% v/v
Stored at	*4°C*

4.3.3 CHEMICALS AND INDUCTION OF U2OS-TREX CELL LINES

A list of the chemical used in cell culture experiments is provided in Table 5.

Table 5 – Chemicals used for cell culture experiments

Chemical	Final concentration	Source
MG-132	20 µM	Sigma-Aldrich
Cytochalasin B	4.5 µg/mL	Sigma-Aldrich
BrdU	100 µM or 10 µM	Roche

The inducible system of U2OS derived cell lines was based on a T-REx induction system (Life Technologies, Darmastadt, Germany), where addition of tetracycline triggers transgene overexpression. Appropriate tetracycline concentrations for each cell line were determined experimentally and are presented in Table 6.

Table 6 – Tetracycline concentration used for transgene induction

Cell line	Tetracycline concentration
U2OS-eGFP	0.5 µg/mL
U2OS-eGFP-STIL	4.0 µg/mL
U2OS-eGFP-PLK4	2.0 µg/mL
U2OS-eGFP-SAS6	1.0 µg/mL

4.3.4 CATIONIC POLYMER-MEDIATED TRANSFECTION OF DNA

Transfection of adherent cell lines was performed with Turbofect transfection reagent (Life Technologies, Darmastadt, Germany) according to manufacturer's instructions. Turbofect is a cationic polymer that forms stable positively-charged complexes with DNA. These complexes protect DNA from degradation and allow delivery to the cells.

The day before transfection, cells were seeded on coverslips in 3 cm plastic or glass-bottomed dishes (Ibidi, Munich, Germany) at a concentration that allowed to obtain 80% confluency on the day of transfection. Immediately before transfection, growth medium was removed and 2 mL of fresh medium were added. Transfection mixture was prepared prior to use and incubated for 20 minutes at room temperature. A volume of reaction mixture correspondent to 10% of the growth medium volume present in the dish was added drop-wise to the cells. The dish was gently rocked to allow even distribution of the mixture and moved to the incubator until harvest or imaging.

A complete list of the condition used for transfection is provided in Table 7.

Table 7 – Cationic-polymer mediated transfection conditions

Vector	OptiMEM reaction volume	DNA	DNA:Turbofect Ratio
pYOY152	200 µL	1 µg	1:2
pMX230	200 µL	1 µg	1:2
pH2B_mCherry_IRES_neo3	200 µL	0.5 µg	1:2

4.4 IMMUNOFLUORESCENCE AND IMAGING METHODS

4.4.1 INDIRECT IMMUNOFLUORESCENCE

Cells grown on coverslips were briefly rinsed with PBS (see 4.3.1). Cytoplasm was extracted with 0.5% Triton X-100 in PHEM-buffer, washed for 5 minutes in PHEM-buffer and then fixed in 4% PFA or ice-cold methanol for 10 minutes.

PHEM buffer	
PIPES	60 mM
HEPES	25 mM
EGTA	8 mM
$MgCl_2$	2 mM
pH	*6.9*

Following fixation, coverslips were rehydrated in PBS for 5 minutes, permeabilized for 5 minutes with 0.5% Triton X-100 in PBS, blocked in 10% normal goat serum in PBS for 30 minutes, and incubated with primary antibodies for 1 hour.

A complete list of the primary antibodies used for immunofluorescence is provided in Table 8.

Table 8 – Primary antibodies used for immunofluorescence

Antigen	Clone	Species (clonality)	Dilution	Source
α-tubulin	DM1A	Mouse (m)	1:500	Sigma
γ-tubulin	TU-30	Mouse (m)	1:1000	Exbio
phopsho-γ-H2A.X (ser139)		Rabbit (p)	1:200	Abcam
Centrin	20H5	Mouse (m)	1:1000	Millipore
PCNT		Rabbit (p)	1:1000	Abcam
CREST		Human (p)	1:10	New England Biolabs
CP110		Rabbit (p)	1:100	Proteintech
CEP170		Rabbit (p)	1:500	Abcam
CEP152		Rabbit (p)	1:2000	Bethyl Laboratories
Centrobin		Mouse (m)	1:500	Abcam
Polyglutamylated- γ-tubulin	GT335	Rabbit (p)	1:2000	Adipogen
EB1	KT51	Rat (m)	1:200	Abcam
BubR1		Mouse (m)	1:100	BD Biosciences
BrdU		Rat (m)	1:100	BD Biosciences

Abbreviations: m, monoclonal; p, polyclonal.

After primary antibody incubation, coverslips were washed three times for five minutes in PBS and incubated with appropriate species-specific secondary antibodies. After three more PBS washes, coverslips were washed in ddH_2O and dehydrated in ethanol. DNA was counterstained with Hoechst 33342, diluted 1:1000 in PBS, and coverslips were mounted in Vectashield antifade medium.

A complete list of the secondary antibodies used for immunofluorescence is provided in Table 9.

Table 9 – Secondary antibodies used for immunofluorescence

Antigen	Fluorochrome	Species (clonality)	Dilution	Source
Mouse IgG	Alexa Fluor 488	Goat (p)	1:1000	Molecular Probes Life Technologies
Mouse IgG	Alexa Fluor 568			
Mouse IgG	Alexa Fluor 647			
Rabbit IgG	Alexa Fluor 488			
Rabbit IgG	Alexa Fluor 568			
Rabbit IgG	Alexa Fluor 647			
Rat IgG	Alexa Fluor 568			
Human IgG	Alexa Fluor 488			
Human IgG	Alexa Fluor 568			
Human IgG	Alexa Fluor 647			

Abbreviations: p, polyclonal.

4.4.2 MICROTUBULE REGROWTH ASSAY

Microtubule regrowth assay was performed as previously described[82]. Briefly, cells grown on coverslips were first incubated with ice-cold medium for 1 hour at 4°C. Subsequently microtubules were allowed to re-polymerize for 30 seconds at 37°C in fresh medium and cells were immediately fixed in ice-cold methanol. Cells were stained as described in chapter 4.4.1 and microtubule numbers sprouting from the centrosomes were assessed manually.

4.4.3 IMAGE ACQUISITION

Fixed-cell images were acquired with a 63X 1.4 NA Plan Apochromat objective on a Zeiss Cell Observer.Z1 system equipped with an AxioCam MRm camera (Carl Zeiss, Göttingen, Germany). Z-stacks were collected at a 0.2 µM interval, 40 stacks were acquired for each position. Alternatively an Axiovert 200M equipped with an AxioCam MRm camera (Carl Zeiss, Göttingen, Germany) was employed.

Live-cell imaging was performed on a Zeiss Cell Observer.Z1 system equipped with an AxioCam CCD camera. Images were acquired with a 20X 0.8 NA Plan Apochromat objective. Z-stacks were collected at 2 µM interval, 7 stacks were acquired for each position. Positions were imaged every 5 minutes.

Fluorochromes were imaged with appropriate dichroic filters.

4.4.4 CRITERIA FOR IMAGE ANALYSIS

Images were analyzed using ImageJ (Wayne Rasband, USA) or ZEN lite 2011 (Carl Zeiss, Göttingen, Germany) softwares.

Centrosomes at mitosis were detected as isolated pericentrin ring-shaped signals and cells were classified as bearing centriole rosettes, if the number of centrin signals exceeded two per mitotic pole.

In metaphase, mitoses with supernumerary spindle poles were classified as clustered, if chromosomes were congressed on a single line and centrosomes were grouped on the two sides of the metaphase plate. In anaphase, mitoses were classified as clustered if multiple pericentrin rings were visible in at least one daughter cell.

To score lagging chromosomes, cells in anaphase were analyzed for the presence of chromosomes, isolated from the main chromosome masses, and characterized by the presence of a CREST signal.

For measurement of interkinetochore tension, cells were scored as metaphases only if the vast majority of chromosomes congressed on a well-focused equatorial plate. Kinetochore sister pairs were detected by

CREST staining and their three-dimensional coordinates recorded. The distance between the two sister kinetochores was calculated and the average stretch was assessed for each cell.

Micronuclei were identified according to standard guidelines[86]. Only micronuclei with an area between 1/3rd and 1/256th of the nucleus, isolated or with visible boundaries were considered.

To score chromosome missegregation rate with FISH after cytochalasin B exposure, cells were assumed to have divided if they appeared as binucleated and isolated from the others. Chromosomes were scored as missegregated, if they were present in unequal numbers in the two nuclei and if the total number of signals in sister nuclei was an even number.

4.4.5 FLUORESCENCE SIGNAL QUANTIFICATION

Quantification of fluorescence signals was performed as previously described[136] using ImageJ.

For BubR1 and PCNT stainings, two Regions of interest (ROI) were measured. Both ROI were centered on the signal, but differed in their size. The small ROI (A_{small}) contained the signal at its best-of-focus, the larger ROI (A_{large}) was 60% larger and contained the signal plus the local background surrounding it. Integrated density fluorescence was measured as the sum of all pixel values contained in ROIs (F_{large} and F_{small}). Local background fluorescence was calculated by subtracting the integrated density fluorescence of A_{small} from A_{large}. Corrected integrated intensity values ($F_{corrected}$) were produced by subtraction of the inferred background fluorescence intensity from the corresponding total fluorescence intensity. The mathematical formula used to calculate the signal intensity is provided:

$$F_{corrected} = F_{small}\left[\left(F_{large} - F_{small}\right)\frac{A_{small}}{A_{large}}\right]$$

For quantification of cold-stable spindle fibers, cells grown on coverslips were incubated for 30 minutes in ice-cold medium and then processed for immunofluorescence. Sum intensity projections of z-stack series containing mitotic cells were produced, and spindle fluorescence intensity was calculated using the method described above. In this case A_{small} was centered on the mitotic spindle.

For total microtubule polymer fluorescence intensity, background was subtracted using a rolling ball filter, sum intensity projections of z-stack series of interphase cells were produced and their integrated fluorescence intensity was calculated. Polygonal ROIs encircling cells were defined and their integrated fluorescence intensity and area were measured.

Similarly, for EB1 dot counts, after background subtraction, maximum intensity projections were produced and EB1 dots were automatically enumerated via a find maxima algorithm.

4.4.6 IMAGEJ MACROS

To accelerate data collection from image analysis and fluorescence quantification, ImageJ macro were coded.

4.4.6.1 BubR1 AND PCNT SIGNAL MEASUREMENT MACRO

```
var size = 6;
var     snRadius = round(size/2);
var     bgRadius = round(snRadius*1.6);

var pmCmds = newMenu("Popup Menu",
newArray("Remove last signal", "Measure signals", "-", "Start new count", "-", "Signal size"));


macro "Sample Tool - C0a0L18f8L818f" {

        getCursorLoc(x, y, z, flags);

        makeRectangle(x-snRadius,y-snRadius,snRadius*2,snRadius*2);
        roiManager("add");

        makeRectangle(x-bgRadius,y-bgRadius,bgRadius*2,bgRadius*2);
        roiManager("add");


}



macro "Sample Tool Options" {

        size = getNumber("Signal size: ", size);
        snRadius = round(size/2);
        bgRadius = round(snRadius*1.6);

}

macro "Popup Menu" {
        cmd = getArgument();
        if (cmd=="Remove last signal") {
                count = roiManager("count");
                sn = count - 1;
                bg = count - 2;
                var lastSignal = newArray(sn, bg);
                if (count == 0)
                        showMessage("List is empty");
                else {
                        roiManager("select", lastSignal);
                        roiManager("delete");
                }
        }
        if (cmd=="Start new count") {
                a = getBoolean("Do you really want to start a new count?");
                if (a==true) {
                        if (roiManager("count")>0) {
                                roiManager("deselect");
                                roiManager("delete");

                        }
                        run("Clear Results");
                }
        }
        if (cmd=="Signal size") {
                size = getNumber("Signal size: ", size);
                snRadius = round(size/2);
                bgRadius = round(snRadius*1.6);
        }
        if (cmd=="Measure signals") {
                roiManager("deselect");
                roiManager("measure");
                String.copyResults();
        }
}
```

```
macro "Zup [n9]" {
	slice = getSliceNumber();
	if(nSlices > slice + 3) {
		setSlice(slice + 3);
		} else {
	}
}

macro "Zdown [n3]" {
	slice = getSliceNumber();
	if(slice - 3 > 0) {
		setSlice(slice - 3);
		} else {
	}
}

macro "toggle channel [n7]" {
	Stack.getActiveChannels(string);
	if(string == "1100000") {
		Stack.setActiveChannels("1000000");
	} else if(string == "1000000") {
		Stack.setActiveChannels("1100000");
	}
}
```

4.4.6.2 KINETOCHORE FIBERS QUANTIFICATION MACRO

```
var size = 6;
var	snRadius = round(size/2);
var	bgRadius = round(snRadius*1.6);

var pmCmds = newMenu("Popup Menu",
newArray("Remove last signal", "Measure signals", "-", "Start new count", "-", "Signal size"));


macro "Sample Tool - C0a0L18f8L818f" {

	getCursorLoc(x, y, z, flags);
	Stack.setChannel(3);

	makeOval(x-snRadius,y-snRadius,snRadius*2,snRadius*2);
	roiManager("add");

	makeOval(x-bgRadius,y-bgRadius,bgRadius*2,bgRadius*2);
	roiManager("add");

	roiManager("measure");
	roiManager("reset");


}



macro "Sample Tool Options" {

	size = getNumber("Signal size: ", size);
	snRadius = round(size/2);
	bgRadius = round(snRadius*1.6);

}

macro "Popup Menu" {
	cmd = getArgument();
	if (cmd=="Remove last signal") {
		count = roiManager("count");
		sn = count - 1;
		bg = count - 2;
		var lastSignal = newArray(sn, bg);
		if (count == 0)
			showMessage("List is empty");
		else {
			roiManager("select", lastSignal);
			roiManager("delete");
```

```
                }
        }
        if (cmd=="Start new count") {
                a = getBoolean("Do you really want to start a new count?");
                if (a==true) {
                        if (roiManager("count")>0) {
                                roiManager("deselect");
                                roiManager("delete");

                        }
                        run("Clear Results");
                }
        }
        if (cmd=="Signal size") {
                size = getNumber("Signal size: ", size);
                snRadius = round(size/2);
                bgRadius = round(snRadius*1.6);
        }
        if (cmd=="Measure signals") {
                roiManager("deselect");
                roiManager("measure");
                String.copyResults();
        }
}


macro "Zup [n9]" {
        slice = getSliceNumber();
        if(nSlices > slice + 3) {
                setSlice(slice + 3);
                } else {
        }
}

macro "Zdown [n3]" {
        slice = getSliceNumber();
        if(slice - 3 > 0) {
                setSlice(slice - 3);
                } else {
        }
}

macro "toggle channel [n7]" {
        Stack.getActiveChannels(string);
        if(string == "1100000") {
                Stack.setActiveChannels("1000000");
        } else if(string == "1000000") {
                Stack.setActiveChannels("1100000");
        }
}
```

4.4.6.3 EB1 PARTICLE COUNT AND MICROTUBULE POLYMER QUANTIFICATION MACRO

```
var pmCmds = newMenu("Popup Menu",
newArray("Process"));


macro "Popup Menu" {
        cmd = getArgument();

        if (cmd=="Process") {
                if(selectionType != -1) {
                        Dialog.create("Error");
                        Dialog.addMessage("Remove the selection from screen");
                        Dialog.show();
                }
                if(roiManager("count") == 0) {
                        Dialog.create("Error");
                        Dialog.addMessage("No selection list!");
                        Dialog.show();
                }
                else {
//run batch mode and clear result table
                        run("Clear Results");
                        setBatchMode(true);
```

```
//duplication of on-focus stacks
                        selectImage(nImages);
                        Stack.getPosition(channel, slice, frame);
                        a = slice - 2;
                        b = slice + 2;
                        run("Duplicate...", "duplicate slices=&a-&b");
                        print("duplicate: " + a + " " + b);

//separating channels and closing the ones not needed

                        run("Split Channels");
                        selectImage(nImages-1);
                        close();
                        selectImage(nImages-3);
                        close();

//eb1 max intensity projection
                        selectImage(nImages-1);
                        print("EB1 MAX Selected: " + getTitle());
                        run("Z Project...", "projection=[Max Intensity]");
                        run("Subtract Background...", "rolling=5 disable");
                        selectImage(nImages-2);
                        close();

//tubulin sum intensity projection
                        selectImage(nImages-2);
                        print("TUBULIN SUM Selected: " + getTitle());
                        run("Subtract Background...", "rolling=5 disable stack");
                        run("Z Project...", "projection=[Sum Slices]");
                        selectImage(nImages-3);
                        close();

//measure tubulin intensity per cell
                        selectImage(nImages-1);
                        print("measuring tubulin: " + getTitle());
                        roiManager("deselect");
                        roiManager("measure");

//measure eb1 dots
                        selectImage(nImages-2);
                        String.copyResults();
                        for (i=0; i < roiManager("count"); i++){
                                roiManager("select", i);
                                run("Find Maxima...", "noise=1200 output=Count");
                                count = getResult("Count", nResults-1);
                                setResult("Count", i, count);


                        }
                        n = roiManager("count");
                        IJ.deleteRows(n,n*2);

                        String.copyResults();

//close windows
                        close("MAX*");
                        close("SUM*");

//close batch mode and clear ROI manager
                        setBatchMode("exit and display");
                        roiManager("reset");

                }
        }

}
```

4.4.7 FLOW CYTOMETRY

Adherent cells were harvested from plates using trypsin-EDTA, washed with PBS and resuspended in 250 µL of PBS. 700 µL of ice-cold methanol were added dropwise, while slowly vortexing the tube. The fixed cell suspension was incubated at 4°C for at least 1 hour.

$1x10^6$ cells were washed with PBS and resuspended in 200 µL of 0.01 mg/mL PI in PBS, supplemented with 0.25 mg/mL RNase A. After 30 minutes incubation in the dark, cell suspension was diluted with PBS and analyzed.

An Accuri C6 flow cytometer (BD Biosciences, Heidelberg, Germany) was used. Apoptotic cells and debris were excluded and at least $3x10^4$ cells per sample were measured. Cell doublets were gated out using a PI-signal area vs. PI-signal width plot. Analysis of cell cycle profiles was done with BD Accuri C6 software (BD Biosciences, Heidelberg, Germany).

4.5 MOLECULAR CYTOGENETICS METHODS

4.5.1 FLUORESCENCE IN SITU HYBRIDIZATION

FISH is used to detect and localize specific DNA sequences on chromosomes. FISH uses a fluorescent DNA probe that binds to the correspondent sequence of the cell interphase nuclei or mitotic chromosomes, thanks to the double strand complementarity of DNA.

Cells were fixed in ice-cold methanol, and processed for FISH according to standard procedures.

Coverslips were washed in 2X saline-sodium citrate buffer (SSC) for 5 minutes. RNA was digested by incubation with RNase A working solution for 1 hour at 37°C. After three washes in 2X SSC, coverslips were incubated with pepsin/HCl solution for 12 minutes, washed two times with PBS/$MgCl_2$ solution, fixed with 1% formaldehyde and dehydrated by sequential 3 minutes washes in 70%, 85% and 100% ethanol.

RNAse A stock solution	
RNAse A	20 mg/mL
Tris/HCl pH 7.5	10 mM
NaCl	15 mM
Stored at	*-20°C*

Pepsin stock solution	
Pepsin	10% w/v
Stored at	*-20°C*

20X SSC	
NaCl	150 mM
$Na_3Citrate*2H_2O$	15 mM

RNAse A working solution	
RNAse A stock	1:1000

Pepsin/HCl solution	
Pepsin	50 µg/mL
HCl	0.01 M

PBS/MgCl2	
PBS	
$MgCl_2$	50 mM

Centromere-specific fluorescent labeled probes were incubated on coverslips, which were mounted on slides and sealed with Fixogum (Marabu, Germany). DNA denaturation was performed for 5 minutes at 76°C in a hybridization chamber, and then samples were left to hybridize overnight at 42°C.

The following day excess probe was removed by a 10 minutes wash in 2X SSC solution at 66°C, followed by two more washes in 0.2X SSC solution for 7 minutes. Finally, coverslips were shortly immerged in 0.4X SSC/0.2% Tween-20, counterstained with DAPI and mounted in Vectashield antifade.

4.5.2 NICK TRANSLATION

Bacterial artificial chromosomes (BAC) containing centromere-specific alphoid sequences were propagated as described in chapter 4.2 and isolated with a Quiagen MaxiPrep kit according to manufacturer's instructions.

A list of the probes used in this work is provided in Table 10.

Table 10 – BAC probes used for FISH

Probe	Chromosome	Backbone	Resistance	Reference
pAL1	1	Bluescribe	Ampicillin	Archidiacono N et al.[137]
pBS4D	2	Bluescribe	Ampicillin	Rocchi M et al.[138]
pAE0.68	3	Bluescribe	Ampicillin	Baldini A et al.[139]
pZ8.4	8	Bluescribe	Ampicillin	Archidiacono N et al.[137]
pZ17-14	17	pUC19	Ampicillin	Archidiacono N et al.[137]

The isolated BACs were labeled by nick translation. In this procedure, single strand breaks (nicks) are induced on the double stranded DNA. The nicks constitute new sites of DNA synthesis, where the exonuclease activity removes the old, unlabeled strand and polymerase activity substitutes it with a new one. The newly synthetized strand will be labeled thanks to the addition of a fluorochrome-conjugated nucleotide to the reaction mixture.

The nick translation mixture was prepared on ice as follows:

Table 11 – Nick translation reaction components

Reagents	Quantity
β-mercaptoethanol 4.3 M	5 µL
dNTP mix 10X	5 µL
NT buffer 10X	5 µL
labeled-dUTP	1 µL
DNA	1 µg
Dnase working solution	3 µL
H2O	Bring to 30 µL
E.Coli DNA Pol I	1 µL

Table 12 – Fluorochrome-conjugated nucleotides used for nick translation

Labeled-dUTP	Fluorochrome	Source
DY-495-dUTP	DY-495 (green)	Dyomics
DY-547-dUTP	DY-547 (orange)	Dyomics

The mixture was incubated at 16°C for 90 minutes. Reaction was stopped by adding 50 µL of stop solution.

For quality control purposes, nick translation products in the range of 200-700 base pairs were detected on a 1.2% agarose gel as described in chapter 4.2.6.
Products were stored at -20°C.

DNAse stock solution	
DNAse	1 mg/mL
NaCl	0.15 M
Glycerin	50%
Stored at	*-20°C*

NT buffer 10X	
Tris/HCl pH 7.5	0.5 mM
$MgCl_2$	50 mM
BSA	0.5 mg/mL
Stored at	*-20°C*

Stop solution	
Dextran blue	0.5%
NaCl	0.1%
EDTA	20 mM
Tris/HCl pH 7.5	20 mM
Stored at	*4°C*

DNAse working solution	
DNAse stock solution	1:1000

dNTPs mix 10X	
A,G,C nucleotides 0.1 M	5 µL each
T nucleotide 0.1 M	1 µL
Stored at	*-20°C*

4.5.3 PROBE ISOLATION

The nick translation product was isolated by ethanol precipitation to remove excess labeled nucleotides not incorporated during the reaction. 5 µL of salmon sperm DNA (Sigma-Aldrich, Munich, Germany) were added to 20 µL of nick translation products and mixed 1:3 v/v with ethanol. The mixture was incubated at -80°C for 2 hours and centrifuged for 30 min at 15000 x g at 4°C. The supernatant was removed and the pellet air-dried.

Probe DNA was resuspended in 6.5 µL of 70% hybridization solution and 3.5 µL of 20% dextran sulfate.

70% Hybridization solution

SSC 20X	100 µL
HCl 1N	7 µL
Formammide	700 µL
ddH_2O	Bring to 1 mL
Stored at	*-20°C*

The probe was then stored at -20°C until use.

4.6 PROTEIN BIOCHEMISTRY METHODS

4.6.1 PROTEIN LYSATES FOR WESTERN BLOT ANALYSIS

Adherent cells were harvested using trypsin-EDTA to detach them from plates and washed with PBS. Cells were then pelleted and resuspended in RIPA buffer supplemented with Complete Protease Inhibitor (Roche, Basel, Switzerland) and PhosSTOP Phosphatase Inhibitor (Roche, Basel, Switzerland). Samples were incubated on ice for 30 minutes and vortexed at 10 minutes intervals. Lysates were pelleted by centrifugation for 10 minutes at 18000 x g at 4°C and supernatant was transferred to a new precooled reaction tube. Samples were stored at -80°C until further use.

RIPA buffer

Tris/HCl pH 7.5	50 mM
NaCl	150 mM
Sodium-deoxycholate	0.25% w/v
Nonidet P40	1% v/v
EDTA	1 mM

Protein concentration was determined by Bradford protein assay. 1 µL of protein lysate was added to 1 mL of dye reagent for the Quick Start Bradford Protein Assay (Bio-Rad, Munich, Germany), mixed vigorously and incubated for 5 minutes to allow the colorimetric reaction to take place. To determine protein amount,

absorbance was measured at 595 nm by spectrophotometry (Eppendorf, Hamburg, Germany) using a BSA standard curve as reference.

4.6.2 SDS-PAGE

Sodium-dodecyl-sulfate (SDS) polyacrylamide gel electrophoresis (SDS-PAGE) under denaturing conditions was performed to separate proteins according to their molecular weight. 6 - 12% acrylamide running gels (3 M Tris, pH 8.9) were used according to the protein range to be resolved. A 5% stacking gel (0.47 M Tris, pH 6.7) was used. 70 µg of protein in 1X SDS loading buffer were boiled for 5 minutes at 95°C and loaded onto gel. Separation was performed at 120V in Mini-Protean Tetra cells (Bio-Rad, Munich, Germany) filled with tris-glycine running buffer.

6X SDS loading buffer

Tris/HCl pH 6.8	240 mM
B-mercaptoethanol	30% v/v
SDS	6% w/v
Glycerol	30% v/v
Bromophenol blue	0.002% w/v

Tris-glycine running buffer

Glycin	380 mM
Tris	50 mM
SDS	0.1% w/v

4.6.3 WESTERN BLOT

Proteins separated by SDS-PAGE were transferred onto a PVDF membrane by semi-dry transfer. PVDF membranes were activated in methanol for 1 minute. A wet sandwich, equilibrated in transfer buffer, was assembled in the following order: isolation pads, whatman paper, membrane, gel, whatman paper, isolation pads. The sandwich was correctly oriented between electrodes in a Mini Trans-Blot Electrophoretic Transfer cell (Bio-Rad, Munich, Germany) and transfer was performed for 1.5 hours at 350 mA.

Borate transfer buffer

Boric acid	20 mM
EDTA	1.3 mM
pH	8.8

Following transfer, membranes were blocked for 1 hour with 5% skimmed milk powder or 3% BSA in 0.1% Tween-20 in PBS (PBS-T). Primary antibodies were diluted in blocking solution and incubated with membranes overnight. Excess antibodies were washed three times for 10 minutes with PBS-T, while rocking. Membranes were then incubated with secondary antibodies for 1 hour at room temperature and washed three additional times in PBS-T. Membranes were stored in PBS-T at 4°C until signal detection.

A comprehensive list of antibodies used for western blot is given in tables 13 and 14.

Table 13 – Primary antibodies used for western blot

Antigen	Clone	Species (clonality)	Dilution	Source
P53		mouse(m)	1:5000	Progen
P21		mouse(m)	1:1000	Millipore
Actin	I-19	rabbit(p)	1:2000	Santa Cruz
MCM7	141.2	mouse(m)	1:1000	Santa Cruz
Cyclin B1	H-433	rabbit(p)	1:1000	Santa Cruz
Phospho-Eg5		rabbit(m)	1:2000	Novus Biologicals

Table 14 – Secondary antibodies used for western blot

Antigen	Specifications	Species (clonality)	Dilution	Source
Mouse IgG	HRP-conjugated	Goat (p)	1:5000	Santa Cruz
Rabbit IgG				

The signal from horseradish peroxidase-conjugated secondary antibodies was detected by enhanced chemiluminescence method with Pierce ECL western blotting substrate (Thermo Fisher Scientific, Lafayette; USA) according to manufacturer's instructions. Signals were detected via exposure and development of photographic films (Amersham Hyperfilm ECL, GE Healthcare, Buckinghamshire, UK).

4.7 STATISTICAL ANALYSIS

Statistical analysis was performed using Sigma Plot (Systat Software Inc., San Jose, USA) or Excel software (Microsoft Corporation, Redmond, USA). Experiments were repeated in triplicates unless otherwise stated. Samples were processed in technical duplicates or triplicates. A Shapiro-Wilk test and an equal variance test were performed on raw datasets. Upon passing both tests, data sets were subjected to a Student's *t*-test, otherwise a Mann-Whitney rank-sum test was performed. A difference was considered to be statistically significant if the two-tailed p-value was smaller than 0.05. Different p-value thresholds were represented as follows: $p < 0.05$ (*), $p < 0.01$ (**), $p < 0.001$ (***). Pearson product-moment correlation coefficient was used to measure linear correlation between two variables.

INDEX

LIST OF FIGURES

LIST OF TABLES

LIST OF ABBREVIATIONS

AML	Acute myeloid leukemia
BAC	Bacterial artificial chromosome
BMNC	Bone marrow mononucleated cells
BrdU	5-bromo-2'-deoxyuridine
BSA	Bovine serum albumine
BubR1	Bub1-related kinase
CCD	Charge-coupled device
CDK	Cyclin dependent kinase
CDK5RAP2	CDK5 regulatory subunit associated protein 2
CEP135	Centrosomal protein 135kDa
CEP152	Centrosomal protein 152kDa
CEP170	Centrosomal protein 170kDa
CEP192	Centrosomal protein 192kDa
CIN	Chromosomal instability
CPAP	Centrosomal P4.1-associated protein
CREST	Calcinosis, Raynaud's phenomenon, Esophageal dysmotility, Sclerodactyly and Telangiectasia
DMSO	Dimethyl sulfoxide
ECL	Enhanced chemoluminescence
EDTA	Ethylenediaminetetraacetic acid
eGFP	Enhanced green fluorescent protein
EGTA	Ethylene glycol tetraacetic acid
FCS	Fetal calf serum
FISH	Fluorescence in situ hybridization
HA	Hemoagglutinin

HEPES	4-(2-hydroxyethyl)-1-piperazineethanesulfonic acid
HRP	Horseradish peroxidase
IRES	Internal ribosome entry site
IU	International units
KIF2B	Kinesin family member 2B
LB	Luria's broth
MCAK	Mitotic centromere-associated kinesin
MCM7	Mini-chromosome maintenance complex protein 7
MN	Micronucleus
MTOC	Microtubule organizing center
N.A.	Not available
PAGE	Polyacrilamide gel electrophoresis
PBS	Phosphate buffered saline
PBS-T	Phosphate buffered saline - Triton
PCM	Pericentriolar material
PCNT	Pericentrin
PI	Propidium iodide
PIPES	Piperazine-N,N'-bis(2-ethanesulfonic acid)
PLK1	Polo-like kinase 1
PLK4	Polo-like kinase 4
PVDF	Polyvinylidene fluoride
RIPA	Radioimmunoprecipitation assay buffer
ROI	Region of interest
s.e.m.	Standard error of the mean
SAC	Spindle assembly checkpoint
SAS6	Spindle assembly abnormal 6 homolog
$SCF\beta^{TrCP}$	Skp1-Cul1-F-box β-transducin repeat-containing protein

SD	Standard deviation
SDS	Sodium dodecyl sulfate
SOC	Super optimal broth with catabolite repression
STIL	SCL/TAL1 interrupting locus
tet	Tetracycline
γ-TURC	γ-tubulin ring complex

BIBLIOGRAPHY

1. Pihan, G. A. Centrosome dysfunction contributes to chromosome instability, chromoanagenesis, and genome reprograming in cancer. *Front. Oncol.* **3,** 277 (2013).
2. Azimzadeh, J. & Bornens, M. Structure and duplication of the centrosome. *J. Cell Sci.* **120,** 2139–2142 (2007).
3. Hoyer-Fender, S. Centriole maturation and transformation to basal body. *Semin. Cell Dev. Biol.* **21,** 142–147 (2010).
4. Carvalho-Santos, Z., Azimzadeh, J., Pereira-Leal, J. B. & Bettencourt-Dias, M. Evolution: Tracing the origins of centrioles, cilia, and flagella. *J. Cell Biol.* **194,** 165–175 (2011).
5. Graser, S. *et al.* Cep164, a novel centriole appendage protein required for primary cilium formation. *J. Cell Biol.* **179,** 321–330 (2007).
6. Lüders, J. & Stearns, T. Microtubule-organizing centres: a re-evaluation. *Nat. Rev. Mol. Cell Biol.* **8,** 161–167 (2007).
7. Hirono, M. Cartwheel assembly. *Philos. Trans. R. Soc. Lond. B. Biol. Sci.* **369,** (2014).
8. Arquint, C., Gabryjonczyk, A.-M. & Nigg, E. A. Centrosomes as signalling centres. *Philos. Trans. R. Soc. Lond. B. Biol. Sci.* **369,** (2014).
9. Stearns, T. & Winey, M. The cell center at 100. *Cell* **91,** 303–309 (1997).
10. Fabunmi, R. P., Wigley, W. C., Thomas, P. J. & DeMartino, G. N. Activity and Regulation of the Centrosome-associated Proteasome. *J. Biol. Chem.* **275,** 409–413 (2000).
11. O'Connell, C. B. & Khodjakov, A. L. Cooperative mechanisms of mitotic spindle formation. *J. Cell Sci.* **120,** 1717–1722 (2007).
12. Woodruff, J. B., Wueseke, O. & Hyman, A. A. Pericentriolar material structure and dynamics. *Philos. Trans. R. Soc. Lond. B. Biol. Sci.* **369,** (2014).
13. Andersen, J. S. *et al.* Proteomic characterization of the human centrosome by protein correlation profiling. *Nature* **426,** 570–574 (2003).
14. Sonnen, K. F., Schermelleh, L., Leonhardt, H. & Nigg, E. A. 3D-structured illumination microscopy provides novel insight into architecture of human centrosomes. *Biol. Open* **1,** 965–976 (2012).
15. Lawo, S., Hasegan, M., Gupta, G. D. & Pelletier, L. Subdiffraction imaging of centrosomes reveals higher-order organizational features of pericentriolar material. *Nat. Cell Biol.* **14,** 1148–1158 (2012).
16. Lacey, K. R., Jackson, P. K. & Stearns, T. Cyclin-dependent kinase control of centrosome duplication. *Proc. Natl. Acad. Sci. U. S. A.* **96,** 2817–2822 (1999).
17. Fırat-Karalar, E. N. & Stearns, T. The centriole duplication cycle. *Philos. Trans. R. Soc. Lond. B. Biol. Sci.* **369,** (2014).
18. Kim, T.-S. *et al.* Hierarchical recruitment of Plk4 and regulation of centriole biogenesis by two centrosomal scaffolds, Cep192 and Cep152. *Proc. Natl. Acad. Sci. U. S. A.* **110,** E4849–4857 (2013).
19. Gibbons, I. R. & Grimstone, A. V. On flagellar structure in certain flagellates. *J. Biophys. Biochem. Cytol.* **7,** 697–716 (1960).
20. Guichard, P., Chrétien, D., Marco, S. & Tassin, A.-M. Procentriole assembly revealed by cryo-electron tomography. *EMBO J.* **29,** 1565–1572 (2010).
21. Schmidt, T. I. *et al.* Control of centriole length by CPAP and CP110. *Curr. Biol. CB* **19,** 1005–1011 (2009).
22. Kong, D. *et al.* Centriole maturation requires regulated Plk1 activity during two consecutive cell cycles. *J. Cell Biol.* **206,** 855–865 (2014).
23. Tsou, M.-F. B. *et al.* Polo kinase and separase regulate the mitotic licensing of centriole duplication in human cells. *Dev. Cell* **17,** 344–354 (2009).
24. Guarguaglini, G. *et al.* The Forkhead-associated Domain Protein Cep170 Interacts with Polo-like Kinase 1 and Serves as a Marker for Mature Centrioles. *Mol. Biol. Cell* **16,** 1095–1107 (2005).

25. Wang, W.-J., Soni, R. K., Uryu, K. & Tsou, M.-F. B. The conversion of centrioles to centrosomes: essential coupling of duplication with segregation. *J. Cell Biol.* **193,** 727–739 (2011).
26. Rogers, G. C., Rusan, N. M., Roberts, D. M., Peifer, M. & Rogers, S. L. The SCF Slimb ubiquitin ligase regulates Plk4/Sak levels to block centriole reduplication. *J. Cell Biol.* **184,** 225–239 (2009).
27. Kleylein-Sohn, J. *et al.* Plk4-induced centriole biogenesis in human cells. *Dev. Cell* **13,** 190–202 (2007).
28. Habedanck, R., Stierhof, Y.-D., Wilkinson, C. J. & Nigg, E. A. The Polo kinase Plk4 functions in centriole duplication. *Nat. Cell Biol.* **7,** 1140–1146 (2005).
29. Peel, N., Stevens, N. R., Basto, R. & Raff, J. W. Overexpressing centriole-replication proteins in vivo induces centriole overduplication and de novo formation. *Curr. Biol. CB* **17,** 834–843 (2007).
30. Strnad, P. *et al.* Regulated HsSAS-6 levels ensure formation of a single procentriole per centriole during the centrosome duplication cycle. *Dev. Cell* **13,** 203–213 (2007).
31. Vulprecht, J. *et al.* STIL is required for centriole duplication in human cells. *J. Cell Sci.* **125,** 1353–1362 (2012).
32. Arquint, C. & Nigg, E. A. STIL microcephaly mutations interfere with APC/C-mediated degradation and cause centriole amplification. *Curr. Biol. CB* **24,** 351–360 (2014).
33. Arquint, C., Sonnen, K. F., Stierhof, Y.-D. & Nigg, E. A. Cell-cycle-regulated expression of STIL controls centriole number in human cells. *J. Cell Sci.* **125,** 1342–1352 (2012).
34. Wong, C. & Stearns, T. Centrosome number is controlled by a centrosome-intrinsic block to reduplication. *Nat. Cell Biol.* **5,** 539–544 (2003).
35. Vitre, B. D. & Cleveland, D. W. Centrosomes, chromosome instability (CIN) and aneuploidy. *Curr. Opin. Cell Biol.* **24,** 809–815 (2012).
36. Musacchio, A. & Salmon, E. D. The spindle-assembly checkpoint in space and time. *Nat. Rev. Mol. Cell Biol.* **8,** 379–393 (2007).
37. Lengauer, C., Kinzler, K. W. & Vogelstein, B. Genetic instability in colorectal cancers. *Nature* **386,** 623–627 (1997).
38. McGranahan, N., Burrell, R. A., Endesfelder, D., Novelli, M. R. & Swanton, C. Cancer chromosomal instability: therapeutic and diagnostic challenges. *EMBO Rep.* **13,** 528–538 (2012).
39. Bakhoum, S. F. & Compton, D. A. Chromosomal instability and cancer: a complex relationship with therapeutic potential. *J. Clin. Invest.* **122,** 1138–1143 (2012).
40. Sheltzer, J. M., Torres, E. M., Dunham, M. J. & Amon, A. Transcriptional consequences of aneuploidy. *Proc. Natl. Acad. Sci. U. S. A.* **109,** 12644–12649 (2012).
41. Sheltzer, J. M. *et al.* Aneuploidy drives genomic instability in yeast. *Science* **333,** 1026–1030 (2011).
42. Pavelka, N. *et al.* Aneuploidy confers quantitative proteome changes and phenotypic variation in budding yeast. *Nature* **468,** 321–325 (2010).
43. Greaves, M. & Maley, C. C. Clonal evolution in cancer. *Nature* **481,** 306–313 (2012).
44. Lee, A. J. X. *et al.* Chromosomal instability confers intrinsic multidrug resistance. *Cancer Res.* **71,** 1858–1870 (2011).
45. Swanton, C. *et al.* Chromosomal instability determines taxane response. *Proc. Natl. Acad. Sci. U. S. A.* **106,** 8671–8676 (2009).
46. Salmon, E. D., Cimini, D., Cameron, L. A. & DeLuca, J. G. Merotelic kinetochores in mammalian tissue cells. *Philos. Trans. R. Soc. Lond. B. Biol. Sci.* **360,** 553–568 (2005).
47. Gregan, J., Polakova, S., Zhang, L., Tolić-Nørrelykke, I. M. & Cimini, D. Merotelic kinetochore attachment: causes and effects. *Trends Cell Biol.* **21,** 374–381 (2011).
48. Cimini, D., Moree, B., Canman, J. C. & Salmon, E. D. Merotelic kinetochore orientation occurs frequently during early mitosis in mammalian tissue cells and error correction is achieved by two different mechanisms. *J. Cell Sci.* **116,** 4213–4225 (2003).

49. Cimini, D. & Degrassi, F. Aneuploidy: a matter of bad connections. *Trends Cell Biol.* **15,** 442–451 (2005).
50. Anderhub, S. J., Krämer, A. & Maier, B. Centrosome amplification in tumorigenesis. *Cancer Lett.* **322,** 8–17 (2012).
51. Cimini, D., Cameron, L. A. & Salmon, E. D. Anaphase spindle mechanics prevent mis-segregation of merotelically oriented chromosomes. *Curr. Biol. CB* **14,** 2149–2155 (2004).
52. Cimini, D., Wan, X., Hirel, C. B. & Salmon, E. D. Aurora kinase promotes turnover of kinetochore microtubules to reduce chromosome segregation errors. *Curr. Biol. CB* **16,** 1711–1718 (2006).
53. Cimini, D. *et al.* Merotelic kinetochore orientation is a major mechanism of aneuploidy in mitotic mammalian tissue cells. *J. Cell Biol.* **153,** 517–527 (2001).
54. Torosantucci, L., De Santis Puzzonia, M., Cenciarelli, C., Rens, W. & Degrassi, F. Aneuploidy in mitosis of PtK1 cells is generated by random loss and nondisjunction of individual chromosomes. *J. Cell Sci.* **122,** 3455–3461 (2009).
55. Kline-Smith, S. L., Khodjakov, A., Hergert, P. & Walczak, C. E. Depletion of centromeric MCAK leads to chromosome congression and segregation defects due to improper kinetochore attachments. *Mol. Biol. Cell* **15,** 1146–1159 (2004).
56. Bakhoum, S. F., Thompson, S. L., Manning, A. L. & Compton, D. A. Genome stability is ensured by temporal control of kinetochore-microtubule dynamics. *Nat. Cell Biol.* **11,** 27–35 (2009).
57. Bakhoum, S. F., Genovese, G. & Compton, D. A. Deviant kinetochore microtubule dynamics underlie chromosomal instability. *Curr. Biol. CB* **19,** 1937–1942 (2009).
58. Manning, A. L. *et al.* The kinesin-13 proteins Kif2a, Kif2b, and Kif2c/MCAK have distinct roles during mitosis in human cells. *Mol. Biol. Cell* **18,** 2970–2979 (2007).
59. Bakhoum, S. F. & Compton, D. A. Kinetochores and disease: keeping microtubule dynamics in check! *Curr. Opin. Cell Biol.* **24,** 64–70 (2012).
60. Boveri, T. Concerning the origin of malignant tumours by Theodor Boveri. Translated and annotated by Henry Harris. *J. Cell Sci.* **121 Suppl 1,** 1–84 (2008).
61. Godinho, S. A. & Pellman, D. Causes and consequences of centrosome abnormalities in cancer. *Philos. Trans. R. Soc. Lond. B. Biol. Sci.* **369,** (2014).
62. Chan, J. Y. A clinical overview of centrosome amplification in human cancers. *Int. J. Biol. Sci.* **7,** 1122–1144 (2011).
63. Nigg, E. A. Origins and consequences of centrosome aberrations in human cancers. *Int. J. Cancer J. Int. Cancer* **119,** 2717–2723 (2006).
64. D'Assoro, A. B. *et al.* Amplified centrosomes in breast cancer: a potential indicator of tumor aggressiveness. *Breast Cancer Res. Treat.* **75,** 25–34 (2002).
65. Fukasawa, K. Oncogenes and tumour suppressors take on centrosomes. *Nat. Rev. Cancer* **7,** 911–924 (2007).
66. Löffler, H., Fechter, A., Liu, F. Y., Poppelreuther, S. & Krämer, A. DNA damage-induced centrosome amplification occurs via excessive formation of centriolar satellites. *Oncogene* **32,** 2963–2972 (2013).
67. Macmillan, J. C., Hudson, J. W., Bull, S., Dennis, J. W. & Swallow, C. J. Comparative expression of the mitotic regulators SAK and PLK in colorectal cancer. *Ann. Surg. Oncol.* **8,** 729–740 (2001).
68. Erez, A. *et al.* Sil overexpression in lung cancer characterizes tumors with increased mitotic activity. *Oncogene* **23,** 5371–5377 (2004).
69. Khodjakov, A. *et al.* De novo formation of centrosomes in vertebrate cells arrested during S phase. *J. Cell Biol.* **158,** 1171–1181 (2002).
70. Rodrigues-Martins, A., Riparbelli, M., Callaini, G., Glover, D. M. & Bettencourt-Dias, M. Revisiting the role of the mother centriole in centriole biogenesis. *Science* **316,** 1046–1050 (2007).

71. La Terra, S. *et al.* The de novo centriole assembly pathway in HeLa cells: cell cycle progression and centriole assembly/maturation. *J. Cell Biol.* **168,** 713–722 (2005).
72. Mikule, K. *et al.* Loss of centrosome integrity induces p38-p53-p21-dependent G1-S arrest. *Nat. Cell Biol.* **9,** 160–170 (2007).
73. Fujiwara, T. *et al.* Cytokinesis failure generating tetraploids promotes tumorigenesis in p53-null cells. *Nature* **437,** 1043–1047 (2005).
74. Meraldi, P., Honda, R. & Nigg, E. A. Aurora-A overexpression reveals tetraploidization as a major route to centrosome amplification in p53-/- cells. *EMBO J.* **21,** 483–492 (2002).
75. Krzywicka-Racka, A. & Sluder, G. Repeated cleavage failure does not establish centrosome amplification in untransformed human cells. *J. Cell Biol.* **194,** 199–207 (2011).
76. Zack, T. I. *et al.* Pan-cancer patterns of somatic copy number alteration. *Nat. Genet.* **45,** 1134–1140 (2013).
77. Dewhurst, S. M. *et al.* Tolerance of whole-genome doubling propagates chromosomal instability and accelerates cancer genome evolution. *Cancer Discov.* **4,** 175–185 (2014).
78. Ring, D., Hubble, R. & Kirschner, M. Mitosis in a cell with multiple centrioles. *J. Cell Biol.* **94,** 549–556 (1982).
79. Ganem, N. J., Godinho, S. A. & Pellman, D. A mechanism linking extra centrosomes to chromosomal instability. *Nature* **460,** 278–282 (2009).
80. Silkworth, W. T., Nardi, I. K., Scholl, L. M. & Cimini, D. Multipolar spindle pole coalescence is a major source of kinetochore mis-attachment and chromosome mis-segregation in cancer cells. *PloS One* **4,** e6564 (2009).
81. Stewénius, Y. *et al.* Structural and numerical chromosome changes in colon cancer develop through telomere-mediated anaphase bridges, not through mitotic multipolarity. *Proc. Natl. Acad. Sci. U. S. A.* **102,** 5541–5546 (2005).
82. Godinho, S. A. *et al.* Oncogene-like induction of cellular invasion from centrosome amplification. *Nature* **510,** 167–171 (2014).
83. Matov, A. *et al.* Analysis of microtubule dynamic instability using a plus-end growth marker. *Nat. Methods* **7,** 761–768 (2010).
84. Zimmerman, W. C., Sillibourne, J., Rosa, J. & Doxsey, S. J. Mitosis-specific anchoring of gamma tubulin complexes by pericentrin controls spindle organization and mitotic entry. *Mol. Biol. Cell* **15,** 3642–3657 (2004).
85. Wiese, C. & Zheng, Y. Microtubule nucleation: gamma-tubulin and beyond. *J. Cell Sci.* **119,** 4143–4153 (2006).
86. Fenech, M. Cytokinesis-block micronucleus cytome assay. *Nat. Protoc.* **2,** 1084–1104 (2007).
87. Crasta, K. *et al.* DNA breaks and chromosome pulverization from errors in mitosis. *Nature* **482,** 53–58 (2012).
88. Heng, H. H. Q. *et al.* Karyotype heterogeneity and unclassified chromosomal abnormalities. *Cytogenet. Genome Res.* **139,** 144–157 (2013).
89. Cimini, D., Fioravanti, D., Salmon, E. D. & Degrassi, F. Merotelic kinetochore orientation versus chromosome mono-orientation in the origin of lagging chromosomes in human primary cells. *J. Cell Sci.* **115,** 507–515 (2002).
90. Cimini, D. Merotelic kinetochore orientation, aneuploidy, and cancer. *Biochim. Biophys. Acta* **1786,** 32–40 (2008).
91. Thompson, S. L. & Compton, D. A. Chromosome missegregation in human cells arises through specific types of kinetochore-microtubule attachment errors. *Proc. Natl. Acad. Sci. U. S. A.* **108,** 17974–17978 (2011).

92. DeLuca, J. G. Kinetochore-microtubule dynamics and attachment stability. *Methods Cell Biol.* **97,** 53–79 (2010).
93. Sivakumar, S., Daum, J. R. & Gorbsky, G. J. Live-cell fluorescence imaging for phenotypic analysis of mitosis. *Methods Mol. Biol. Clifton NJ* **1170,** 549–562 (2014).
94. Cassimeris, L. & Skibbens, R. V. Regulated assembly of the mitotic spindle: a perspective from two ends. *Curr. Issues Mol. Biol.* **5,** 99–112 (2003).
95. Yang, Z., Loncarek, J., Khodjakov, A. & Rieder, C. L. Extra centrosomes and/or chromosomes prolong mitosis in human cells. *Nat. Cell Biol.* **10,** 748–751 (2008).
96. Kwon, M. *et al.* Mechanisms to suppress multipolar divisions in cancer cells with extra centrosomes. *Genes Dev.* **22,** 2189–2203 (2008).
97. Lampson, M. A. & Kapoor, T. M. The human mitotic checkpoint protein BubR1 regulates chromosome-spindle attachments. *Nat. Cell Biol.* **7,** 93–98 (2005).
98. Leber, B. *et al.* Proteins required for centrosome clustering in cancer cells. *Sci. Transl. Med.* **2,** 33ra38 (2010).
99. Cimini, D. Detection and correction of merotelic kinetochore orientation by Aurora B and its partners. *Cell Cycle Georget. Tex* **6,** 1558–1564 (2007).
100. Tanaka, T. U. Kinetochore–microtubule interactions: steps towards bi-orientation. *EMBO J.* **29,** 4070–4082 (2010).
101. Wan, X., Cimini, D., Cameron, L. A. & Salmon, E. D. The coupling between sister kinetochore directional instability and oscillations in centromere stretch in metaphase PtK1 cells. *Mol. Biol. Cell* **23,** 1035–1046 (2012).
102. Holland, A. J. *et al.* The autoregulated instability of Polo-like kinase 4 limits centrosome duplication to once per cell cycle. *Genes Dev.* **26,** 2684–2689 (2012).
103. Krämer, A., Neben, K. & Ho, A. D. Centrosome aberrations in hematological malignancies. *Cell Biol. Int.* **29,** 375–383 (2005).
104. Neben, K., Giesecke, C., Schweizer, S., Ho, A. D. & Krämer, A. Centrosome aberrations in acute myeloid leukemia are correlated with cytogenetic risk profile. *Blood* **101,** 289–291 (2003).
105. Nolte, F. *et al.* Centrosome aberrations in bone marrow cells from patients with myelodysplastic syndromes correlate with chromosomal instability. *Ann. Hematol.* **92,** 1325–1333 (2013).
106. Loh, J.-K. *et al.* Differential expression of centrosomal proteins at different stages of human glioma. *BMC Cancer* **10,** 268 (2010).
107. Telentschak, S., Soliwoda, M., Nohroudi, K., Addicks, K. & Klinz, F.-J. Cytokinesis failure and successful multipolar mitoses drive aneuploidy in glioblastoma cells. *Oncol. Rep.* **33,** 2001–2008 (2015).
108. Chan, J. Y. A Clinical Overview of Centrosome Amplification in Human Cancers. *Int. J. Biol. Sci.* **7,** 1122–1144 (2011).
109. Khodjakov, A. & Pines, J. Centromere tension: a divisive issue. *Nat. Cell Biol.* **12,** 919–923 (2010).
110. Zhou, J., Panda, D., Landen, J. W., Wilson, L. & Joshi, H. C. Minor alteration of microtubule dynamics causes loss of tension across kinetochore pairs and activates the spindle checkpoint. *J. Biol. Chem.* **277,** 17200–17208 (2002).
111. Cimini, D., Moree, B., Canman, J. C. & Salmon, E. D. Merotelic kinetochore orientation occurs frequently during early mitosis in mammalian tissue cells and error correction is achieved by two different mechanisms. *J. Cell Sci.* **116,** 4213–4225 (2003).
112. Nicklas, R. B. & Ward, S. C. Elements of error correction in mitosis: microtubule capture, release, and tension. *J. Cell Biol.* **126,** 1241–1253 (1994).
113. Ertych, N. *et al.* Increased microtubule assembly rates influence chromosomal instability in colorectal cancer cells. *Nat. Cell Biol.* **16,** 779–791 (2014).

114. Wollman, R. *et al.* Efficient chromosome capture requires a bias in the 'search-and-capture' process during mitotic-spindle assembly. *Curr. Biol. CB* **15,** 828–832 (2005).
115. Lee, M., Chang, J., Chang, S., Lee, K. S. & Rhee, K. Asymmetric spindle pole formation in CPAP-depleted mitotic cells. *Biochem. Biophys. Res. Commun.* **444,** 644–650 (2014).
116. Gregan, J. *et al.* The kinetochore proteins Pcs1 and Mde4 and heterochromatin are required to prevent merotelic orientation. *Curr. Biol. CB* **17,** 1190–1200 (2007).
117. Debec, A., Sullivan, W. & Bettencourt-Dias, M. Centrioles: active players or passengers during mitosis? *Cell. Mol. Life Sci.* **67,** 2173–2194 (2010).
118. Sir, J.-H. *et al.* Loss of centrioles causes chromosomal instability in vertebrate somatic cells. *J. Cell Biol.* **203,** 747–756 (2013).
119. Tulu, U. S., Fagerstrom, C., Ferenz, N. P. & Wadsworth, P. Molecular requirements for kinetochore-associated microtubule formation in mammalian cells. *Curr. Biol. CB* **16,** 536–541 (2006).
120. Uetake, Y. & Sluder, G. Prolonged prometaphase blocks daughter cell proliferation despite normal completion of mitosis. *Curr. Biol. CB* **20,** 1666–1671 (2010).
121. Schvartzman, J.-M., Sotillo, R. & Benezra, R. Mitotic chromosomal instability and cancer: mouse modelling of the human disease. *Nat. Rev. Cancer* **10,** 102–115 (2010).
122. Birkbak, N. J. *et al.* Paradoxical relationship between chromosomal instability and survival outcome in cancer. *Cancer Res.* **71,** 3447–3452 (2011).
123. Korzeniewski, N., Hohenfellner, M. & Duensing, S. The centrosome as potential target for cancer therapy and prevention. *Expert Opin. Ther. Targets* **17,** 43–52 (2013).
124. Raab, M. S. *et al.* GF-15, a novel inhibitor of centrosomal clustering, suppresses tumor cell growth in vitro and in vivo. *Cancer Res.* **72,** 5374–5385 (2012).
125. Krämer, A., Maier, B. & Bartek, J. Centrosome clustering and chromosomal (in)stability: a matter of life and death. *Mol. Oncol.* **5,** 324–335 (2011).
126. Rebacz, B. *et al.* Identification of griseofulvin as an inhibitor of centrosomal clustering in a phenotype-based screen. *Cancer Res.* **67,** 6342–6350 (2007).
127. Karna, P. *et al.* A novel microtubule-modulating noscapinoid triggers apoptosis by inducing spindle multipolarity via centrosome amplification and declustering. *Cell Death Differ.* **18,** 632–644 (2011).
128. Bennett, R. A., Izumi, H. & Fukasawa, K. Induction of centrosome amplification and chromosome instability in p53-null cells by transient exposure to subtoxic levels of S-phase-targeting anticancer drugs. *Oncogene* **23,** 6823–6829 (2004).
129. Bian, M. *et al.* Short exposure to paclitaxel induces multipolar spindle formation and aneuploidy through promotion of acentrosomal pole assembly. *Sci. China Life Sci.* **53,** 1322–1329 (2010).
130. Zasadil, L. M. *et al.* Cytotoxicity of paclitaxel in breast cancer is due to chromosome missegregation on multipolar spindles. *Sci. Transl. Med.* **6,** 229ra43 (2014).
131. Dodson, H., Wheatley, S. P. & Morrison, C. G. Involvement of centrosome amplification in radiation-induced mitotic catastrophe. *Cell Cycle Georget. Tex* **6,** 364–370 (2007).
132. Pontén, J. & Saksela, E. Two established in vitro cell lines from human mesenchymal tumours. *Int. J. Cancer J. Int. Cancer* **2,** 434–447 (1967).
133. Stone, K. R., Mickey, D. D., Wunderli, H., Mickey, G. H. & Paulson, D. F. Isolation of a human prostate carcinoma cell line (DU 145). *Int. J. Cancer J. Int. Cancer* **21,** 274–281 (1978).
134. Kaighn, M. E., Narayan, K. S., Ohnuki, Y., Lechner, J. F. & Jones, L. W. Establishment and characterization of a human prostatic carcinoma cell line (PC-3). *Invest. Urol.* **17,** 16–23 (1979).
135. Cailleau, R., Young, R., Olivé, M. & Reeves, W. J. Breast tumor cell lines from pleural effusions. *J. Natl. Cancer Inst.* **53,** 661–674 (1974).

136. Hoffman, D. B., Pearson, C. G., Yen, T. J., Howell, B. J. & Salmon, E. D. Microtubule-dependent changes in assembly of microtubule motor proteins and mitotic spindle checkpoint proteins at PtK1 kinetochores. *Mol. Biol. Cell* **12,** 1995–2009 (2001).

137. Archidiacono, N. *et al.* Comparative mapping of human alphoid sequences in great apes using fluorescence in situ hybridization. *Genomics* **25,** 477–484 (1995).

138. Rocchi, M. *et al.* Chromosome-specific subsets of human alphoid DNA identified by a chromosome 2-derived clone. *Genomics* **8,** 705–709 (1990).

139. Baldini, A., Smith, D. I., Rocchi, M., Miller, O. J. & Miller, D. A. Cloning and analysis of 100kb of pericentromeric repetitive (alphoid) DNA from human chromosome 3. *Am J Hum Genet* **45,** A129 (1989).